The IOCG(U) Mineral System:

Characteristics of K-Fe Alteration in the Northern Yorke Peninsula

Thesis submitted in accordance with the requirements of the University of Adelaide for an Honours Degree in Geology/Geophysics

Nicholas D. Owen

November 2015

THE UNIVERSITY of ADELAIDE

CHARACTERISTICS OF K-FE ALTERATION IN RELATION TO IOCG(U) MINERALISATION IN THE NORTHERN YORKE PENINSULA

ALTERATION & IOCG(U) MINERALISATION IN THE NYP

ABSTRACT

The Moonta-Wallaroo area in the Northern Yorke Peninsula (NYP) is inferred to have been associated with the major deformation, metamorphic and magmatic event at ca. 1600-1575 Ma that affected much of eastern Proterozoic Australia. Wide spread K-Fe (biotite-magnetite) alteration is genetically linked with the main pyrite ±chalcopyrite mineralising event within the Doora Member of the Wandearah Formation. Zones of high mineralisation were seen to correspond with coarsening grainsize of biotite in petrological and hand sample and were supported by geochemical trends between Fe_2O_3, S and Cu. Later stage hematite bearing phase of alteration resulted in intense alteration and pyrite-chalcopyrite mineralisation locally within carbonate bearing zones. It is suggested that uranium enrichment is also associated with biotite-magnetite alteration but was later stripped from the highly mineralised zones by less pervasive hydrothermal fluids.

U-Pb isotope analysis of zircon grains constrain the age of formation of the basement in which mineralisation occurs. The Moonta Porphyry revealed an age of 1752 ±6Ma. Based on its interdigitising relationship with the Moonta Porphyry a maximum age of sedimentation of the Doora Member is proposed at ca. 1752 Ma. The protolithic material of the Harlequin stone was determined to be similar to that of the Doora Member and was sourced mainly from the ca. 1850 Ma Donington Suite Granitoids. A Pb^{207}/Pb^{206} age of ca. 1708 Ma suggests a wider age of formation of the Wallaroo Group than previously reported in literature.

Alteration within the Oorlano Metasomatite metasedimentary samples showed a clear deviation in chemical characteristics from the Doora Member suggesting different styles of alteration in relation to their proximity to the Arthurton and Tickera Granites.

KEYWORDS

K-Fe metasomatism, IOCG(U), Harlequin Stone, Gawler Craton, Proterozoic, magmatism

Contents

Characteristics of K-Fe Alteration in Relation to IOCG Mineralisation in the Northern Yorke Peninsula i
Alteration & IOCG Mineralisation in the NYP i
Abstract i
Keywords i
List of Figures and Tables iii
Introduction 1
Geological Setting/Background 3
Methods 9
Logging and sampling 9
Petrological analysis 9
Whole Rock Geochemistry 10
Zircon U-Pb Geochronology 10
Observations and Results 11
Core Logging - DDH 114 & DDH 200 (Doora-Vulcan Trend) 11
Petrology 17
Whole Rock Geochemistry 22
Zircon U-Pb Geochronology 27
Moonta Porphyry 27
Sample Description 27
Zircon Characteristics 27
Sample Data 27
Geochronological Interpretation 28
Oorlano Metasomatite (Harlequin Stone) 30
Sample Description 30
Zircon Characteristics 31
Sample Data 31
Geochronological Interpretation 31
Discussion 34
Geochronology 34
Moonta Porphyry 34
Oorlano Metasomatite (Harlequin Stone) 34

Alteration 36
Doora Member 36
Oorlano Metasomatite 39
Relationship of Alteration Oorlano Metasomatite vs Doora Member 45
Relationships between Alteration and Mineralisation 47
Uranium in Yorke Peninsula 48
Relationships with Eastern Proterozoic Australia 49
Conclusions 52
Acknowledgments 53
References 53
Appendix A: Whole Rock Geochemical Data 57
Appendix B: Geochronological Data 61

LIST OF FIGURES AND TABLES

Figure 1: A regional map showing the Olympic Domain in the eastern Gawler Craton. The locations of major IOCG deposits within the Olympic Domain are shown including Prominent Hill, Olympic Dam, Carrapateena, the historic Moonta-Wallaroo Cu-Au region and the newly discovered skarn associated Hillside deposit. The rectangular box in the SE of the Gawler Craton shows the extent of the Northern Yorke Peninsula and includes the Moonta-Wallaroo District. Also shown (insert bottom left) are the locations of the main IOCG(U) regions in the Paleo-Mesoproterozoic Australia including the Olympic Domain in the Gawler Craton, the Curnamona Province and the Cloncurry District in the Mt Isa Inlier. Modified from Conor et al. (2010). 2
Figure 2: Interpretation of the geology in the Northern Yorke Peninsula in the southern Olympic Domain. The locations of the historic Wallaroo and Moonta Cu-Au mining fields are shown along the north western coast and the skarn associated Hillside deposit on the south eastern coast of the Northern Yorke Peninsula. Additionally, the locations of the Poona Mine, Oorallaw Quarry, the Doora-Vulcan trend and the locations from which the Doora Member samples were taken are also shown. Modified from Conor et al. (2010)..... 7
Figure 3: Stratigraphy within the Northern Yorke Peninsula showing the relative timing of emplacement of the formations after Cowley et al. (2003) with additional information from Schwarz (2003), Reid et al. (2008) and Conor et al. (2010). 8
Figure 4: Representative drill core from DDH 114 and DDH 200; a) unaltered sediments with small fractures offsetting planar compositional banding; b) unaltered metasediments containing folded compositional banding with fine grained biotite foliation axial to fold hinges and thin 1cm pegmatite intruding along foliation; c) moderately altered sediments dominated by medium grained biotite foliation; d) moderately altered sediments containing folded compositional banding cross cut by large pegmatite which intrudes along foliation; e) highly altered sediments containing hematite alteration with pegmatite and sulphide mineralisation along foliation; f) highly altered sediments with sulphides developed along foliation axial to fold plane; g) highly altered sediments with hematite/pegmatite vein cross cutting and locally folded coarse-grained biotite foliation; h) highly altered sediments with disrupted pegmatite and an intense biotite shear zone in which the foliation has been folded by a later event..... 14
Figure 5: Detailed visual log of a section DDH 114 showing the physical changes in the structure of the core in response to folding and shearing with depth. The logged section of represents one broad alteration progression with a gradual change from less altered with low sulphide mineralisation to highly altered with high sulphide mineralisation. To show the relationship between of sulphide mineralisation and biotite-magnetite alteration the coarseness of biotite grains was plotted with the total percentage sulphide mineralisation. 15
Figure 6: Detailed visual log of a section DDH 200 showing the physical changes in the structure of the core in response to folding and shearing with depth. Several alteration progressions occur across the logged section. To show the relationship between of sulphide mineralisation and biotite-magnetite alteration the coarseness of biotite grains was plotted with the total percentage sulphide mineralisation. 16
Figure 7: Photomicrographs of unaltered through to altered lithologies. a) unaltered sediment preserving compositional layering with fine grained matrix of quartz and feldspar (DDH 200, 144.5m); b) and c) unaltered sediment containing a vein of coarse

grained biotite which has been overprinted by pyrite and chalcopyrite mineralisation (DDH 200, 486.1m); d) and e) moderately altered sediment with clear compositional layering and a distinct separation between fine grained quartz-feldspar-biotite and coarser grained biotite-quartz-feldspar. The compositional layering forms a tight fold with a strong biotite foliation axial to the fold hinge. Small blotches of pyrite mineralisation occur within the coarse grained layer (DDH 200, 158.5m); f) to h) moderately altered sediment containing orthopyroxene alteration and pyrite-chalcopyrite mineralisation restricted to layers containing coarse grained biotite (DDH 200, 164.3m); i) to k) moderately altered sediment containing a pegmatite vein which cross cuts compositional layering. Coarse grained biotite and magnetite alteration occurs within the vein indicating that the development of coarse biotite occurred either syn or post-pegmatite veining. Identified on the images by the dashed line are the edges of the pegmatite vein (DDH 200, 158.5m). Abbreviations: Fg - fine grained, cg - coarse grained, qtz - quartz, feld - feldspar, bt - biotite, cpx - clinopyroxene, mt - magnetite, py - pyrite, cpy - chalcopyrite..... 19
Figure 8: Photomicrographs of highly altered sediments a) to l) (above) and m) to u) (next page). a) and b) coarse grained biotite which has been altered to chlorite. Large 1 - 1.5 mm Tourmaline grains overgrow coarse grained biotite and are in turn overprinted by fine grained chlorite which forms fissure like veins through both the biotite foliation and tourmaline grains (DDH 200, 146.9m); d) and e) coarse grained biotite which has undergone clinopyroxene alteration (DDH 200, 147.5m); c) and f) two different generations of carbonate with small amounts of an Fe-oxide (most likely hematite) forming at the reaction margin. Additionally, the large grain which is light grey in cross polars (f) has formed secondary carbonate laminae indicating its instability some stage after formation (DDH 200, 159.1m); g) and h) heavy magnetite alteration of an Fe-carbonate. At the centre of the stage are titanate and uraninite grains encased in coarse grained biotite. The biotite foliation post-dates coarse grained quartz but pre-dates the magnetite alteration (DDH 200, 159.1m); i) and l) coarse grained biotite-magnetite alteration with associated sulphide mineralisation (DDH 114, 160m); j) to k) poikiloblastic hornblende surrounding quartz, biotite, magnetite and pyrite (DDH 114, 160m); m) and n) thick (2 mm) veins of fine grained chlorite surrounded by a matrix of fine grained quartz and biotite. Associated with the chlorite vein are blobs of pyrite and chalcopyrite mineralisation (DDH 200, 146.9m); o) and r) large heavily metamict allanite grain surrounded by blue green hornblende and a grain of high bioinfringence orthopyroxene. Late stage pyrite and chalcopyrite mineralisation occurs within cracks and around the edges of the allanite grain (DDH 114 194.2m); p) and q) coarse chlorite and biotite grains within altered carbonate and vein like pyrite-chalcopyrite mineralisation (DDH 200, 162.7); s) to u) coarse grained quartz and biotite surrounding a large carbonate containing extensive hematitic alteration. Within cracks and extensively altered sections of the carbonate are large amounts of pyrite and chalcopyrite mineralisation (DDH 200, 162.7). Abbreviations: fg - fine grained, cg - coarse grained, qtz - quartz, feld - feldspar, bt - biotite, hbl - hornblende, tur - tourmaline cpx - clinopyroxene, aln - allanite, mt - magnetite, py - pyrite, cpy - chalcopyrite. 20
Figure 9: Backscatter Electron Microscope images of uraninite grains; (left) Uraninite grain contained within poikiloblastic hornblende with direct association with magnetite. Large halo extends well beyond the grain boundaries; (right) two neighbouring uraninite

grains, one contained within coarse-grained biotite and the other with magnetite (from left to right). 21
Figure 10: Element ratio plots of geochemistry data from drill holes DDH 114 and DDH 200. (a) to (i) show a range of elements plotted against Fe_2O_3. Fe_2O_3 is used as a measure of the intensity of alteration ranging from relatively unaltered samples with low concentrations of Fe_2O_3 up to highly altered samples containing high concentrations of Fe_2O_3; j) and k) proportional relationship between Cu, Au and S with a large spike in Cu and Au values occurring in sample 2129383; l) to n) show a linear relationship between LREE's Ce and La and a roughly proportional relationship of both of these with Y. 25
Figure 11: a) CL images of representative zircon grains from the Moonta Porphyry sample recovered from the Poona Cu-Au Mine; b) concordia plot for the Moonta Porphyry sample recovered from the Poona Cu-Au Mine. Insert bottom right shows the calculated concordia intercept yielding an age of 1757 ± 7.3 Ma. Data used to calculate the weighted mean is within ten percent of concordancy; c) weighted Mean of the Moonta Porphyry sample collected from Poona Cu-Au Mine. Data used to calculate the weighted mean is within ten percent of concordancy. 30
Figure 12: a) CL images of representative zircon grains from the Oorlano Metasomatite sample recovered from the Oorallaw Quarry; b) probability density plot of LA-ICPMS results from the Oorlano Metasomatite which all within the range of 10 % from concordancy. 33
Figure 13: A paragenetic sequence diagram summarising the relative timing of alteration and mineralisation in the Doora Member observed in thin section. Grouping of alteration type as either Propylitic or Potassic and the temperature ranges therein are based on Taylor & Pollard (2006). 37
Figure 14: Geochemical ratio plots (a) to (c) show trace elements Vanadium, Nickel and Chromium from the Oorlano Metasomatite plotted against Silica. Mafic lithologies contained high Vanadium, Nickel and Chromium and low Silica while felsic lithologies contained an abundance of silica with low Vanadium, Nickel and Chromium. Metasediments were contained moderate amounts of Vanadium, Nickel, Chromium and Silica. 40
Figure 15: Isocon plots constructed from the average elemental composition of rocks with a similar interpreted protolith at varying levels of alteration. The dashed lines represent the minimum and maximum Isocon gradients at each level of alteration. Where any data points fall outside of this range either a net gain or loss is recorded for the element in question. (a) Moderate Alteration in the Doora Member (b) High Alteration in the Doora Member and (c) Oorlano Metasomatite. Only values separated as metasediments in Figure 14 were used for Isochron analysis. All three alteration types were plotted against the average of the least altered Doora Member samples. All data used to create the Isochron plots are given in Appendix 3. 44

Table 1: Representative geochemical data from drill holes DDH 114 and DDH 200. Samples for geochemistry were taken across three alteration sequences with one broad sequence selected from DDH 114 and two narrow sequences selected from DDH 200. An X value is used where element concentrations were below detection limit. 24
Table *2*: Summary of LA-ICPMS U-Pb zircon data from the Moonta Porphyry sample recovered from the Poona Cu-Au Mine. 28

Table 3: Summary of the LA-ICPMS U-Pb results from the Oorlano Metasomatite sample recovered from the Oorallaw Quarry. 31
Table 4: Geochemical data from Oorlano Metasomatite samples at various locations. For each drill hole a basement sample number of either B1 or B2 is given to show the relative depth of each sample where B1 is the shallower of the two. A protolith was prescribed based on elemental ratios as shown in Figure 14. The calculated values for the Alteration Index (AI), Silicification Index (SI) and the Chlorite-Carbonate-Pyrite Index (CCPI) are also shown. 41
Table 5: Whole rock geochemistry data from the metasediments of the Doora Member and the Oorlano Metasomatite metasedimentary samples. Samples are split into levels of alteration and a multiplication factor was applied to generate average concentration values between 0 and 30 to enable the data to be plotted on isocron diagrams. 42

INTRODUCTION

Eastern Proterozoic Australia hosts numerous deposits including iron oxide-copper-gold (IOCG) deposits at Olympic Dam, Prominent Hill, Carrapateena and the Moonta-Wallaroo Region in the Olympic Domain as well the Cloncurry District in the Mount Isa area (Figure 1). The role of hydrothermal fluids and their relationship to mineralisation and metasomatism are well understood for some areas including the Cloncurry District (Williams *et al.* 2001, Mark *et al.* 2006), Olympic Dam (Haynes *et al.* 1995, Johnson & McCulloch 1995, Direen & Lyons 2007) and Prominent Hill (Belperio *et al.* 2007) however are less understood within the northern Yorke Peninsula (NYP) in the southern Olympic Domain (Figure 1) (Conor 1995, Conor 2002, Conor *et al.* 2010).

Mineralisation and metasomatism in the Moonta-Wallaroo area in the NYP (Figure 2) are inferred to have been associated with the major deformation, metamorphic and magmatic event at ca. 1600-1575 Ma (Conor 2002, Morales Ruano *et al.* 2002, Hand *et al.* 2007, Conor & Forbes 2012, Reid & Hand 2012) that effected much of eastern Proterozoic Australia (e.g. Gauthier *et al.* 2001, Giles & Nutman 2002, Fanning *et al.* 2007, Hand *et al.* 2007, Forbes *et al.* 2008, Conor *et al.* 2010, Forbes *et al.* 2011, Conor & Forbes 2012). Intense metasomatism in the area is suggested to have been associated with K-Fe rich hydrothermal fluids, resulting in development of a magnetite-biotite mineral assemblage (Morales Ruano *et al.* 2002, Conor *et al.* 2010, Conor & Forbes 2012, Kontonikas-Charos *et al.* 2014) that is contemporaneous with mineralisation (Conor *et al.* 2010). The K-Fe (biotite-magnetite) metasomatism is associated with high strain zones (e.g. shearing, folding) and growth of coarse biotite as a result of shearing

(Conor *et al.* 2010). However, the processes of K-Fe metasomatism and absolute time constraints on the development of metasomatic assemblages in relation to mineralisation and magmatism in the NYP are not well constrained.

This study aims to provide constraints on the timing of volcanism and sedimentation in the northern Yorke Peninsula. Detailed core logging, petrological analysis and whole rock geochemistry of prospective lithologies which showed the progression of K-Fe

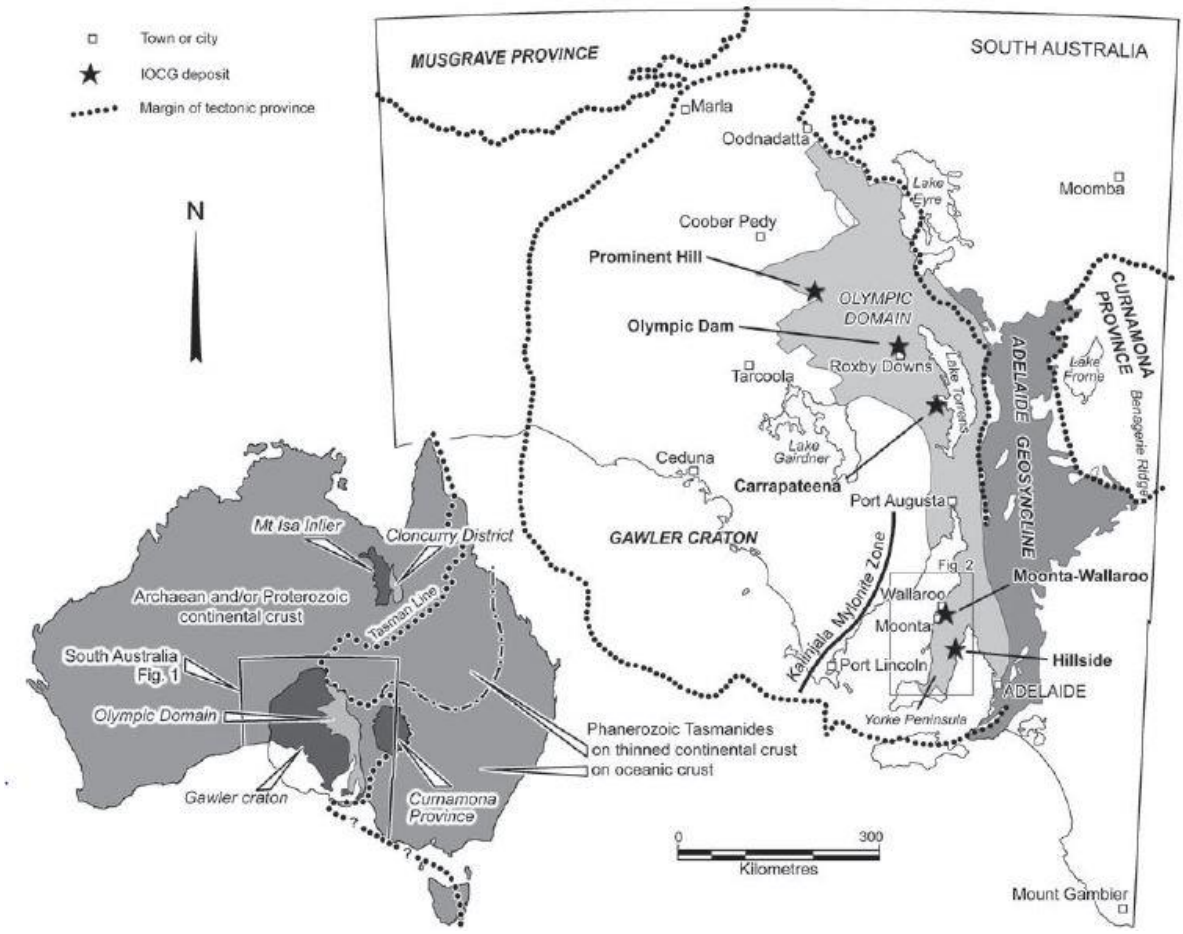

Figure 1: A regional map showing the Olympic Domain in the eastern Gawler Craton. The locations of major IOCG deposits within the Olympic Domain are shown including Prominent Hill, Olympic Dam, Carrapateena, the historic Moonta-Wallaroo Cu-Au region and the newly discovered skarn associated Hillside deposit. The rectangular box in the SE of the Gawler Craton shows the extent of the Northern Yorke Peninsula and includes the Moonta-Wallaroo District. Also shown (insert bottom left) are the locations of the main IOCG(U) regions in the Paleo-Mesoproterozoic Australia including the Olympic Domain in the Gawler Craton, the Curnamona Province and the Cloncurry District in the Mt Isa Inlier. Modified from Conor et al. (2010).

metasomatism with sulphide mineralisation was used to examine the processes that occur during K-Fe metasomatism and their relationship to IOCG-style mineralisation in the NYP. New geochemical data for the Doora Member of the Wandearah Formation was compared to whole rock geochemical data collected by Dr Caroline Forbes in order to analyse the range of chemical signatures of the Oorlano Metasomatite (Figure 3). The relationship of the NYP in the context of mineralisation, magmatism, deformation and metasomatism associated with the ca. 1600-1580Ma event that affected eastern Proterozoic Australia is then discussed along with the distribution of uranium in magnetite hosted IOCG deposits.

GEOLOGICAL SETTING/BACKGROUND

The Olympic Domain in the eastern Gawler Craton hosts zones of extensive alteration and mineralisation resulting in one of the largest known concentrations of economic IOCG deposits of any geological province world-wide (Conor *et al.* 2010). Known major deposits in the Olympic Domain include the world class Olympic Dam deposit, as well as the Prominent Hill and Carrapateena deposits, the skarn associated Hillside deposit and the Moonta-Wallaroo Cu-Au deposits (Figure 1) (Ferris *et al.* 2002, Conor *et al.* 2010).

The Moonta-Wallaroo Cu-Au deposits are located within the southern extension of the Olympic Domain in the northern Yorke Peninsula (Figure 1). Mineralisation is hosted within the ca. 1750 Ma Wallaroo Group (Conor 2002, Cowley *et al.* 2003, Conor *et al.* 2010). The Wallaroo Group stratigraphy (Figure 3) has been discussed in Cowley *et al.* (2003) however detail of the stratigraphy remains conjectural due to the poor exposure of the Paleoproterozoic rocks. The most expansive unit within the Wallaroo Group is

the Wanderah Formation, which is a package of fine sandstones and calcsilicate metasediments and includes the iron rich calcsilicates of the Doora Member (Figure 3) (Cowley *et al.* 2003). Felsic and mafic volcanogenic sequences of the Weetulta and Matta Formations respectively were extruded contemporaneously with deposition of the Wandearah Formation metasediments. The Weetulta Formation of which the Moonta Porphyry is the type example includes rhyodacites and ignimbrites (Figure 3) which are intercalated with the Doora Member near Kadina (Drexel et al. 1993, Cowley *et al.* 2003). The ca. 1748 ±15Ma (Fanning *et al.* 2007) Moonta Porphyry is a metamorphosed rhyodacite in part affected by K-Fe metasomatic alteration (Cowley *et al.* 2003).

Deformation of the Wallaroo Group resulted in development of two fold generations. The first generation of folds are isoclinal, and are suggested to have developed early during the ca. 1600-1580 Ma (Conor 2002, Morales Ruano *et al.* 2002, Hand *et al.* 2007, Conor & Forbes 2012, Reid & Hand 2012) Olarian Orogeny (Conor 2002, Hand *et al.* 2007, Conor & Forbes 2012) but the possibility of it relating to the ca. 1730-1690 Ma Kimban Orogeny (Conor *et al.* 2010) cannot be discarded. The second generation of folds is open and upright and is suggested to have developed at ca. 1600-1575 Ma (Conor *et al.* 2010). Amphibolite rich calc-silicate hydrothermal alteration is preserved within the axial planes of later stage open folds. There is no alteration associated with earlier isoclinal folds. Also included with the ca. 1600-1580 Ma event is the intrusion of the Tickera and Arthurton Granites in the NYP (Hand *et al.* 2007, Conor *et al.* 2010, Conor & Forbes 2012) at ca. 1577 ±7 Ma and 1582 ±7 Ma respectively (Fanning *et al.* 2007). These granites are suggested to be equivalent to the more extensive Hiltaba Granite Suite (Conor 2002, Fanning *et al.* 2007, Conor *et al.* 2010) that is associated

with IOCG mineralisation throughout the Gawler Craton (Conor 2002, Cowley *et al.* 2003, Conor *et al.* 2010, Conor & Forbes 2012). Granites of the NYP are variably deformed and metamorphosed/altered.

Alteration associated with intrusion of the Tickera and Arthurton Granites is interpreted to have resulted in development of the Oorlano Metasomatite (Figure 3) (Cowley *et al.* 2003). The Oorlano Metasomatite is a general term for all intensely altered metasomatic rocks with no easily recognisable geological precursor due to the pervasive and intense nature of the alteration which has taken place within it (Conor 2002, Cowley *et al.* 2003). Mineral assemblages are diverse but include albite, K-feldspar, amphibole, clinopyroxene, scapolite, epidote, biotite, magnetite and hematite (Conor 2002, Cowley *et al.* 2003).

Metasomatic alteration and mineralisation in the northern Yorke Peninsula is generally structurally controlled being focussed within faults, shear zones and fold hinges (Conor 2002, Morales Ruano *et al.* 2002), K-Fe alteration is recognised as an increase in the growth of coarse grained biotite. Morales Ruano *et al.* (2002) give evidence for a four stage hydrothermal process of alteration and mineralisation in the NYP within the historic Moonta-Wallaroo District (Figure 2). The first two fluid phases include Fe-oxide as magnetite. Na-Ca-Fe alteration (Conor *et al.* 2010, Kontonikas-Charos *et al.* 2014), which is represented by kilometre scale albite ± calc-silicate ± magnetite alteration zones in the Moonta-Wallaroo District (Kontonikas-Charos *et al.* 2014) form wide spread high intensity magnetic anomalies commonly proximal to the Tickera and Arthurton granites (Conor *et al.* 2010). Na-K-Fe alteration is represented by the mineral

assemblage of biotite-magnetite-albite (Conor *et al.* 2010, Kontonikas-Charos *et al.* 2014) and is found to coexist with the Na-Ca-Fe alteration making the relative timing and overprinting relationship between the two stages difficult to constrain (Conor *et al.* 2010). A third fluid phase was dominated by Fe-sulphides (Morales Ruano *et al.* 2002, Conor *et al.* 2010) followed by the final fluid phase which overprinted earlier alteration during cooler hematite-stable conditions. This resulted in a chlorite-hematite-quartz-K feldspar alteration mineral assemblage which is associated with the Cu-Fe-Co-Au-Zn-Pb mineralisation of the copper-gold lodes in the Moonta-Wallaroo mining fields (Conor *et al.* 2010). It is widely suggested that the alteration fluids have a magmatic source and are derived from the Arthurton and Tickera Granites (Both *et al.* 1993) however Morales Ruano *et al.* (2002), Conor *et al.* (2010) also suggest coupled interaction with an upper crustal fluid source including the host Wallaroo Group (Wurst 1994). This is demonstrated by what is interpreted as disseminated syngenetic Cu mineralisation in volcanoclastic metasedimentary rocks overlying the Moonta Porphyry near Wheal Hughes (Conor *et al.* 2010) and by tourmaline geochemistry (Wurst 1994). This suggests metallic enrichment of the upper crust within the NYP prior to the intrusion of the Tickera and Arthurton Granites, possibly during the emplacement of the ca. 1748 ±15Ma (Fanning *et al.* 2007) Moonta Porphyry and other magmatic rocks of the Weetulta and Matta Formations (Figure 3).

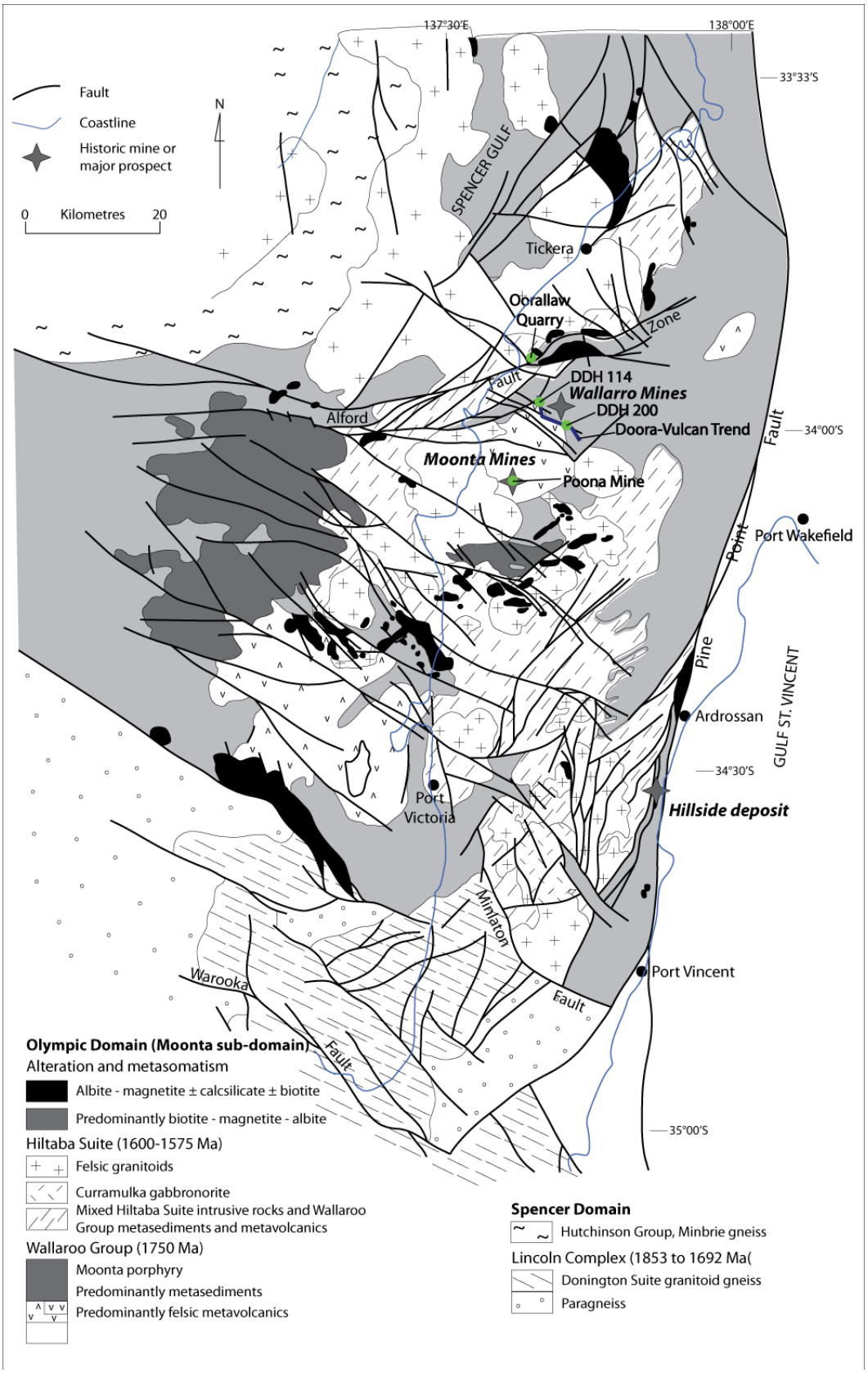

Figure 2: Interpretation of the geology in the Northern Yorke Peninsula in the southern Olympic Domain. The locations of the historic Wallaroo and Moonta Cu-Au mining fields are shown along the north western coast and the skarn associated Hillside deposit on the south eastern coast of the Northern Yorke Peninsula. Additionally, the locations of the Poona Mine, Oorallaw Quarry, the Doora-Vulcan trend and the locations from which the Doora Member samples were taken are shown. Modified from Conor et al. (2010).

Group/Suite	Formation	Member	Lithological description
Alteration	Magnetite alteration?		Albite-magnetite ± calcsilicate ± biotite
	Oorlano Metasomatite		Skarn-like metasomatic rock. Calcsilicate (feldspar, scapolite, actinolite, diopside, carbonate, phlogopite, epidote, magnetite, pyrite), feldspathic (albite>>microcline, lesser opaques and calcsilicate minerals) and iron-rich (magnetite>>hematite, feldspar, biotite, pyrite) metasomatite; precursor lithology usually obliterated or uncertain. Local kaolin alteration (± siderite ± alunite ± pyrite ± chalcocite) [late phase of metasomatism??]
Hiltaba Suite (ca. 1600-1580 Ma)	Tickera Granite		Variable I- and S-type granitoids; monzogranite, quartz monzonite, leucotonalite, commonly intensely deformed
	Arthurton Granite		A-type granite, monzogranite, quartz monzonite, generally undeformed
	Curramulka Gabbronorite		Gabbronorite comprising plagioclase, clinopyroxene (augite), orthopyroxene, hornblende, biotite ± quartz or orthoclase.
Hiltaba Suite?	Bute Metadolerite		Metadolerite comprising albitised and sericitised plagioclase laths, amphibole, biotite and/or chlorite replacing interstitial pyroxene, accessory epidote, opaques, carbonate, sericite and sphene, ophitic texture. Mostly massive, locally sheared. Locally metagabbro with feldspar glomerophenocrysts.
Wallaroo Group (ca. 1750 Ma) Metasediments, felsic and mafic metavolcanics and minor associated subvolcanic intrusives	Wandearah Formation		Clastic and chemical metasediments.
		Wokurna Member	Dominantly laminated muscovite-bearing argillite interlayered with quartz siltstone, occasionally graded, minor iron-oxide, carbonate, albite and calcsilicate, pale green and buff reduction spotting common. Locally becomes more siltstone- to sandstone-rich with disseminated magnetite and hematite as accessory phases; or chloritic metasediments, carbonaceous or calcareous. Includes thin calcsilicate, carbonate and albitic units.
		Delken Member	Cherty', finely laminated, layer parallel albite-quartz metasediment, trace amphibole, magnetite and calcite.
		New Cornwall Member	Metasiltstone and chemical sediments, often layered. Variable proportions of calcsilicate, minor limestone and dolomite, laminated albitite, layered albite-magnetite ironstone, graphitic and calcareous metasiltstone, argillite and metasandstone.
		Doora Member	Schistose, medium-grained, thinly planar layered to laminated metasediments of variable composition including quartz-plagioclase rich, iron-rich and calcsilicate metasediments (e.g. quartz-amphibole (actinolite and cummingtonite)-biotite ± magnetite calcsilicate; biotite-quartz-albite pelite; quartz-albite-magnetite-biotite iron formation). Minor marble and quartz-albitite.
		Aagot Member	Planar to bedded micaceous metasandstone or psammite, sandy or tuffaceous argillite with minor interlayered calcsilicate and albitic rocks. Locally includes volcanoclastic conglomerate.
	Weetulta Formation		Felsic volcanics - porphyritic rhyodacite, dacite, latite with bedded tuff and tuffaceous siltstone.
		Mona Volcanics Member	Acid porphyry (dacite to rhyodacite) with plagioclase phenocrysts (altering to K-feldspar or sericite) with lesser quartz and altered ferromagnesian minerals in quartz + plagioclase or flow banded K-feldspar ± chlorite ± quartz ± Fe-oxides, locally amygdaloidal and spherulitic; and thinly bedding tuffaceous siltstone to tuff with local microphenocrysts, minor crystal tuff and lapilli tuff.
		Moonta Porphyry Member	Plagioclase-phyric rhyodacite locally showing volcanic or ignimbritic characteristics. Plagioclase phenocrysts altered to K-feldspar.
		Wardang Volcanics Member	Plagioclase-phyric rhyodacite, dacite and latite, locally rhyolite; locally preserves flow banding, flow folding, columnar cooling structures and hyaloclastics.
	Matta Formation		Mafic volcanics - amphibolite intrusives and gneisses
		Willamulka Metabasalt Member	Fine- to medium-grained, massive to amygdaloidal basalt, replaced by albite, chlorite, biotite, amphibole, calcite, quartz and accessory minerals. Amygdales filled with quartz, chlorite and/or carbonate.
		Renowden Metabasalt Member	Basalt with crystals (phenocrysts?) of hornblende and plagioclase. Locally contains quartz-rich vesicles that may be scoriaceous texture.
		Wandilta Amphibolite Member	Amphibolite and layered plagioclase-hornblende-biotite rock.
Donington Suite (ca. 1850 Ma)			Intrusives of variable composition including gabbro, gabbronorite, charnockite, and granodiorite to alkali granite.

Figure 3: Stratigraphy within the Northern Yorke Peninsula showing the relative timing of emplacement of the formations after Cowley et al. (2003) with additional information from Schwarz (2003), Reid et al. (2008) and Conor et al. (2010).

METHODS

Logging and sampling

Two drill holes 23633 (DDH 114) and 23042 (DDH 200) were chosen for logging and sampling based on their location within the Doora-Vulcan mineralisation zone south of Kadina in the Moonta Wallaroo area (Figure 2). Selected zones of the drill holes were logged in detail to note progression from reasonably un-altered to highly K-Fe altered metasediments, alteration being evidenced by biotite component and grain size, modal abundance of sulphides and relative strain intensity. DDH 114 was logged and sampled at DSD Core Library in Kadina while DDH 200 was logged and sampled at DSD Core Library in Glenside.

Fourteen samples representative of unaltered through to altered rock were collected for thin section analysis. Eleven of these samples that are representative of the alteration sequences were used for whole rock geochemistry. Two samples were selected from relatively unaltered sections of DDH 200 for detrital zircon geochronology.

A sample of the Harlequin Stone from the Oorallaw Quarry (745132mE, 6245017mS; Figure 2) and a sample of meta-rhyodacite Moonta Porphyry from the Poona Mine (740800mE, 6228950mS, Figure 2) were collected for zircon geochronology.

Petrological analysis

Petrological analysis was done using standard transmitted and reflected light microscopy to note the mineralogy of the unaltered versus altered rocks. This was achieved by noting the modal proportion of biotite and magnetite in the samples along

with the grain size of biotite and the presence/absence/type of sulphide minerals in relation to these factors. Any additional phases accessory to the coarse-grained biotite phase or otherwise were also recorded.

Whole Rock Geochemistry

Eleven samples of the Doora Member were analysed at Genalysis Laboratories in Adelaide using standard fire assay, ICP-MS and ICP-OES techniques. Representative data is given in Tables 1 and 2, all data including standard values are included in Appendix 1 and 2.

Zircon U-Pb Geochronology

Zircon grains from the Harlequin Stone and the Moonta Porphyry were mounted in polished resin mounts and imaged using either a FEI Quanta600 SEM or a Philips XL20 SEM with Cathodoluminescence (CL) at Adelaide Microscopy to determine the location of any chemical zonation within the grains. Representative images are shown in Figure 11 and 14.

Metamict zircon was recovered from the Arthurton and Tickera Granites making constraining the timing of magmatism impossible. Zircon geochronology was planned for 2 samples of the Doora Member however no zircon could be recovered. Additionally, *in situ* monazite geochronology was intended to constrain the timing of K-Fe metasomatism in the Doora Member however no dateable minerals could be found.

A New Wave 213 laser coupled with a 7500cx ICP-MS was used to obtain U-Pb isotope ratios by means of Laser Ablation Inductively Coupled Plasma Mass Spectrometry (LA-

ICP-MS) at Adelaide Microscopy. The laser was fired in a He ablation atmosphere using a beam diameter of 30 µm at a frequency of 5 Hz and a laser output of 55%. To gain correct measurements of background isotopic ratios before each ablation the system was run for 20 seconds without firing, the laser then fired for 10 seconds with the shutter closed to allow beam stabilisation before a 30 second period of sample ablation. Matrix matched standards were run prior to every 15 samples in order to calibrate the measurements and correct for fractionation (Appendix 4**,** 5).

The isotopes measured for zircon analysis were 204Pb, 206Pb, 207Pb, 208Pb, 232U and 238U. The program Glitter developed by Macquarie University in Sydney (Griffin *et al.* 2008) was used for real-time isotope data analysis and was used for any data noise corrections. Isoplot (Ludwig 2003) was then used to plot the data.

OBSERVATIONS AND RESULTS

Core Logging - DDH 114 & DDH 200 (Doora-Vulcan Trend)

Both intervals of the Doora Member in DDH 114 and DDH 200 showed similar characteristics in terms of the alteration mineralogy associated with the deformation. Overall, DDH 114 was more highly altered than DDH 200, which was reflected by a higher coarse-grained biotite content and a higher degree of strain.

Unaltered lithologies (Figure 4a-b) generally consist of light grey fine to medium-grained, well bedded, calcareous metasandstone containing an abundance of quartz, feldspar, fine to medium grained biotite (<1mm) with little magnetite or sulphide. Compositional layering is well displayed by bands of light and dark material. Small

scale (<3cm) folds are occasionally present. Unaltered lithologies are preserved in shear separated zones that vary in thickness ranging from less than a meter (e.g. Figure 5) up to six meters thick (e.g. Figure 6).

Moderately altered lithologies (Figure 4c-d) are comprised of quartz, feldspar, biotite, magnetite, pyrite and chalcopyrite and are more deformed and consistently folded throughout (Figure 4d). The grain size of biotite increases (up to 1.5mm) proximal to and within areas of higher strain (Figures 5 and 6) and locally biotite foliation is intense and parallel to shear structure (Figure 4c). Biotite foliation from least to most altered rock is in the same orientation. Extensive magnetite alteration occurs proximal to deformed zones containing pegmatite (quartz + K-feldspar) veins. Minor magnetite is present in less deformed zones.

Highly altered lithologies (Figure 4e-h) containing quartz, feldspar, biotite, amphibole, magnetite, hematite, pyrite and chalcopyrite are very deformed with complete loss of primary compositional banding. Where primary compositional layering is absent, a schistose foliation is dominant defined by coarse grained biotite. Biotite grains vary up to 3mm in size and coexist with magnetite. Brecciation occurs in and around high strain pegmatite (quartz + K-feldspar) rich zones. The proportion of sulphides is increased in highly deformed and altered zones where 5-15% pyrite and chalcopyrite are present as large (10cm) blebs or even locally dominate the rock. Hematite occurs in thin 1mm veins which cross-cut biotite foliation (Figure 4g). An intense shear zone containing extremely coarse-grained biotite with no magnetite or sulphide mineralisation was

observed at the end of DDH 200 (Figure 4h and Figure 6), where the foliation had been intensely folded.

Overall the intensity of biotite and magnetite alteration as well as the modal proportion of sulphide mineralisation shows a marked increase from unaltered relatively undeformed rocks through to altered highly deformed rocks.

Figure 4: Representative drill core from DDH 114 and DDH 200; a) unaltered metasediments with small fractures offsetting planar compositional banding; b) unaltered metasediments containing folded compositional banding with fine grained biotite foliation axial to fold hinges and thin 1cm pegmatite intruding along foliation; c) moderately altered metasediments dominated by medium grained biotite foliation; d) moderately altered metasediments containing folded compositional banding cross cut by large pegmatite which intrudes along foliation; e) highly altered metasediments containing hematite alteration with pegmatite and sulphide mineralisation along foliation; f) highly altered metasediments with sulphides developed along foliation axial to fold plane; g) highly altered metasediments with hematite/pegmatite vein cross cutting and locally folded coarse-grained biotite foliation; h) highly altered metasediments with disrupted pegmatite and an intense biotite shear zone in which the foliation has been folded by a later event.

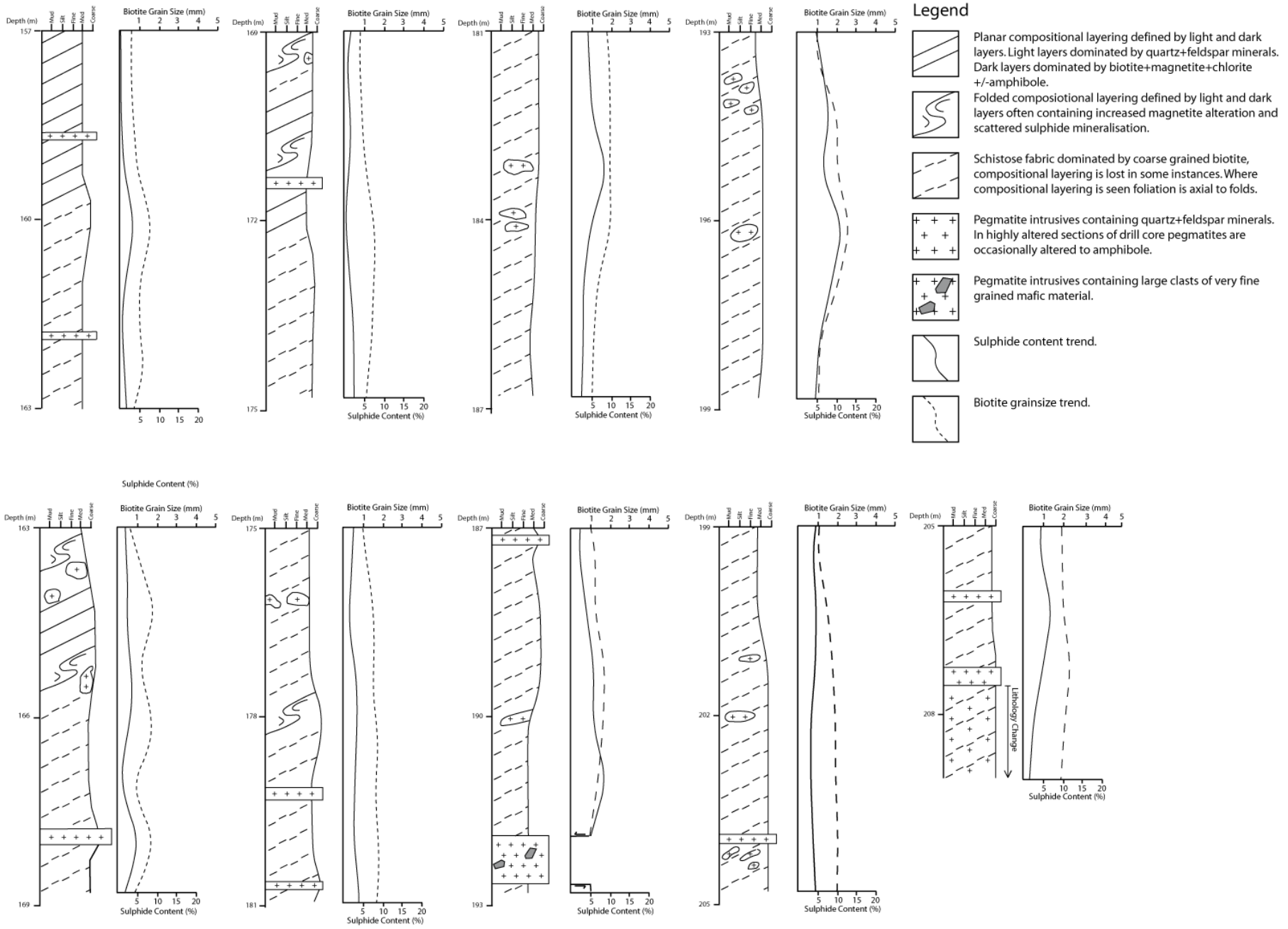

Figure 5: Detailed visual log of a section DDH 114 showing the physical changes in the structure of the core in response to folding and shearing with depth. The logged section of represents one broad alteration progression with a gradual change from less altered with low sulphide mineralisation to highly altered with high sulphide mineralisation. To show the relationship between of sulphide mineralisation and biotite-magnetite alteration the coarseness of biotite grains was plotted with the total percentage sulphide mineralisation.

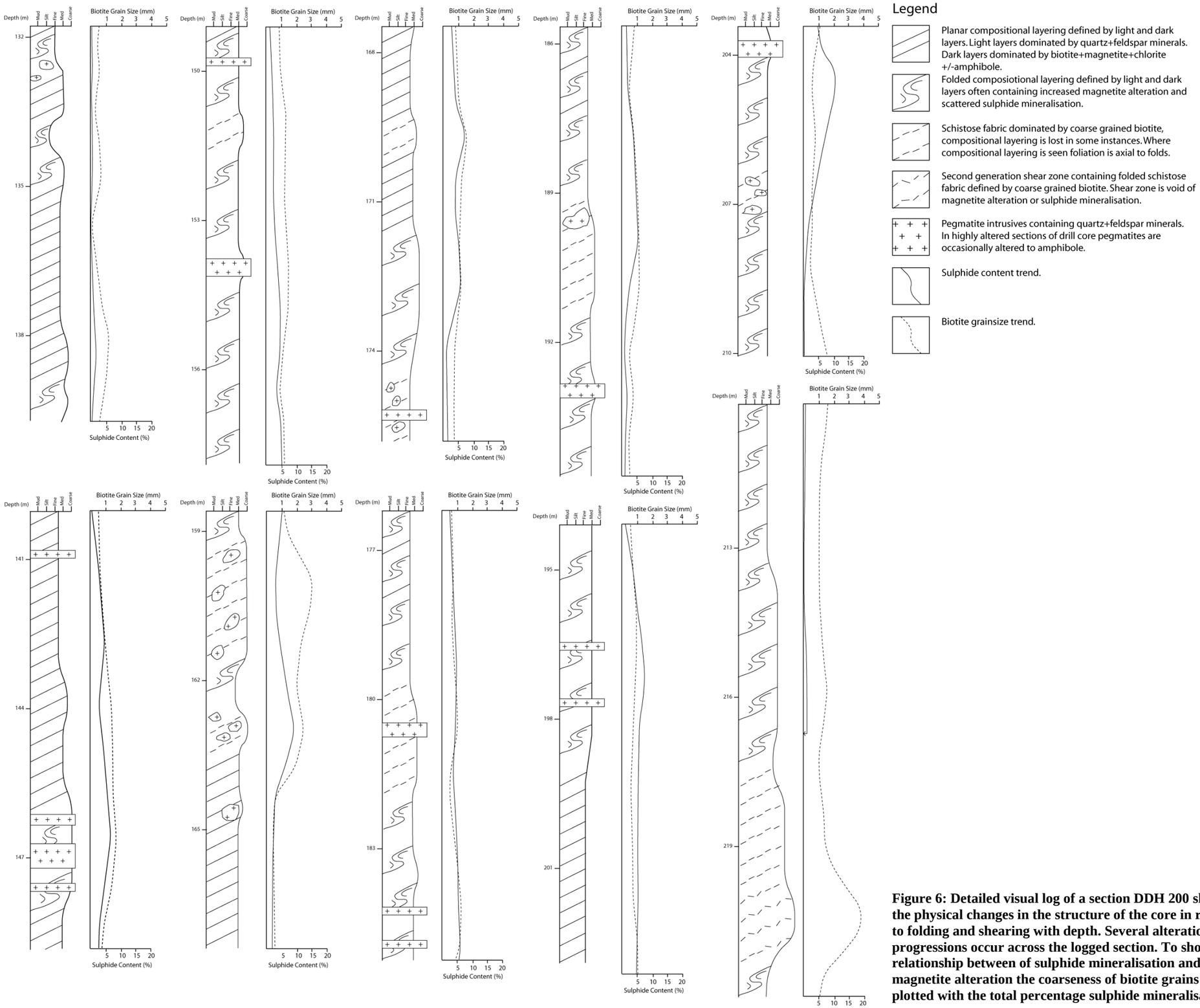

Legend

- Planar compositional layering defined by light and dark layers. Light layers dominated by quartz+feldspar minerals. Dark layers dominated by biotite+magnetite+chlorite +/-amphibole.
- Folded composiotional layering defined by light and dark layers often containing increased magnetite alteration and scattered sulphide mineralisation.
- Schistose fabric dominated by coarse grained biotite, compositional layering is lost in some instances. Where compositional layering is seen foliation is axial to folds.
- Second generation shear zone containing folded schistose fabric defined by coarse grained biotite. Shear zone is void of magnetite alteration or sulphide mineralisation.
- Pegmatite intrusives containing quartz+feldspar minerals. In highly altered sections of drill core pegmatites are occasionally altered to amphibole.
- Sulphide content trend.
- Biotite grainsize trend.

Figure 6: Detailed visual log of a section DDH 200 showing the physical changes in the structure of the core in response to folding and shearing with depth. Several alteration progressions occur across the logged section. To show the relationship between of sulphide mineralisation and biotite-magnetite alteration the coarseness of biotite grains was plotted with the total percentage sulphide mineralisation.

Petrology

Six samples from DDH 114 and eight from DDH 200 were chosen to assess the petrology of unaltered through to altered lithologies. One broad alteration progression was assessed from DDH 114, and two shorter alteration progressions were assessed from DDH 200.

Samples with minor alteration (Figure 7a-c) contain a background matrix of fine grained (<0.3mm) quartz and biotite. The compositional layering observed in hand specimen is defined by bands containing increased abundance of fine-grained (<0.1mm) foliated biotite and coarse (<1mm wide) pyrite and chalcopyrite veins. Scatterings of medium grained chlorite locally overprint earlier biotite mineralisation (Figure 7a). Thin zones of coarse grained (1mm) foliated biotite with sulphides mineralisation along their centre are parallel to foliation (Figure 7b-c).

Moderately altered lithologies are dominated by layers of fine to medium-grained (<0.7mm) biotite, quartz and feldspar (Figure 7d-k) oblique to bedding. An intense foliation defined by medium to coarse grained (<0.7mm) biotite is preserved within the axial plane of micro scale folds that deform the compositional layering (Figure 7d). Minor mineralisation occurs throughout the coarse-grained biotite bands (Figure 7e, h, k) while very little to no mineralisation is preserved in bands containing fine-grained biotite. Thin (~2mm) veins comprised of fine grained quartz and feldspar with minor clinopyroxene, coarse-grained biotite and pyrite are also observed axial planar to micro scale folding (Figure 7f-g). These veins are often cross-cut by bands of coarse biotite (Figure 7f-g, i-j).

Samples containing a high degree of alteration (Figure 8) show variable mineralogy. Highly altered samples are dominated by coarse grained (1-2mm) biotite which has been overprinted by chlorite (Figure 8a-b, d-e). Associated with the coarse-grained biotite, magnetite and hornblende are small (<0.2mm) uraninite grains (Figure 8g, Figure 9). Zoned tourmaline grains which overprint coarse-grained biotite and chlorite alteration are cross cut by fissure like veins of fine grained chlorite (Figure 8a-b). Poikiloblastic hornblende surrounds coarse grained biotite-magnetite and sulphides (Figure 8j-k). Allanite is surrounded by coarse hornblende and is preserved as heavily metamict glassy grains with pyrite and chalcopyrite in the crystal structure (Figure 8o and r). Sulphide mineralisation is associated with two stages of alteration. Firstly it shows a close relationship with coarse grained biotite-magnetite alteration (Figure 8i and l) and secondly forms an overprinting relationship with coarse grained hematite-carbonate alteration (Figure 8p-q and s-u).

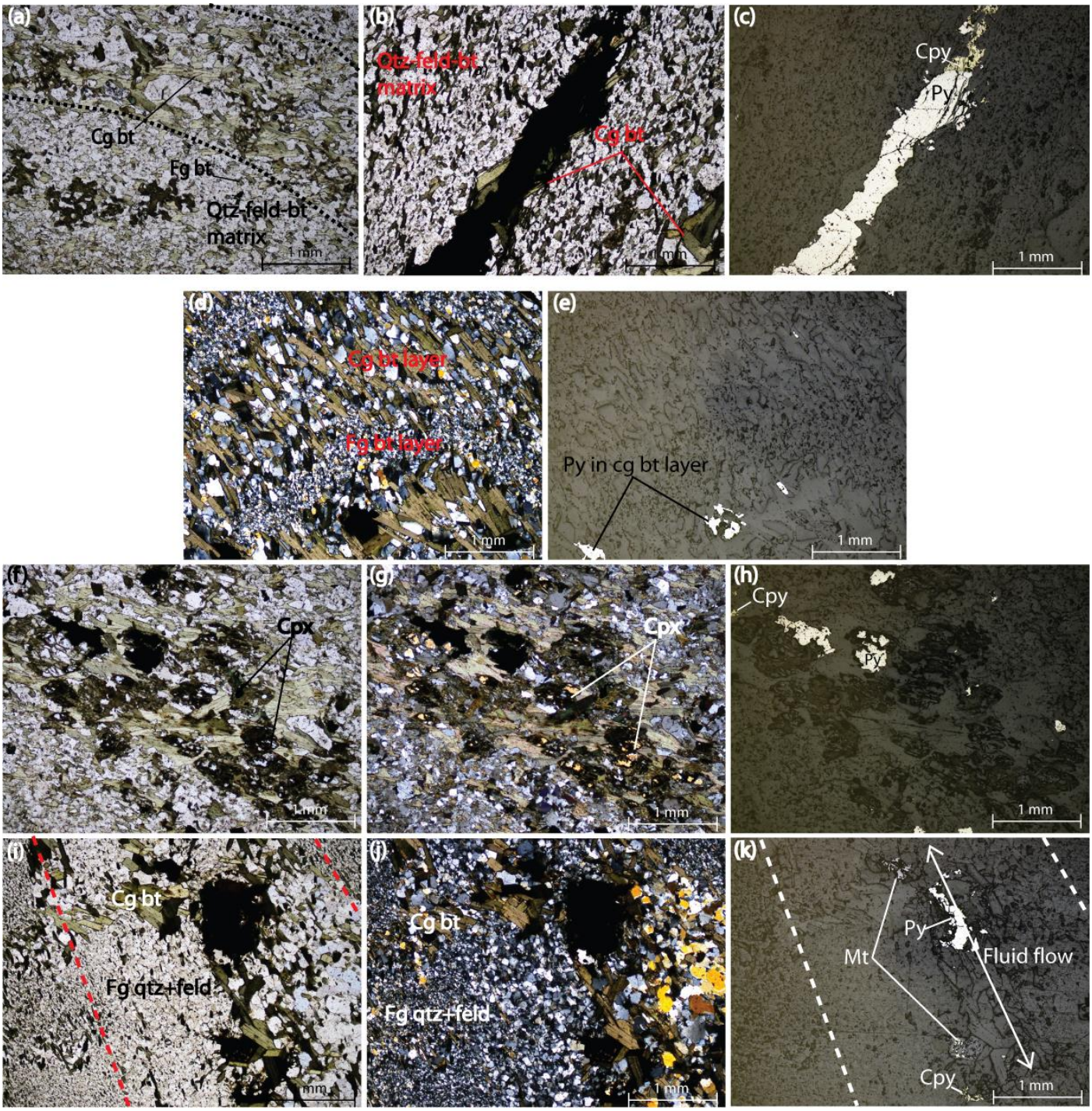

Figure 7: Photomicrographs of unaltered through to altered lithologies. a) unaltered metasediment preserving compositional layering with fine grained matrix of quartz and feldspar (DDH 200, 144.5m); b) and c) unaltered metasediment containing a vein of coarse grained biotite which has been overprinted by pyrite and chalcopyrite mineralisation (DDH 200, 486.1m); d) and e) moderately altered metasediment with clear compositional layering and a distinct separation between fine grained quartz-feldspar-biotite and coarser grained biotite-quartz-feldspar. The compositional layering forms a tight fold with a strong biotite foliation axial to the fold hinge. Small blotches of pyrite mineralisation occur within the coarse grained layer (DDH 200, 158.5m); f) to h) moderately altered metasediment containing orthopyroxene alteration and pyrite-chalcopyrite mineralisation restricted to layers containing coarse grained biotite (DDH 200, 164.3m); i) to k) moderately altered metasediment containing a pegmatite vein which cross cuts compositional layering. Coarse grained biotite and magnetite alteration occurs within the vein indicating that the development of coarse biotite occurred either syn or post-pegmatite veining. Identified on the images by the dashed line are the edges of the pegmatite vein (DDH 200, 158.5m). Abbreviations: Fg - fine grained, cg - coarse grained, qtz - quartz, feld - feldspar, bt - biotite, cpx - clinopyroxene, mt - magnetite, py - pyrite, cpy - chalcopyrite.

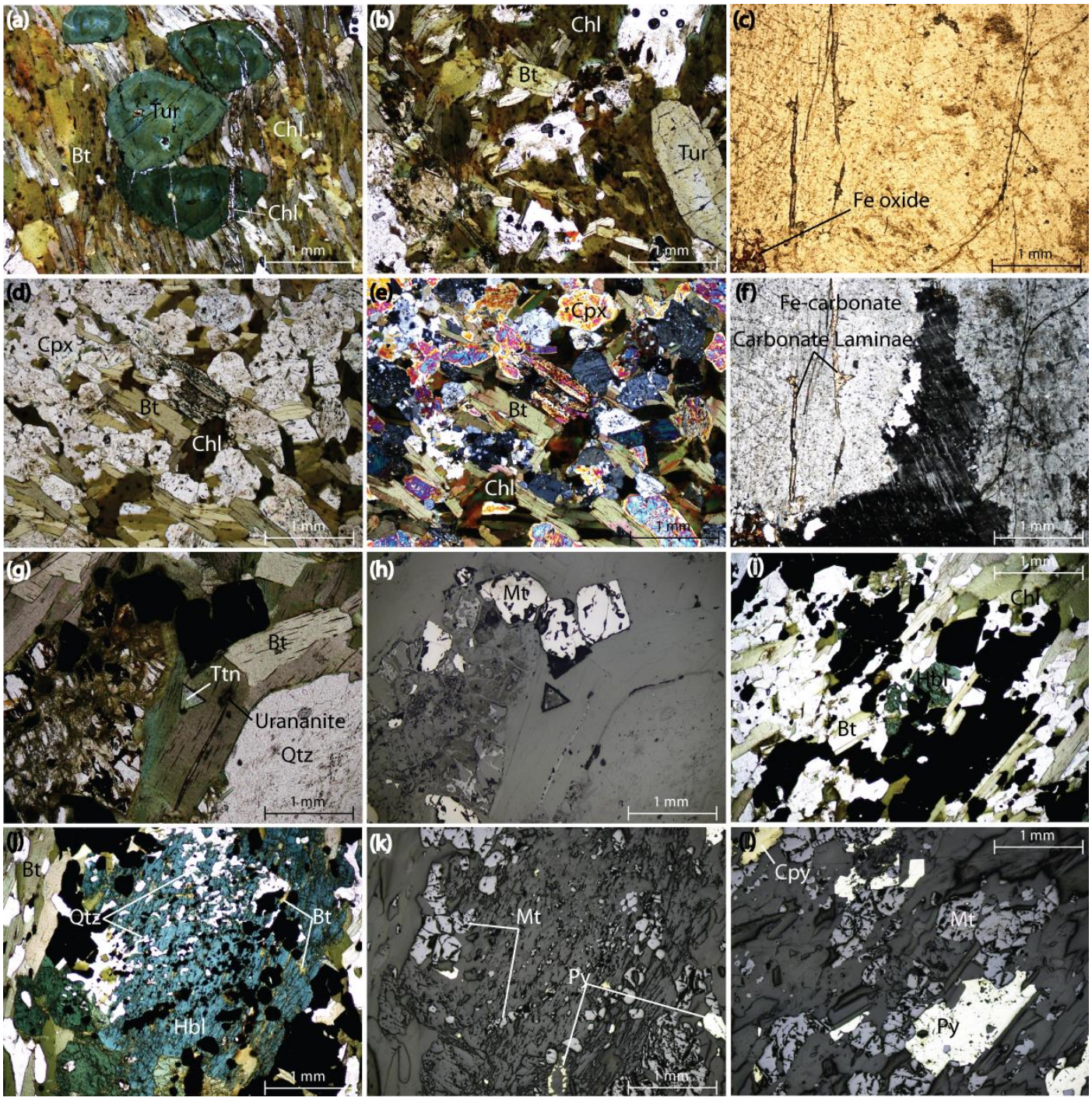

Figure 8: Photomicrographs of highly altered metasediments a) to l) (above) and m) to u) (next page). a) and b) coarse grained biotite which has been altered to chlorite. Large 1 - 1.5 mm Tourmaline grains overgrow coarse grained biotite and are in turn overprinted by fine grained chlorite which forms fissure like veins through both the biotite foliation and tourmaline grains (DDH 200, 146.9m); d) and e) coarse grained biotite which has undergone clinopyroxene alteration (DDH 200, 147.5m); c) and f) two different generations of carbonate with small amounts of an Fe-oxide (most likely hematite) forming at the reaction margin. Additionally, the large grain which is light grey in cross polars (f) has formed secondary carbonate laminae indicating its instability some stage after formation (DDH 200, 159.1m); g) and h) heavy magnetite alteration of an Fe-carbonate. At the centre of the stage are titanate and uraninite grains encased in coarse grained biotite. The biotite foliation post-dates coarse grained quartz but pre-dates the magnetite alteration (DDH 200, 159.1m); i) and l) coarse grained biotite-magnetite alteration with associated sulphide mineralisation (DDH 114, 160m); j) to k) poikiloblastic hornblende surrounding quartz, biotite, magnetite and pyrite (DDH 114, 160m); m) and n) thick (2 mm) veins of fine grained chlorite surrounded by a matrix of fine grained quartz and biotite. Associated with the chlorite vein are blobs of pyrite and chalcopyrite mineralisation (DDH 200, 146.9m); o) and r) large heavily metamict allanite grain surrounded by blue green hornblende and a grain of high bioinfringence orthopyroxene. Late stage pyrite and chalcopyrite mineralisation occurs within cracks and around the edges of the allanite grain (DDH 114 194.2m); p) and q) coarse chlorite and biotite grains within altered carbonate and vein like pyrite-chalcopyrite mineralisation (DDH 200, 162.7); s) to u) coarse grained quartz and biotite surrounding a large carbonate containing extensive hematitic alteration. Within cracks and extensively altered sections of the carbonate are large amounts of pyrite and chalcopyrite mineralisation (DDH 200, 162.7). Abbreviations: fg - fine grained, cg - coarse grained, qtz - quartz, feld - feldspar, bt - biotite, hbl - hornblende, tur - tourmaline cpx - clinopyroxene, aln - allanite, mt - magnetite, py - pyrite, cpy - chalcopyrite.

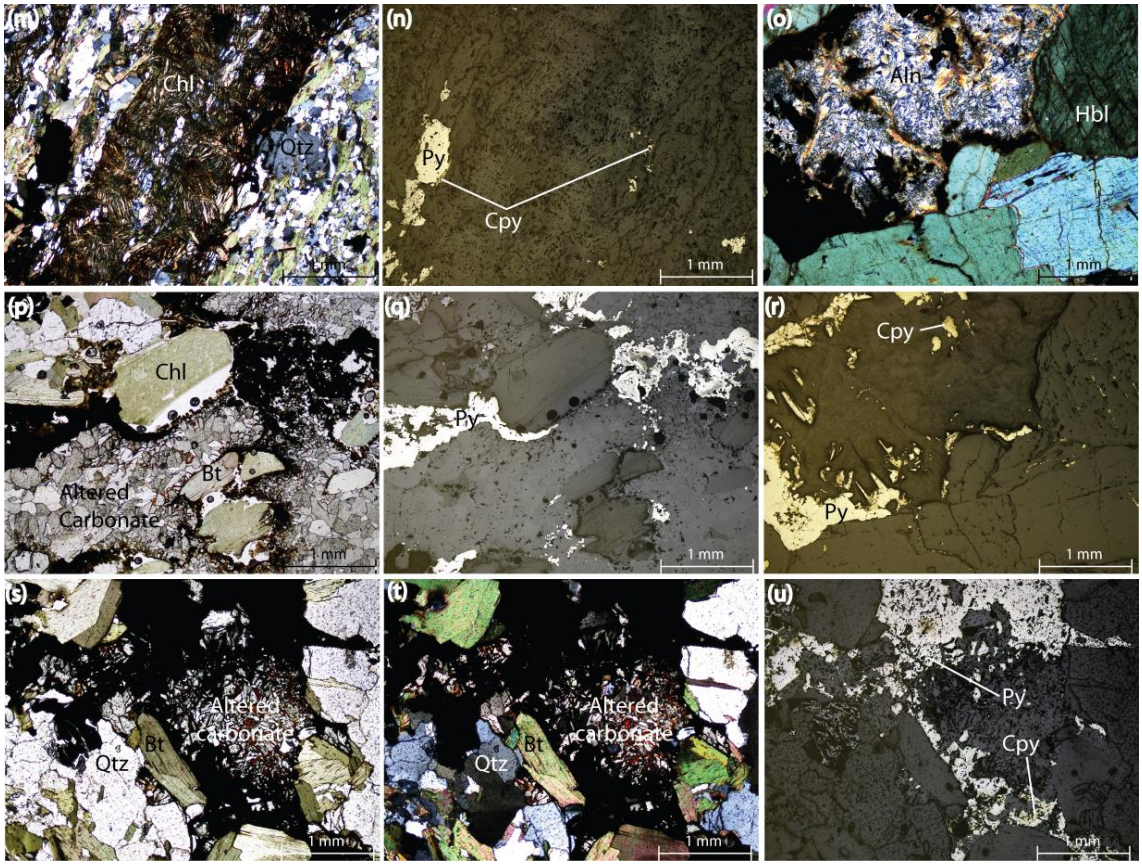

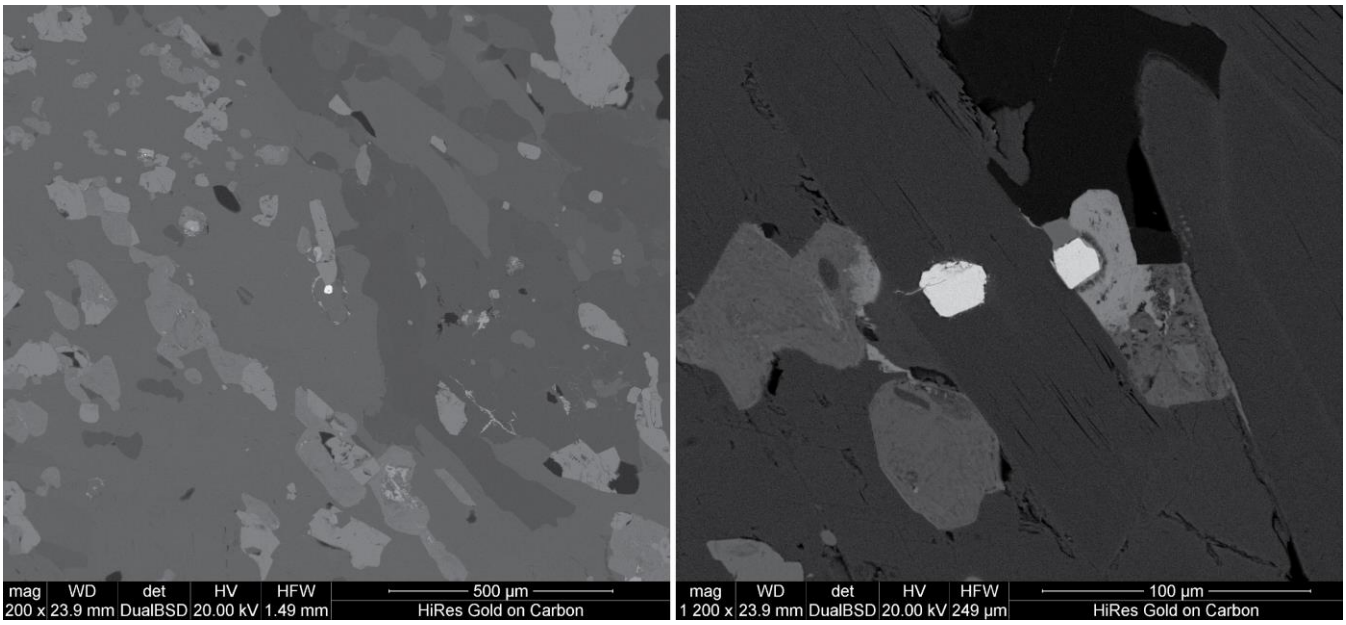

Figure 9: Backscatter Electron Microscope images of uraninite grains; (left) Uraninite grain contained within poikiloblastic hornblende with direct association with magnetite. Large halo extends well beyond the grain boundaries; (right) two neighbouring uraninite grains, one contained within coarse-grained biotite and the other with magnetite (from left to right).

Whole Rock Geochemistry

One broad zone of progressive alteration from the Doora Member was selected from DDH114 as the level of alteration did not fluctuate but increased steadily over the logged section. DDH200 showed a higher degree of variation in the amount of alteration occurring than DDH114 allowing two separate alteration progressions of the Doora Member to be selected from DDH 200.

Samples from unaltered sections of the alteration progressions contain relatively high concentrations of Al2O3, K2O and U at 15.59%, 8.20% and 36.88 ppb respectively (Table 1). Relatively low S and Fe_2O_3 concentrations which ranged from 2386-5650ppm and 8.11-8.16% corresponded with low concentrations of Cu and Au ranging between 205-334 ppm and 1-4 ppb respectively (Figure 10d, h-j). Low concentrations were recorded for Ce, La and Y at less than 55.6ppm, 30.4ppm, and 22.6ppm.

Moderately altered samples contained elevated concentrations of Al_2O_3 and K_2O at 11.47-14.11% and 3.11-8.31%. Na_2O is elevated above 1.90% in samples which contained a moderate or lower degree of alteration (Table 1). S and Fe_2O_3 values increase to moderate levels ranging from 3919-8620 ppm and 11.37-20.92% while containing relatively low concentrations of Cu (238-384 ppm) and $\leq$2 ppb of Au (Figure 10d, h-i). The concentrations of light rare earth elements Ce and La as well as Y show a concordant relationship (Figure 10l-n) increasing moderately from less altered values up to 3101.6 ppm, 2028.2 ppm and 106.1 ppm.

In highly altered samples Al_2O_3, SiO_2 and K_2O show a trend of decreasing concentration with increasing alteration (Figure 10a-c). An opposite trend is observed for Fe_2O_3, Co and MgO which show increases in concentrations up to 47.78%, 540.9ppm and 7.06% respectively (Figure 10e-f). Both peak and very low concentrations for Cu, Au and S ranging from 52-9983 ppm Cu, undetectable to 115 ppb Au and below detection limit to 77532 ppm S are observed (Figure 10d, h-k). Comparable highs and lows were observed in MgO and U values at 6.79 to 2.87 % MgO and 167.80 to 8.70 ppm U respectively (Figure 10f-g). Fe_2O_3 concentrations follow a consistent elevated trend over the highly altered samples which coincided with elevated measurements for Co and LREE's Ce and La and Y up to 3436.2ppm, 2199.7ppm and 118.4ppm respectively (Figure 10l-n).

Table 1: Representative geochemical data from drill holes DDH 114 and DDH 200. Samples for geochemistry were taken across three alteration zones with one broad zone selected from DDH 114 and two narrow zones selected from DDH 200. An X value is used where element concentrations were below detection limit.

Sample no.	Drill Hole	Alteration	K2O (%)	Fe2O3 (%)	Cu (ppm)	Au (ppb)	Al2O3 (%)	SiO2 (%)	Na2O (%)
Detection Limit			0.01	0.01	1	1	0.01	0.01	0.01
2129382	DDH 200	Low	8.2	8.11	334	4	15.59	59.88	2.17
2129385	DDH 200	Low	6.91	8.16	205	1	14.8	59.43	1.9
2131460	DDH 114	Med	3.11	19.73	298	2	12.91	54.47	3.6
2129386	DDH 200	Med	8.31	11.37	238	2	14.11	58.21	1.95
2129389	DDH 200	Med	5.06	12.98	266	X	13.78	56.44	3.2
2131461	DDH 114	High	6.87	20.92	384	X	11.47	47.15	0.58
2131463	DDH 114	High	3.88	29.43	2759	9	8.01	41.11	0.57
2129383	DDH 200	High	7.71	11.47	9983	115	13.46	58.15	0.69
2129384	DDH 200	High	6.41	8.54	52	2	16.4	56.11	2.32
2129387	DDH 200	High	7.63	23.34	127	X	12.51	43.51	0.32
2129388	DDH 200	High	3.13	47.78	2444	6	4.87	28.05	0.15
Sample no.	Drill Hole	Alteration	S (ppm)	MgO (%)	Ce (ppm)	La (ppm)	Co (ppm)	U (ppm)	Y (ppm)
Detection Limit			50	0.01	0.5	0.2	0.1	0.05	0.5
2129382	DDH 200	Low	5650	3.11	55.6	30.4	34	36.88	22.6
2129385	DDH 200	Low	2386	3.44	29.9	18.6	25.4	16.35	22.3
2131460	DDH 114	Med	4924	3.27	12.8	6.8	56.5	8.8	19.2
2129386	DDH 200	Med	3919	4.22	324.2	200.4	34.7	8.5	21.7
2129389	DDH 200	Med	8620	4.36	212.6	132.5	47.6	5.49	22.8
2131461	DDH 114	High	7060	7.06	3101.6	2028.2	71.4	27.1	106.1
2131463	DDH 114	High	23979	6.79	1567.8	1028.9	113.8	167.8	89
2129383	DDH 200	High	15155	4.12	187.4	114.8	14	21.62	62.7
2129384	DDH 200	High	X	3.56	121.2	67.9	17.5	25.1	30.6
2129387	DDH 200	High	2630	7.56	3436.2	2199.7	45.8	21.78	118.4
2129388	DDH 200	High	77532	2.87	646.3	382.1	540.9	8.7	83.8

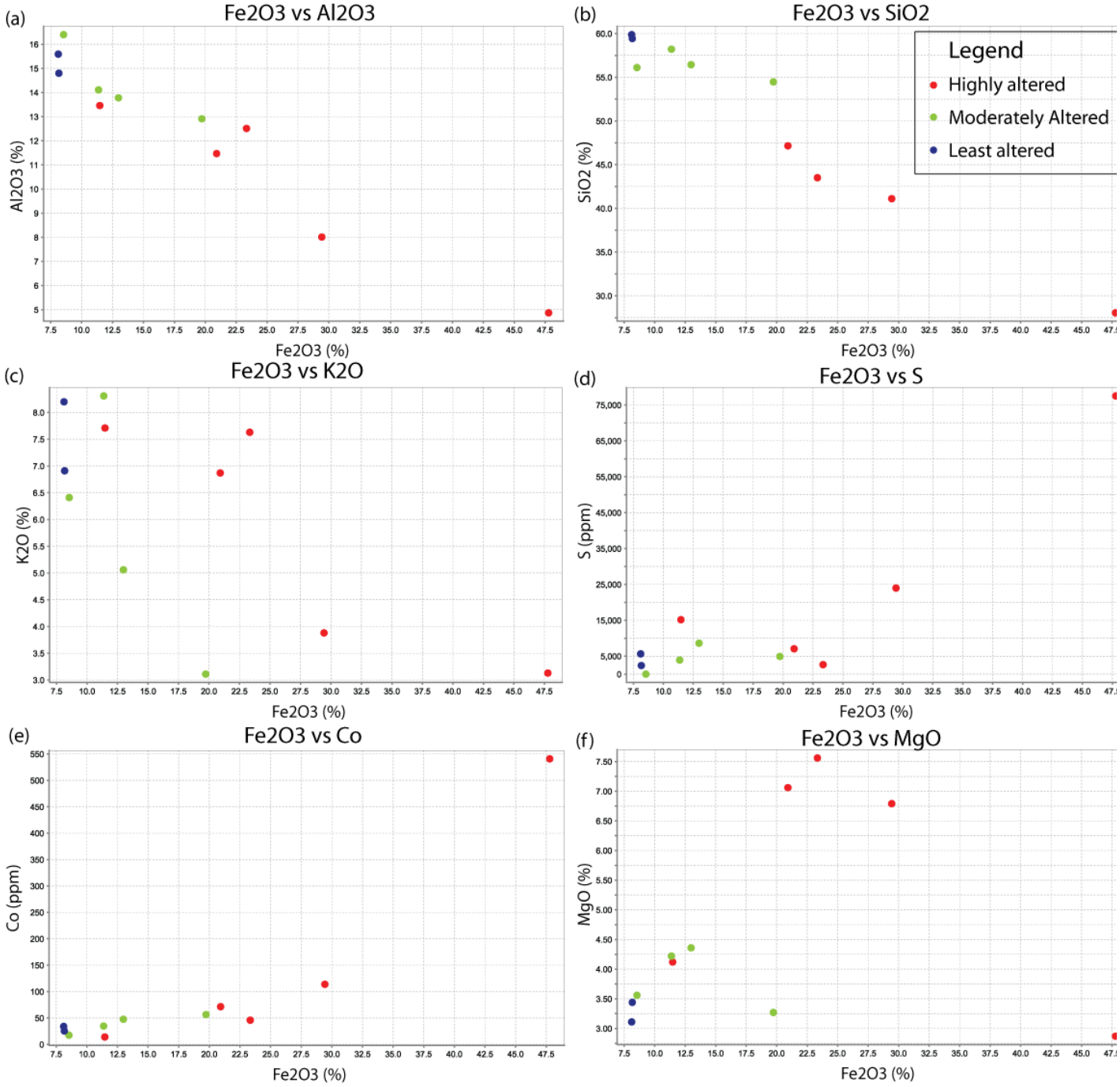

Figure 10: Element ratio plots of geochemistry data from drill holes DDH 114 and DDH 200. (a) to (i) show a range of elements plotted against Fe_2O_3. Fe_2O_3 is used as a measure of the intensity of alteration ranging from relatively unaltered samples with low concentrations of Fe_2O_3 up to highly altered samples containing high concentrations of Fe_2O_3; j) and k) proportional relationship between Cu, Au and S with a large spike in Cu and Au values occurring in sample 2129383; l) to n) show a linear relationship between LREE's Ce and La and a roughly proportional relationship of both of these with Y.

(g)

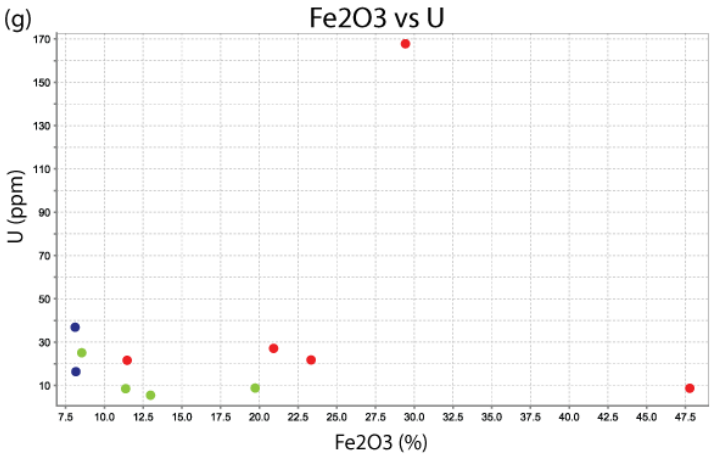
Fe2O3 vs U
U (ppm)
Fe2O3 (%)

(h)

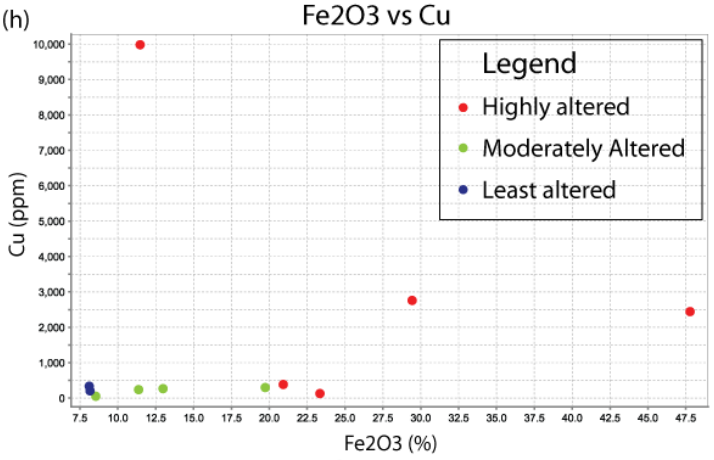
Fe2O3 vs Cu
Legend
Highly altered
Moderately Altered
Least altered
Cu (ppm)
Fe2O3 (%)

(i)

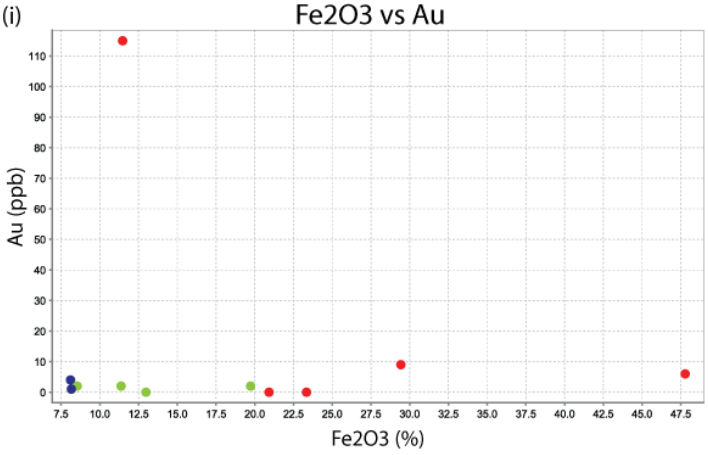
Fe2O3 vs Au
Au (ppb)
Fe2O3 (%)

(j)

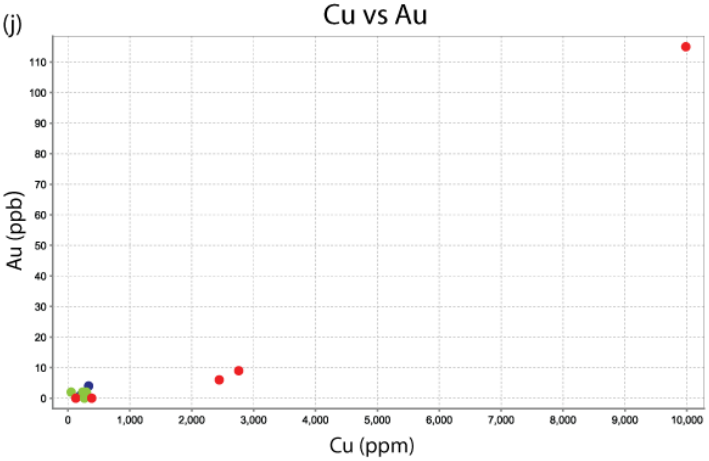
Cu vs Au
Au (ppb)
Cu (ppm)

(k)

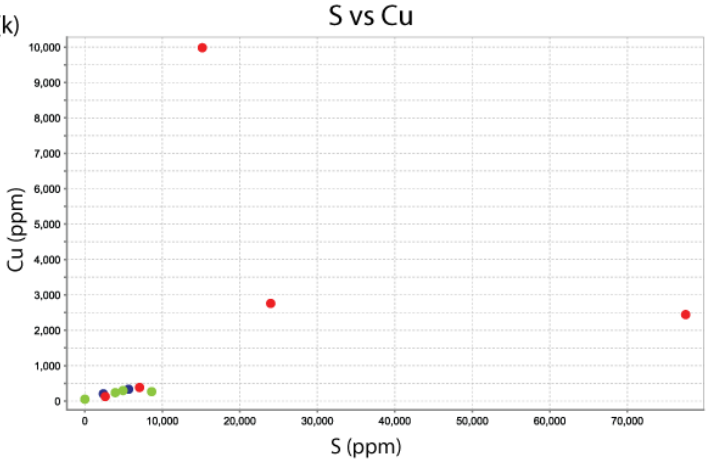
S vs Cu
Cu (ppm)
S (ppm)

(l)

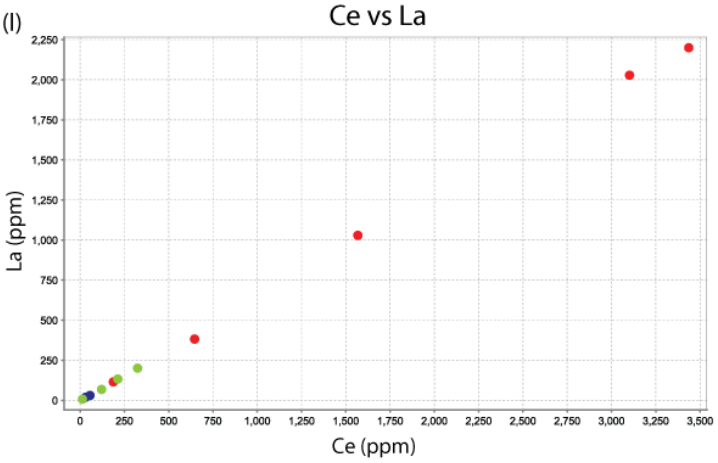
Ce vs La
La (ppm)
Ce (ppm)

(m)

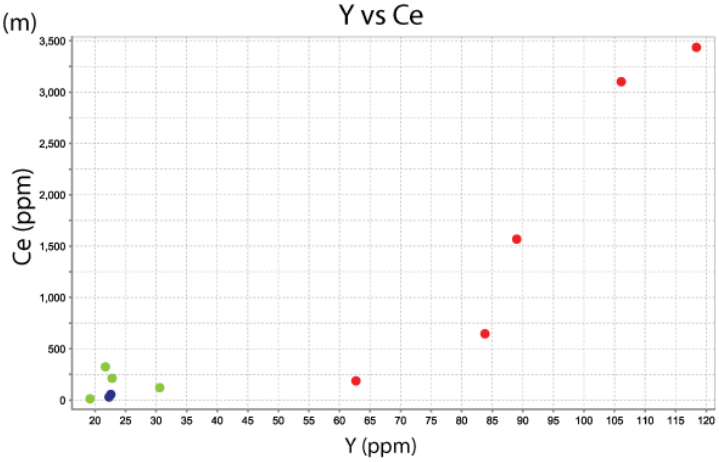
Y vs Ce
Ce (ppm)
Y (ppm)

(n)

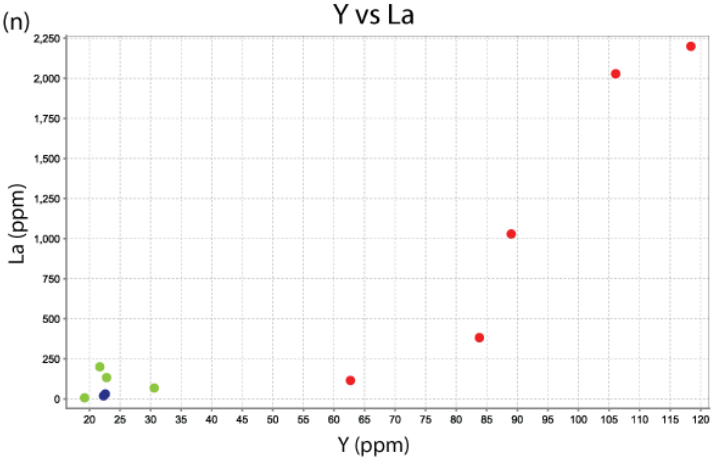
Y vs La
La (ppm)
Y (ppm)

ZIRCON U-PB GEOCHRONOLOGY

Moonta Porphyry

SAMPLE DESCRIPTION

The Moonta Porphyry is a reddish pink porphyritic rhyodacite containing large phenocrysts which have been extensively altered from plagioclase/quartz to K-feldspar. The phenocrysts sit in a fine grained groundmass of quarts, feldspar and biotite. The Moonta Porphyry interfingers with the Doora Member metasediments of the Wallaroo Group indicating a coeval relationship (Conor 1995, Conor 2002, Cowley et al. 2003).

ZIRCON CHARACTERISTICS

Zircon grains from the Moonta Porphyry are sub-angular ranging between 80 µm to over 200 µm in length (Figure 11a). CL images of the internal structure of the grains showed fine zonation with most grains containing small opaque inclusions within the zonation structures.

SAMPLE DATA

Eighty-eight spots were analysed from seventy- eight zircon grains. One grain returned a concordancy value of 2088800% and a Pb207/Pb206 value of 0.1 Ma and was recorded as a null value. Overall the data ranged from 38% to 101% concordancy with fifty-nine data points falling within the 90-110% concordancy range selected for analysis (Table 2). The weighted mean was calculated using data which was within 10% of concordancy. The concordia intercept calculation utilised available analyses to generate a fairly accurate linear trend through the data points (Figure 11). The weighted

mean resulted in an age of 1752 ± 6 Ma (MSWD = 0.77) while the Concordia intercept yielded an upper intercept value of 1757 ± 7 Ma (MSWD = 1.9).

GEOCHRONOLOGICAL INTERPRETATION

The weighted mean resulted in a Pb207/Pb206 age of 1752 ± 6 Ma constraining the age of igneous zircon crystallisation within the sample.

Table *2*: Summary of LA-ICPMS U-Pb zircon data from the Moonta Porphyry sample selected from the Poona Cu-Au Mine.

	Radiogenic Ratios						Age (Ma)						
Grain Spot	Pb206/U238	±	Pb207/U235	±	Pb207/Pb206	±	Pb206/U238	±	Pb207/U235	±	Pb207/Pb206	±	% Disc
1.1	0.3120	0.0042	4.6306	0.0735	0.1076	0.0015	1751	21	1755	13	1760	25	0.5
3.2	0.2977	0.0040	4.6644	0.0695	0.1137	0.0014	1680	20	1761	12	1859	22	9.6
4.1	0.3009	0.0041	4.5079	0.0712	0.1087	0.0015	1696	20	1732	13	1777	25	4.6
5.1	0.3041	0.0040	4.4616	0.0641	0.1064	0.0013	1712	20	1724	12	1739	22	1.5
7.1	0.3097	0.0041	4.5566	0.0707	0.1067	0.0014	1739	20	1741	13	1744	24	0.2
7.2	0.3095	0.0041	4.5763	0.0667	0.1073	0.0013	1738	20	1745	12	1753	22	0.9
9.1	0.3089	0.0041	4.5245	0.0635	0.1062	0.0012	1736	20	1736	12	1736	21	0.0
10.1	0.2991	0.0040	4.3521	0.0661	0.1055	0.0014	1687	20	1703	13	1724	24	2.1
12.1	0.3073	0.0041	4.6143	0.0700	0.1089	0.0014	1728	20	1752	13	1781	23	3.0
13.1	0.2986	0.0040	4.4347	0.0660	0.1077	0.0013	1684	20	1719	12	1761	23	4.4
15.1	0.2843	0.0038	4.1690	0.0613	0.1064	0.0013	1613	19	1668	12	1738	22	7.2
16.1	0.2998	0.0040	4.4426	0.0644	0.1075	0.0013	1690	20	1720	12	1757	22	3.8
17.1	0.2918	0.0039	4.2387	0.0603	0.1054	0.0012	1650	19	1682	12	1721	21	4.1
18.1	0.3154	0.0042	4.6864	0.0715	0.1078	0.0014	1767	21	1765	13	1762	23	-0.3
18.2	0.2813	0.0038	4.1625	0.0652	0.1073	0.0015	1598	19	1667	13	1755	24	8.9
19.1	0.3018	0.0041	4.4603	0.0706	0.1072	0.0015	1700	20	1724	13	1752	25	3.0
19.2	0.2965	0.0040	4.4106	0.0639	0.1079	0.0013	1674	20	1714	12	1764	22	5.1
20.1	0.3065	0.0041	4.4660	0.0663	0.1057	0.0013	1724	20	1725	12	1726	23	0.1
21.1	0.3042	0.0041	4.5103	0.0677	0.1075	0.0014	1712	20	1733	12	1758	23	2.6
22.1	0.3071	0.0041	4.4834	0.0685	0.1059	0.0014	1727	20	1728	13	1730	24	0.2
24.1	0.2816	0.0037	4.0918	0.0584	0.1054	0.0012	1600	19	1653	12	1721	21	7.1
27.1	0.3074	0.0041	4.5164	0.0702	0.1066	0.0014	1728	20	1734	13	1742	24	0.8
31.1	0.2846	0.0039	4.2103	0.0671	0.1073	0.0015	1614	19	1676	13	1754	25	8.0
32.1	0.3003	0.0040	4.3735	0.0676	0.1057	0.0014	1693	20	1707	13	1726	24	1.9
34.1	0.2876	0.0038	4.2347	0.0619	0.1068	0.0013	1630	19	1681	12	1746	22	6.6
35.1	0.2858	0.0038	4.1813	0.0588	0.1061	0.0012	1621	19	1670	12	1734	21	6.5
36.1	0.3028	0.0041	4.4938	0.0697	0.1077	0.0014	1705	20	1730	13	1760	24	3.1

39.1	0.3028	0.0040	4.4572	0.0654	0.1068	0.0013	1705	20	1723	12	1745	22	2.3
40.1	0.3095	0.0042	4.5405	0.0704	0.1064	0.0014	1738	21	1738	13	1739	24	0.1
41.1	0.2971	0.0040	4.3152	0.0689	0.1054	0.0015	1677	20	1696	13	1721	25	2.6
42.1	0.3021	0.0042	4.4402	0.0803	0.1066	0.0017	1702	21	1720	15	1742	29	2.3
44.1	0.3022	0.0041	4.4142	0.0699	0.1060	0.0014	1702	20	1715	13	1731	25	1.7
45.1	0.2978	0.0040	4.5213	0.0722	0.1101	0.0015	1680	20	1735	13	1802	25	6.7
46.1	0.2942	0.0040	4.3837	0.0692	0.1081	0.0015	1663	20	1709	13	1767	25	5.9
47.1	0.2919	0.0039	4.2806	0.0643	0.1064	0.0013	1651	20	1690	12	1738	23	5.0
48.1	0.2797	0.0037	4.0772	0.0601	0.1057	0.0013	1590	19	1650	12	1727	22	7.9
49.1	0.3073	0.0042	4.5553	0.0725	0.1075	0.0015	1727	20	1741	13	1758	25	1.7
50.1	0.3123	0.0042	4.5752	0.0678	0.1063	0.0013	1752	21	1745	12	1736	22	-0.9
52.1	0.2964	0.0040	4.3670	0.0703	0.1069	0.0015	1673	20	1706	13	1747	25	4.2
53.1	0.2990	0.0040	4.4254	0.0660	0.1074	0.0013	1686	20	1717	12	1755	23	3.9
55.1	0.2867	0.0039	4.2932	0.0679	0.1086	0.0015	1625	19	1692	13	1776	25	8.5
56.1	0.3056	0.0041	4.5423	0.0702	0.1078	0.0014	1719	20	1739	13	1763	24	2.5
59.1	0.3175	0.0043	4.7871	0.0736	0.1094	0.0014	1777	21	1783	13	1789	24	0.7
60.1	0.3067	0.0041	4.5859	0.0703	0.1085	0.0014	1724	20	1747	13	1774	24	2.8
60.2	0.3111	0.0042	4.5626	0.0669	0.1064	0.0013	1746	20	1743	12	1738	22	-0.5
61.1	0.3000	0.0041	4.4658	0.0693	0.1080	0.0014	1691	20	1725	13	1766	24	4.2
62.1	0.3082	0.0042	4.5299	0.0750	0.1066	0.0016	1732	21	1737	14	1742	26	0.6
62.3	0.3091	0.0042	4.5625	0.0706	0.1071	0.0014	1736	20	1743	13	1750	24	0.8
63.1	0.3085	0.0042	4.5282	0.0744	0.1065	0.0015	1733	21	1736	14	1740	26	0.4
65.1	0.3112	0.0042	4.6169	0.0727	0.1076	0.0015	1746	21	1752	13	1760	24	0.7
66.1	0.3039	0.0043	4.6586	0.0900	0.1112	0.0020	1711	21	1760	16	1819	32	5.9
67.1	0.3117	0.0042	4.7205	0.0774	0.1099	0.0016	1749	21	1771	14	1797	26	2.7
68.1	0.2943	0.0040	4.4852	0.0730	0.1105	0.0016	1663	20	1728	14	1808	25	8.0
69.1	0.3097	0.0042	4.6217	0.0753	0.1082	0.0015	1739	21	1753	14	1770	26	1.7
69.2	0.2954	0.0040	4.3664	0.0748	0.1072	0.0016	1669	20	1706	14	1753	27	4.8
70.1	0.2955	0.0040	4.3425	0.0676	0.1066	0.0014	1669	20	1702	13	1742	24	4.2
71.2	0.2895	0.0039	4.3024	0.0676	0.1078	0.0015	1639	20	1694	13	1763	24	7.0
72.1	0.3002	0.0041	4.4799	0.0699	0.1083	0.0014	1692	20	1727	13	1770	24	4.4
75.1	0.3066	0.0041	4.5334	0.0835	0.1073	0.0018	1724	20	1737	15	1754	30	1.7

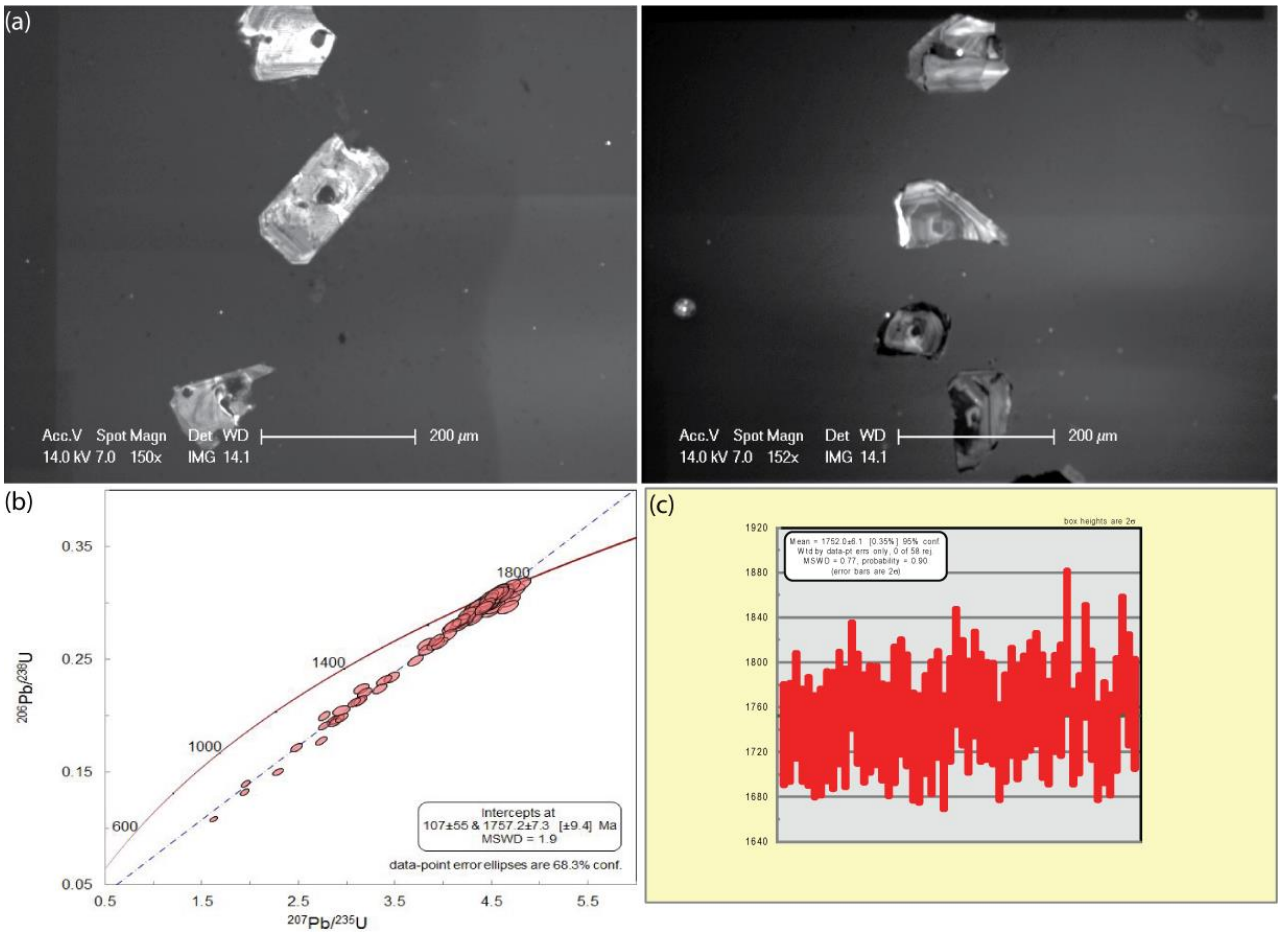

Figure 11: a) CL images of representative zircon grains from the Moonta Porphyry sample recovered from the Poona Cu-Au Mine; b) concordia plot for the Moonta Porphyry sample recovered from the Poona Cu-Au Mine. Insert bottom right shows the calculated concordia intercept yielding an age of 1757 ± 7.3 Ma; c) weighted Mean of the Moonta Porphyry sample collected from Poona Cu-Au Mine. Data used to calculate the weighted mean is within ten percent of concordancy.

Oorlano Metasomatite (Harlequin Stone)

SAMPLE DESCRIPTION

The sample of the Harlequin Stone obtained from the Oorallaw Quarry is a highly altered metasomatic rock containing alkali-feldspar, diopside, amphibole, epidote ± magnetite and occurs in the aureole of the Tickera and Arthurton Granite complex. The lithological precursor is unknown due to the extreme amount of alteration which has occurred within the rock, but may have been a scapolite-rich metasediment derived from calcareous marl.

ZIRCON CHARACTERISTICS

Zircon grains from the Harlequin Stone range from sub to anhedral and vary greatly in size and condition. While some grains are well zoned and maintain good internal structure others are extensively cracked with large opaque inclusions. Some zircon grains are completely metamict with a complete loss of any dateable zonation structures. Representative images are shown in (Figure 12a).

SAMPLE DATA

One hundred and fifty spots from one hundred and thirty-nine zircon grains were chosen for laser ablation. Zircon grains within 10% concordance were selected for analysis. The probability density plot yielded a main peak age at approximately 1854 Ma. Two minor peaks occurred at 2057 Ma and 2446 Ma (Figure 12b). A minimum age of 1708 ±26 Ma was recorded (Table 3).

GEOCHRONOLOGICAL INTERPRETATION

The probability density plot yielded a range of Pb^{207}/Pb^{206} ages with a main peak age at approximately 1870 Ma. Secondary peaks recorded at approximately 2120 Ma with two minor peaks occurring at 2550 Ma and 2660 Ma (Figure 12b).

Table 3: Summary of the LA-ICPMS U-Pb results from the Oorlano Metasomatite sample selected from the Oorallaw Quarry.

	Radiogenic Ratios						Age (Ma)						
Grain Spot	Pb206/U238	±	Pb207/U235	±	Pb207/Pb206	±	Pb206/U238	±	Pb207/U235	±	Pb207/Pb206	±	% Disc
1.1	0.3190	0.0048	4.7951	0.0741	0.1090	0.0012	1785	23	1784	13	1783	20	-0.1
11.1	0.3507	0.0053	6.1554	0.0930	0.1273	0.0014	1938	25	1998	13	2062	19	6
19.1	0.3048	0.0047	4.3978	0.0796	0.1047	0.0016	1715	23	1712	15	1708	27	-0.4
25.1	0.3149	0.0047	5.0770	0.0789	0.1169	0.0013	1765	23	1832	13	1910	20	7.6
31.1	0.3109	0.0047	4.7379	0.0732	0.1105	0.0012	1745	23	1774	13	1808	20	3.5
34.1	0.3270	0.0049	5.1504	0.0791	0.1143	0.0012	1824	24	1845	13	1868	19	2.4

35.1	0.3318	0.0050	5.1944	0.0791	0.1136	0.0012	1847	24	1852	13	1857	19	0.5
36.1	0.3171	0.0048	5.1376	0.0801	0.1175	0.0013	1775	23	1842	13	1919	20	7.5
38.1	0.3013	0.0045	4.5796	0.0709	0.1103	0.0012	1698	22	1746	13	1804	20	5.9
40.1	0.3196	0.0049	5.0034	0.0823	0.1136	0.0014	1788	24	1820	14	1857	22	3.8
41.1	0.3150	0.0047	5.0402	0.0789	0.1161	0.0013	1765	23	1826	13	1897	20	6.9
42.1	0.3232	0.0048	5.0402	0.0768	0.1131	0.0012	1805	24	1826	13	1850	19	2.4
48.1	0.3121	0.0047	4.9257	0.0792	0.1145	0.0014	1751	23	1807	14	1872	21	6.4
48.2	0.3235	0.0049	5.1206	0.0826	0.1148	0.0014	1807	24	1840	14	1877	21	3.8
49.1	0.2964	0.0045	4.6130	0.0715	0.1129	0.0013	1673	22	1752	13	1847	20	9.4
55.1	0.3229	0.0049	5.0693	0.0787	0.1139	0.0013	1804	24	1831	13	1862	20	3.1
55.2	0.3303	0.0050	5.1830	0.0811	0.1138	0.0013	1840	24	1850	13	1861	20	1.1
58.1	0.3018	0.0045	4.5650	0.0715	0.1097	0.0012	1700	22	1743	13	1795	20	5.3
63.1	0.3152	0.0048	5.0295	0.0788	0.1157	0.0013	1766	23	1824	13	1891	20	6.6
69.1	0.2982	0.0045	4.5856	0.0707	0.1115	0.0012	1683	22	1747	13	1825	20	7.8
78.1	0.3061	0.0046	4.6838	0.0732	0.1110	0.0012	1721	23	1764	13	1816	20	5.2
81.1	0.3175	0.0048	5.1315	0.0815	0.1172	0.0014	1778	23	1841	13	1914	21	7.1
88.1	0.3086	0.0047	4.7973	0.0749	0.1128	0.0013	1734	23	1784	13	1844	20	6
90.1	0.2948	0.0045	4.4681	0.0742	0.1100	0.0014	1665	22	1725	14	1799	23	7.4
91.1	0.2989	0.0045	4.4808	0.0734	0.1087	0.0013	1686	22	1727	14	1778	22	5.2
98.1	0.3333	0.0050	5.6587	0.0893	0.1232	0.0014	1854	24	1925	14	2003	20	7.4
99.1	0.3106	0.0047	4.8748	0.0772	0.1139	0.0013	1744	23	1798	13	1862	20	6.4
108.1	0.3040	0.0046	4.8230	0.0774	0.1151	0.0013	1711	23	1789	14	1881	21	9.1
117.1	0.3331	0.0051	5.4074	0.0904	0.1178	0.0015	1854	25	1886	14	1922	22	3.6
121.1	0.3130	0.0048	4.8695	0.0813	0.1129	0.0014	1755	23	1797	14	1846	23	4.9
121.2	0.3154	0.0048	4.8866	0.0819	0.1124	0.0014	1767	24	1800	14	1839	23	3.9
125.1	0.4286	0.0065	9.3868	0.1493	0.1589	0.0018	2299	29	2377	15	2444	19	5.9
126.1	0.3084	0.0047	4.7211	0.0812	0.1110	0.0015	1733	23	1771	14	1816	24	4.6
130.1	0.3170	0.0048	5.0382	0.0812	0.1153	0.0014	1775	23	1826	14	1885	21	5.8
133.1	0.3076	0.0047	4.7128	0.0800	0.1111	0.0014	1729	23	1770	14	1818	23	4.9
139.1	0.3115	0.0047	4.7813	0.0788	0.1114	0.0014	1748	23	1782	14	1822	22	4

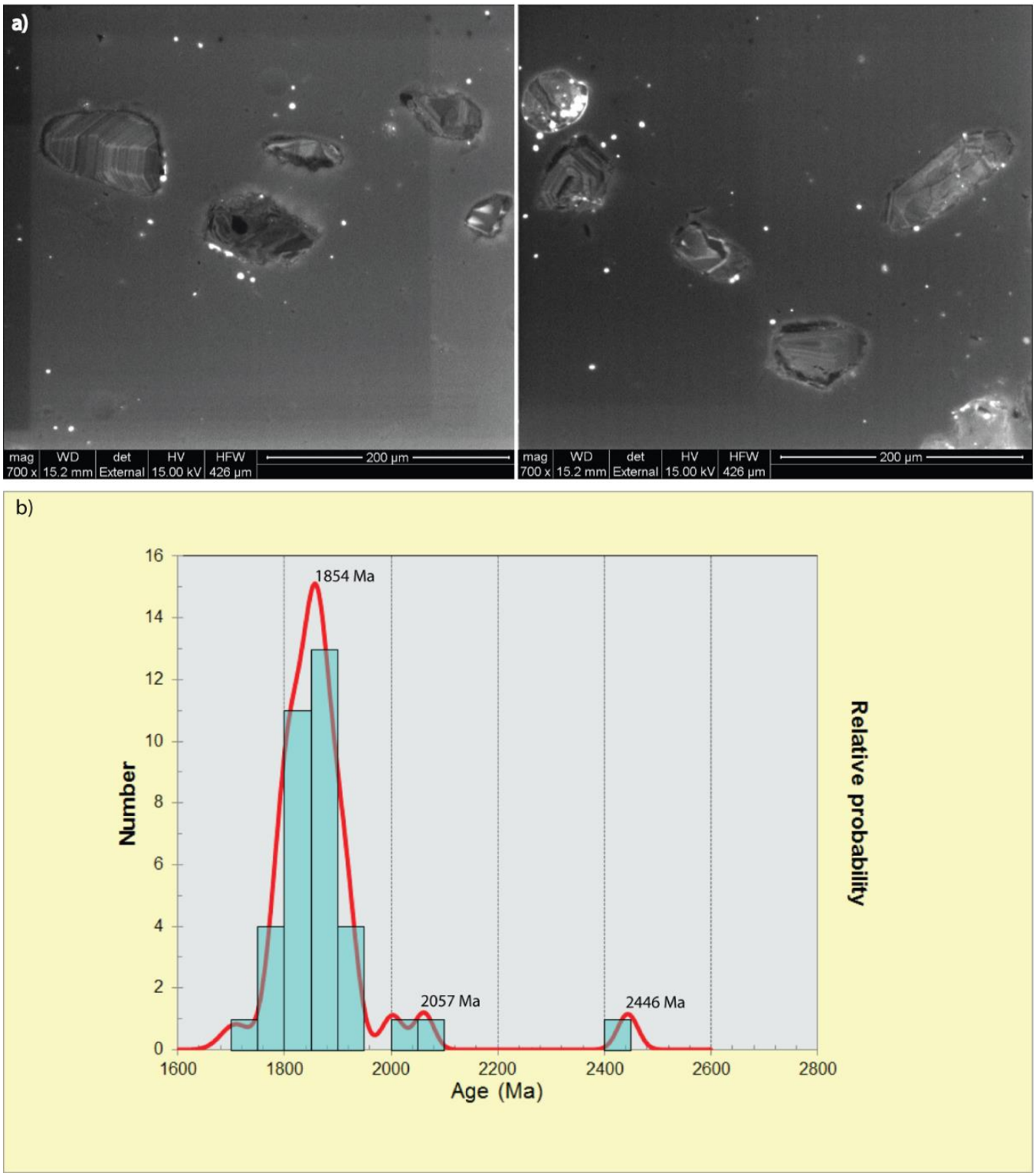

Figure 12: a) CL images of representative zircon grains from the Oorlano Metasomatite sample recovered from the Oorallaw Quarry; b) probability density plot of LA-ICPMS results from the Oorlano Metasomatite which all within the range of 10 % from concordancy.

DISCUSSION

Geochronology

MOONTA PORPHYRY

The crystallisation age of the Moonta Porphyry has previously been not well constrained. While the expectation has been that the Moonta Porphyry should return an age of approximately 1760 Ma (Cowley et al. 2003), zircon U-Pb ages yielded from previous studies have returned ages as young as 1737 ± 5 Ma (Fanning 1997). More recently Fanning et al. (2007) published ages of 1753 ± 8 Ma and 1748 ± 15 Ma. In this study a Pb207/Pb206 crystallisation age of the Moonta Porphyry was determined to be 1752 ± 6 Ma (Figure 11c). Near Kadina the Moonta Porphyry interfingers with metasediments of the Wandearah Formation, namely with the Doora Member (Cowley et al. 2003, Conor et al. 2010). Therefore the age of the Doora Member is suggested to be of similar age to the newly defined age of the Moonta Porphyry.

OORLANO METASOMATITE (HARLEQUIN STONE)

Zircon grains from the Harlequin Stone returned a range of age peaks from the U-Pb analytical data (Figure 12b). One very large peak occurred at ~1854 Ma coinciding with ages similar to that of the Donington Suite granitoids (Figure 3) that underlie younger basement successions in much of the south eastern part of the Gawler Craton (Dutch et al. 2010). In the Southern Yorke Peninsula the Donington Suite granitoids intruded prior to and during the ca. 1850 Ma Cornian Orogeny (Reid et al. 2008, Dutch et al. 2010).

Two minor peaks relating to older periods of magmatism occurred at ~2446 Ma and ~2057 Ma. The earlier age is comparable to magmatism during the Sleafordian Orogeny and is suggested to be related to the intrusion of the Kiana Granite at 2462 ± 10 Ma (Fanning 1997, Fanning et al. 2007, Reid et al. 2008). The later of the two is possibly attributed to the formation of the Miltalie Gneiss at ca. 2000 Ma (Fanning 1997, Fanning et al. 2007). A small number of zircon grains were also analysed to contain U-Pb ages comparable to those of the Moonta Porphyry analyses found in this study (Figure 11b-c) as well as those of the ca. 1790 Ma Myola Volcanics (Fanning et al. 2007) that extruded at the basement near Whyalla (Creaser & Fanning 1993).

From the above it is suggested that the main source of detrital material comprising the Harlequin Stone protolith was sourced from the Donington Suite with minor components being sourced from the Kiana Granite, Miltalie Gneiss, Moonta Porphyry and the Myola Volcanics.

Based on the age of the protolith of the Harlequin, the detrital nature of the zircon grains and the interdigitising relationship it shares with the Moonta Porphyry (Conor 2002, Cowley et al. 2003) the protolith of the Harlequin Stone is interpreted to be similar to that of the Doora Member. A minimum age of sedimentation is suggested to be ca. 1708 Ma based on Pb207/Pb206 zircon grain analysis (Table 3) suggesting a wider age of Wallaroo Group formation than previously suggested by Conor (1995). Due to the coeval relationship shared between the Doora Member and the Moonta Porphyry (Conor 2002, Cowley et al. 2003) it might be expected that larger quantities of ~1760 Ma (Cowley et al. 2003) zircon grains would be inherited due to simultaneous processes

of erosion of the Weetulta Formation and sedimentation of the Wandearah Formation however an analogous situation of zircon-poor metasediments hosting zircon-rich volcanics is seen in the Paleo-Mesoproterozoic Curnamona Province where ~1720-1715 Ma zircon grains characteristic of the Abminga Subsuite volcanics are absent or rare in the enclosing metasediments of the Curnamona Group (Conor pers. comm. 2015). In the Curnamona Province, it is suggested that the lack of detrital volcanogenic zircon grains in the metasediments is evidence for rapid deepening of the basin causing a higher rate of sediment input from zircon-poor sources compared to the rate of erosion of the newly formed volcanic sequences (pers. comm. Conor 2015).

Alteration

DOORA MEMBER

Based on geochemical and petrological analysis the evolution of the Doora Member has been split into three main phases (Figure 13). The first two stages are suggested to have occurred under dynamic metamorphic conditions as evidenced by foliated biotite while the third stage was more under more subtle conditions:

1) The first phase is defined by fine grained biotite, quartz and feldspar with minor coarse grained carbonate minerals, magnetite and no sulphide mineralisation. This mineral assemblage was complimented by high concentrations of Al, SiO_2 and K_2O with low Fe_2O_3 and S in the unaltered samples (Figure 10 a-d).

2) The second phase is defined by coarse grained biotite, magnetite, pyrite and chalcopyrite (Figure 8l, k) and reflected a large increase in Fe_2O_3 and S concentrations (Figure 10d). Very coarse-grained quartz alteration is interpreted to have occurred either during or before the growth of coarse-grained biotite as evidenced by the foliation

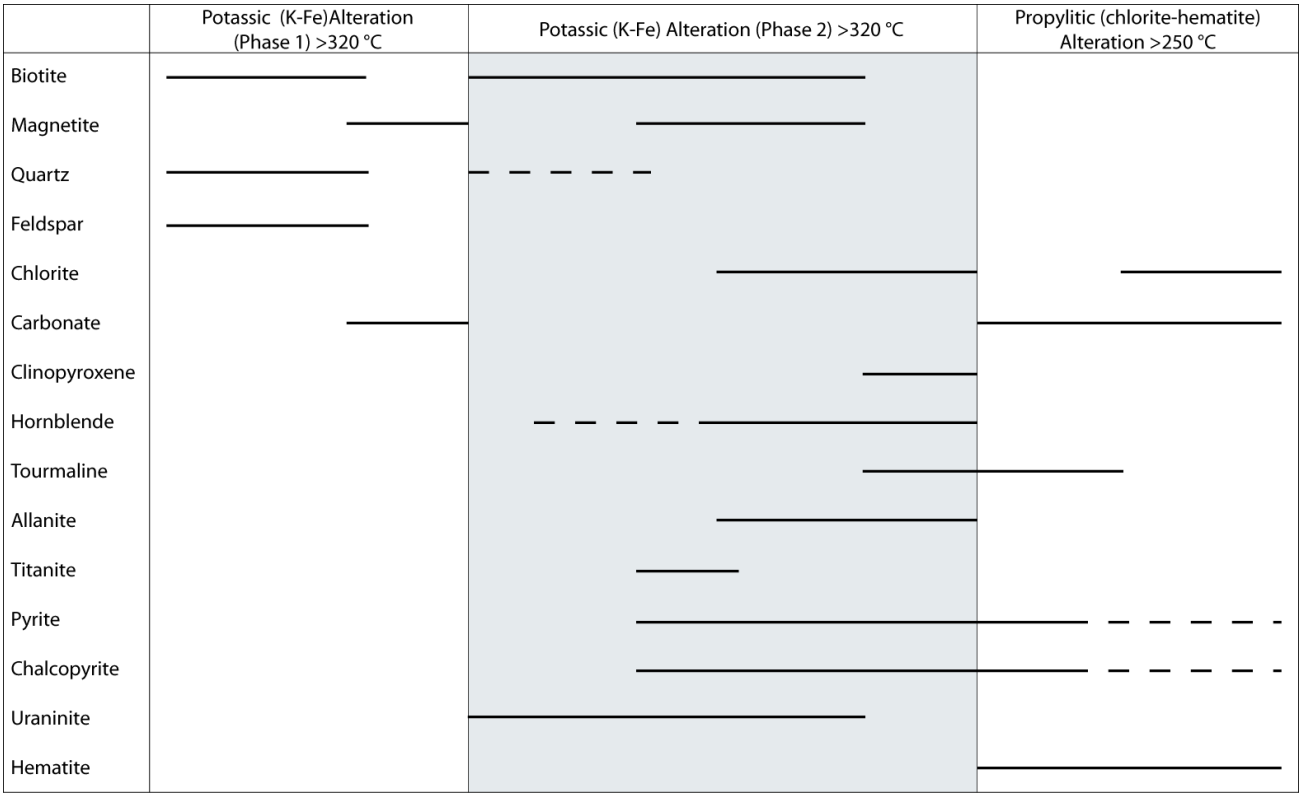

Figure 13: A paragenetic sequence diagram summarising the relative timing of alteration and mineralisation in the Doora Member observed in thin section. Grouping of alteration type as either Propylitic or Potassic and the temperature ranges therein are based on Taylor & Pollard (2006).

following the edge of the quartz grain (Figure 8g-h). Titanite and uraninite are associated with coarse-grained biotite (Figure 8g). Uraninite mineralisation is also associated with magnetite and poikiloblastic hornblende (Figure 9). Coarse-grained poikiloblastic hornblende containing quartz, biotite, and magnetite (Figure 8j-k) followed during or shortly after magnetite-biotite alteration. In some samples allanite was surrounded by coarse grained non poikiloblastic hornblende (Figure 8o, r) indicating that the crystal growth of both minerals likely occurred synchronously. Allanite contained a large amount of pyrite and chalcopyrite which had invaded through cracks in the crystal structure indicating that crystal growth ceased before sulphide mineralisation. The presence of allanite in the highly altered samples of the Doora Member reflects the increase of Ce, La and Y in the geochemistry data (Figure 10l-n). Coarse-grained tourmaline (Figure 8a, b) and clinopyroxene (Figure 8d-e) overprinted

coarse-grained biotite in highly altered samples. Chlorite alteration occurred in two phases, one coarse-grained phase overprinted coarse-grained biotite and later was followed by a much finer grained phase.

3) The later much finer grained phase of chlorite alteration caused fissure like veins along foliation to intrude coarse grained tourmaline, biotite and earlier chlorite alteration (Figure 8a). Early coarse-grained carbonate has been locally altered by a later propylitic phase coupled with the breakdown to hematite (Figure 8c, f). The second phase of carbonate alteration is not apparent however a large amount of oxidised hematite alteration combined with late stage pyrite and chalcopyrite mineralisation exists within the early stage carbonate (Figure 8p-q, s-u).

Based on the relative timing of minerals of the alteration assemblage (Figure 13) in the Doora Member and following scheme proposed by Taylor & Pollard (2006) it is suggested that the variation in temperature of the metasomatic fluids was a major controlling factor of the alteration present in the Doora Member. It is suggested that the metasomatic fluids progressed from a relatively high temperature (>320°C) in the first two phases of alteration before cooler (250°C-320°C) more oxidised fluids were introduced in the final alteration phase. Morales Ruano et al. (2002) suggested a similar mechanism of variance in temperature of the metasomatic fluids at the nearby Moonta Cu-Au deposit, and that fluid temperature was controlled by the coexistence of multiple fluids with varying degrees of magmatic input. The second higher temperature phase of alteration resulted in a more mafic mineral assemblage and likely involved fluids with a higher degree of magmatic content. Although it cannot be assumed that all samples were exposed to the same degree of alteration or the exact same fluid compositions from

unaltered to highly altered samples, there is an overall reduction in felsic elements such as Na, K, Al, Si and Ti (Figure 15a-b) and an increase in elements such as Fe_2O_3, MgO, V, Pb and S (Figure 15b), which are commonly associated with more mafic minerals such as biotite, pyroxene, hornblende and tourmaline (Figure 8a-b, d-e, j-k).

OORLANO METASOMATITE

Fourteen samples of the Oorlano Metasomatite collected by Dr Caroline Forbes from various locations across the NYP are analysed to characterise the alteration chemistry. Three groups were chemically distinguishable using plots of SiO_2 versus V, Ni and Cr (Figure 14). The samples were labelled as either mafic, metasedimentary or felsic components with clear chemical relationships between each of the groups. Mafic components contained elevated values for V (>197ppm), Ni (>94ppm) and Cr (>66ppm) while containing low SiO_2 (<48.72%) (Table 4). Metasedimentary components contained moderate amounts of V, Ni and Cr with moderate amounts of SiO_2. Felsic components contained high values of SiO_2 with negligible V, Ni or Cr (Figure 14).

Comparison of the metasedimentary components of the Oorlano Metasomatite with the moderately and highly altered samples of the Doora Member was done using isocon plots to assess which elements were enriched and depleted during alteration (Figure 15). The data for the metasedimentary components of the Oorlano Metasomatite and the Doora Member were averaged for each. During the calculation any large outliers were excluded to avoid large variance of data points from the displayed data. The data for each element was then assigned a multiplication factor to generate a spread of values between 0 and 30. Minimum and maximum Isocon gradients were assigned based on

elements which were deemed to be immobile during alteration as per Mark et al. (2006). Elements assessed as being immobile in the Doora Member were Al_2O_3, Ga, Ge, Hf and TiO_2 while immobile elements in the Oorlano Metasomatite were Al_2O_3, Ga, Gd, SiO_2, Th, TiO_2 and Tm.

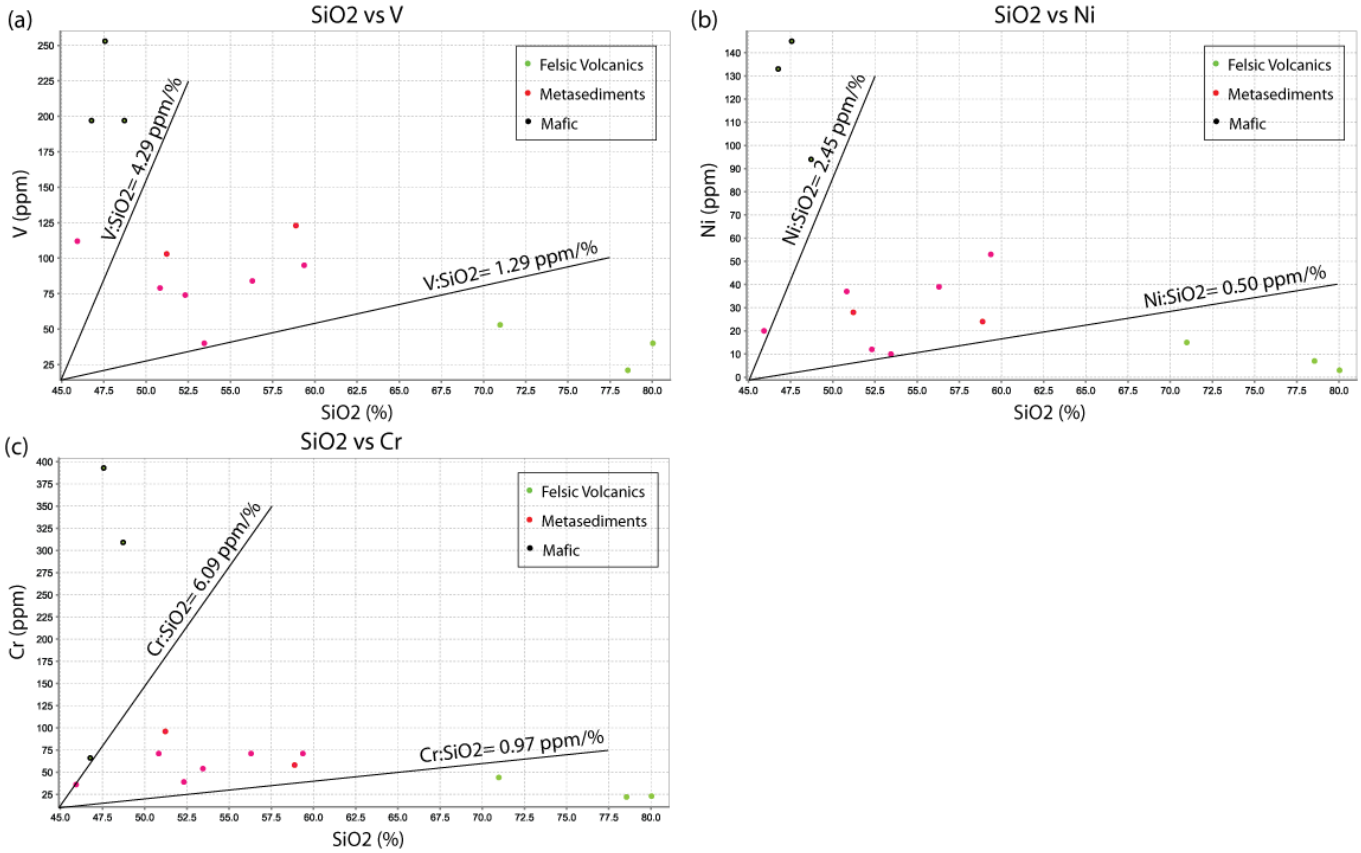

Figure 14: Geochemical ratio plots (a) to (c) show trace elements Vanadium, Nickel and Chromium from the Oorlano Metasomatite plotted against Silica. Mafic lithologies contained high Vanadium, Nickel and Chromium and low Silica while felsic lithologies contained an abundance of silica with low Vanadium, Nickel and Chromium. Metasediments were contained moderate amounts of Vanadium, Nickel, Chromium and Silica.

Table 4: Representative geochemical data of the highly altered Oorlano Metasomatite at various locations across the NYP collected by Dr Caroline Forbes. A mafic, felsic or metasedimentary protolith was determined based on elemental ratios of V, Ni and Cr against SiO_2 as shown in Figure 14.

Sample no.	Drill Hole Number	Eastings	Northings	Zone	Protolith	Cr (ppm)	Ni (ppm)	V (ppm)	SiO2 (%)
1949055	139488	767704	6214605	53	Mafic Volcanic	66	133	197	46.77
1946896	139474	771179	6264821	53	Mafic Volcanic	309	94	197	48.72
1946895	139474	771179	6264821	53	Mafic Volcanic	393	145	253	47.57
1960849	22962	767704	6214605	53	Metasediment	71	53	95	59.37
1949813	23669	751171	6243568	53	Metasediment	54	10	40	53.45
1949812	23669	751171	6243568	53	Metasediment	71	39	84	56.30
1949780	139488	759504	6267846	53	Metasediment	58	24	123	58.88
1949009	30060	777888	6243276	53	Metasediment	71	37	79	50.83
1933086	143968	761879	6160620	53	Metasediment	36	20	112	45.93
1933085	143968	761879	6160620	53	Metasediment	39	12	74	52.32
1933076	23265	747787	6247265	53	Metasediment	96	28	103	51.22
1949051	23674	759856	6246503	53	Felsic Volcanic	44	15	53	70.98
1949050	23674	759856	6246503	53	Felsic Volcanic	22	7	21	78.55
1933075	23265	747787	6247265	53	Felsic Volcanic	23	3	40	80.03

Table 5: Whole rock geochemistry data from the Doora Member samples and the Oorlano Metasomatite metasedimentary samples. Samples are split into levels of alteration and a multiplication factor was applied to generate average concentration values between 0 and 30 to enable the data to be plotted on isocron diagrams as per Mark *et al.* (2006).

Element	Unit of Concentration	X Factor	Average Unaltered	Average Moderately Altered	Average Highly Altered		X Factor	Average Unaltered	Average Oorlano Metasomatite
Al2O3	%		14.4	12.6	11.1		1.5	14.4	18.7
As	ppm		4.5	7.6	12.8		3	4.5	23.8
Ba	ppm	0.1	12.5	6.1	10.7		0.01	12.5	4
Be	ppm	10	16	21.5	23.2		10	16	24
Ce	ppm	0.02	2.1	33.1	12.6		0.1	2.1	8.4
Co	ppm	0.2	7.5	11.9	9.6		0.2	7.5	6.8
Cr	ppm	0.2	19.1	16.2	11.7		0.2	19.1	11.4
Cs	ppm		10.5	15.2	12.2			10.5	5.4
Cu	ppm	0.01	2.7	3.3	13.5		0.1	2.7	4
Dy	ppm		3.5	16	14.1		4	3.5	13.3
Er	ppm	2	4.5	11.2	15.3		5	4.5	10.7
Eu	ppm	1.8	1.7	2.2	11.1		15	1.7	15.6
Fe2O3	%	0.5	5.9	8.5	12.1		2	5.9	24.7
Ga	ppm		21	21.7	21.9			21	19.6
Gd	ppm	0.4	1.5	14.1	8.2		5	1.5	18.8
Ge	ppm	12	3.7	2.6	3.7		15	3.7	17.9
Hf	ppm	5	18.5	19.8	20.2		5	18.5	26.9
Ho	ppm	5	3.7	12	13.7		30	3.7	21.3
In	ppm	50	2.4	5.4	11.5		500	2.4	15.8
K2O	%	2.5	16.6	14.9	14.4		2.5	16.6	12.3
La	ppm	0.02	1.3	21.6	15.2		0.4	1.3	19.3
Li	ppm	0.2	8.4	8.2	10.9		0.7	8.4	24.9
Lu	ppm	15	5.9	9.6	17		50	5.9	21.2
MgO	%	4	14	22.8	19.9		5	14	21.3
MnO	%	150	5.6	9	12		200	5.6	16.3
Na2O	%	10	24.1	18.9	8.1		10	24.1	14.7
Nb	ppm	0.5	10.4	12	6.1			10.4	13.1
Nd	ppm	0.03	1	1.9	5.8		0.5	1	17
Ni	ppm	0.1	2.6	5.5	10.4			2.6	28.5
P2O5	%	50	8.8	13.8	15.9		80	8.8	18.3
Pb	ppm		3.3	0	6.5		3	3.3	18.3
Pr	ppm	0.1	1	1.9	10.6		2	1	19.7
Rb	ppm	0.05	15.9	20.5	16.9		0.08	15.9	18.7
Re	ppm	1200	3.3	1.8	7.2		8000	3.3	16
S	ppm	0.0005	2.1	3.9	11.9		0.0005	2.1	3.3
Sc	ppm		10	13	12.2		1.5	10	14.8

Se	ppm	4	0.9	12.6	13.2		10	0.9	12.5
SiO2	%	0.5	29	25.9	22.7		0.5	29	26.5
Sm	ppm	0.5	2.3	3.4	16.4		3	2.3	16.3
Sn	ppm		6.5	8.5	12.6			6.5	12.3
Sr	ppm	0.4	21.7	12.7	13.8		0.4	21.7	13.1
Ta	ppm	10	16.3	15.5	10.2		10	16.3	16.4
Tb	ppm	5	2.9	18.1	13		30	2.9	15.4
Te	ppm	40	3.4	7.8	18.2		100	3.4	8
Th	ppm	0.8	13.1	21.7	16.7		1.5	13.1	26.2
TiO2	%	40	21.2	20.2	19.4		40	21.2	20.2
Tl	ppm	15	12.3	17.2	15.1		15	12.3	8.6
Tm	ppm	20	7.4	14.7	22.4		20	7.4	7.4
U	ppm	0.5	8.8	8.1	9.7		0.5	8.8	2.5
V	ppm	0.2	16.7	18.6	26.8		0.2	16.7	16.1
Y	ppm	0.4	8.6	25.8	30.8		0.4	8.6	8.5
Yb	ppm	2.5	6	11	18.3		2.5	6	6
Zn	ppm	0.2	6.1	5.8	13.6		0.2	6.1	10.8
Zr	ppm	0.1	12.1	13.4	13.6		0.1	12.1	17.7

Cu, U, Ba and S were severely depleted from the Oorlano Metasomatite metasedimentary samples with Ce, La, Rb, Na_2O, Cr, Nb, Sr, K_2O also recording substantially decreased concentrations. An increase in MgO and large increases in Hf and Zr were also notable.

Al_2O_3 and SiO_2 remained at a steady concentration (Figure 15c) due to the large amount of feldspar and epidote in the mineralogy (Conor 1995, Cowley et al. 2003). Decreases in Ce and La are likely to be due to the exclusion of allanite and/or monazite. Exclusion of allanite from the mineralogy could also be synchronous with the loss of U from the chemical composition (Figure 15c). Low concentrations of S and Cu was likely contemporaneous with the exclusion of chalcopyrite from the mineralogy and an overall

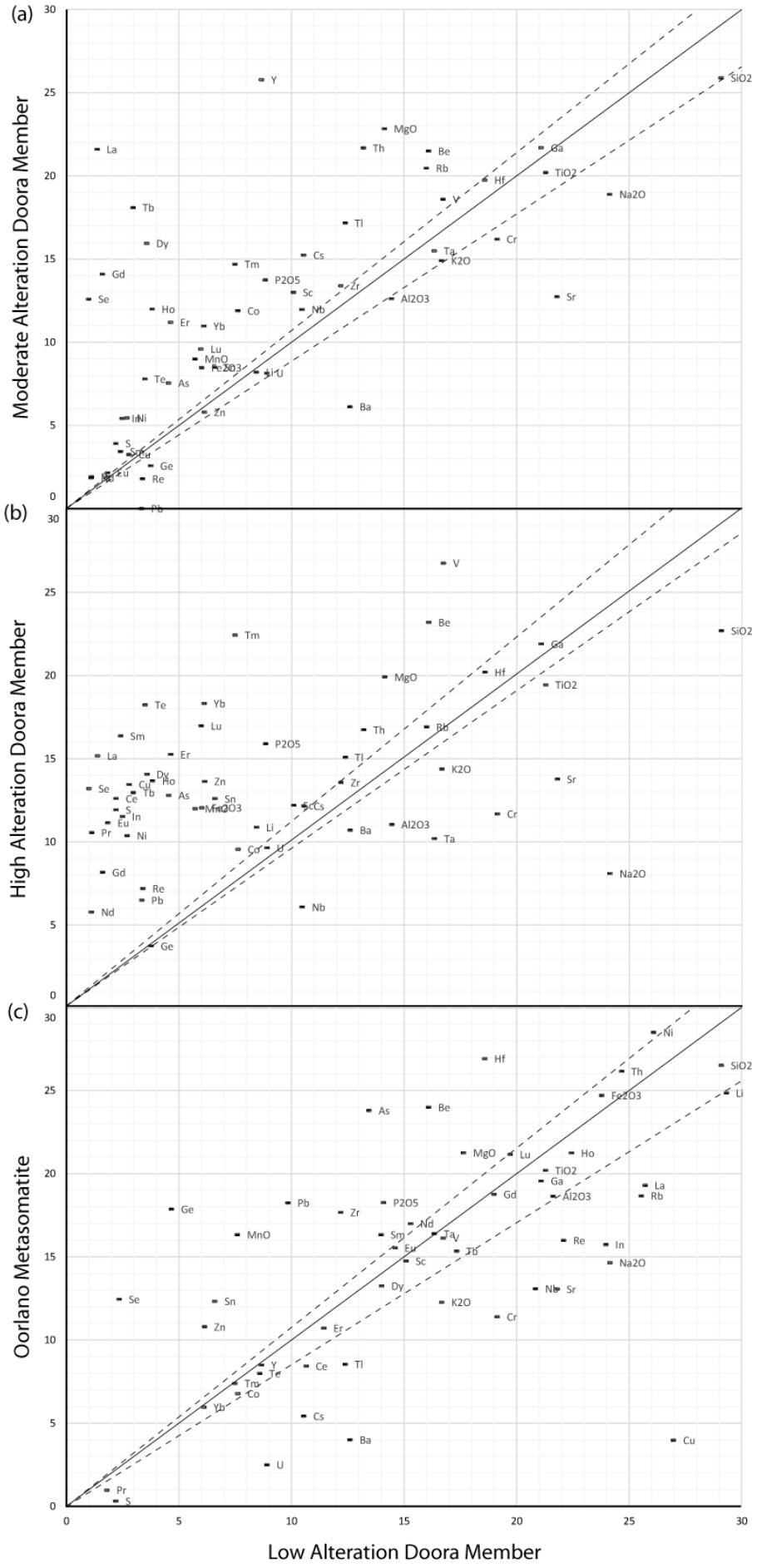

Figure 15: Isocon plots constructed from the average elemental composition of rocks with a similar interpreted protolith at varying levels of alteration. The dashed lines represent the minimum and maximum Isocon gradients at each level of alteration. Where any data points fall outside of this range either a net gain or loss is recorded for the element in question. (a) Moderate Alteration in the Doora Member (b) High Alteration in the Doora Member and (c) Oorlano Metasomatite. Only values separated as metasediments in Figure 14 were used for Isochron analysis. All three alteration types were plotted against the average of the least altered Doora Member samples. All data used to create the Isochron plots are given in Appendix 3.

lack of sulphide minerals. An absence of sulphide minerals is in agreement with a number of studies addressing similar styles of alteration known to occur in the NYP (e.g. Williams et al. 2001, Clark et al. 2005, Conor et al. 2010, Williams et al. 2001) suggested two main hydrothermal fluid phases in the Starra IOCG deposit in the Cloncurry District. The first phase resulted in a mineral assemblage that was barren of copper mineralisation, however fluid inclusions showed that the fluids contained a high concentration of Cu (>1000 ppm) (Williams et al. 2001). Additionally, both Clark et al. (2005) and Conor et al. (2010) have reported on stages of alteration which are barren of Cu mineralisation in the Curnamona Province and the NYP respectively. It is suggested here that the lack of Cu mineralisation in the Oorlano Metasomatite metasedimentary samples is due to either the stripping of sulphide minerals by post mineralisation hydrothermal fluids or omission from conditions in which sulphide mineralisation was stable.

An increase in MgO is attributable to the formation of tremolite, diopside, dolomite and actinolite (Conor 1995, Cowley et al. 2003) while large overall increases in Hf and Zr are possibly with relation to the large amount of zircon found in the Oorlano Metasomatite (e.g. the Harlequin Stone sample from Orallaw Quarry) compared to the complete lack of zircon in all of the Doora Member samples.

RELATIONSHIP OF ALTERATION OORLANO METASOMATITE VS DOORA MEMBER

Conor et al. (2010) and Raymond et al. (2002) discuss two main types of alteration which occurred in the Wallaroo Group. The first is albite-calcsilicate-magnetite alteration with accessory minerals epidote, calcite, titanite, allanite and tourmaline. It is suggested here that this first phase of alteration distally altered the sediments that make

up the Doora Member while pervasively altering those that make the Oorlano Metasomatite due to its proximity to the Tickera Granite (Drexel et al. 1993, Conor 1995, Cooper 1999, Cowley et al. 2003). Albite-calcsilicate-magnetite alteration appear to be generally barren of sulphide mineralisation and where any mineralisation occurs it is attributable to a later event coinciding with either biotite-magnetite or chlorite-quartz-hematite-K feldspar (hematitic alteration from here on in) (Conor et al. 2010). Samples of the Doora Member showing moderate amounts of alteration and metasedimentary samples of the Oorlano Metasomatite showed similar trends in their geochemistry (Figure 15a, c) which reflect albite-calcsilicate-magnetite alteration mineral assemblage. Both rock types showed increases in MgO, MnO, Fe_2O_3, La, Ce and Y with steady background concentrations of S and Cu. Mg and Mn are present in both tourmaline and pyroxene, Fe is present within hornblende, tourmaline, epidote and magnetite while La, Ce and Y are all found within allanite. S and Cu likely remained at baseline concentrations due to the lack of mineralisation associated with albite-calcsilicate-magnetite alteration.

Later alteration localised within the Oorlano Metasomatite further separated the alteration signature from the Doora Member. This relationship is apparent when comparing the large variance of element concentrations between the highly biotite-magnetite altered Doora Member samples and the Oorlano Metasomatite metasedimentary samples. Elements such as SiO_2, Al_2O_3, K2O and TiO_2 are at much higher concentrations in the Oorlano Metasomatite while Cu and S are depleted indicating a trend towards more felsic alteration.

Relationships between Alteration and Mineralisation

The progression of the Doora Member from unaltered to altered at the Doora-Vulcan trend (Figure 2) was represented by both gradual (5-10m) changes and sudden (1-2m) zones of intense shearing (Figure 5 and 8). A biotite foliation was present in all samples and did not define the structure of the rock in unaltered samples containing clear compositional layering (Figure 7a-d). Hand samples that preserve an intense coarse-grained biotite foliation contain sulphide mineralisation in the plane axial to fold hinges (Figure 4e-f). This relationship was well displayed in thin section where magnetite alteration and associated sulphide mineralisation were limited to areas of coarse-grained biotite foliation (Figure 7b-c). This suggests that the bulk of mineralisation occurred within a dynamic metamorphic environment at mid to upper greenschist facies. A later stage of sulphide mineralisation unrelated to biotite-magnetite alteration also occurred but was not as common. This late stage mineralisation was associated with the dissolution of carbonate by hematitic alteration (Figure 8p-q, s-u). Increased modal proportion of biotite-magnetite alteration does not always directly correspond with Cu-sulphide mineralisation in the Doora Member. The lack in corresponding increase of Cu with Fe (Figure 10h) is attributable to the high ratio of pyrite to chalcopyrite mineralisation within the Doora Member samples (Figures 8 and 9). However, whether this truly represents the mineralogy of the Doora Member in the Doora-Vulcan trend is difficult to confirm due to low geochemical sampling density. Additionally, Cu could be introduced during the hematite bearing phase of alteration post biotite-magnetite alteration. A similar case occurs when comparing Fe_2O_3 and K_2O ratios (Figure 10c). The concentration of K_2O sporadically decreases as Fe_2O_3 increases; therefore an

overall trend can be identified of an increase in Fe and a decrease in K with increasing alteration.

Skirrow et al. (2007) report three molybdenite Re-Os alteration ages in the NYP. The earliest age of 1599 ±6Ma (Skirrow et al. 2007) is from veins of calcite-quartz-chlorite-sericite-chalcopyrite-pyrite-molybdenite which cross cut an earlier assemblage of albite-actinolite-epidote-clinosite and recrystallised scapolite (Skirrow et al. 2007). Both assemblages are suggested to have formed without iron oxide alteration due to the low iron content of the host strata (Skirrow et al. 2007). Their Fe-oxide hosting equivalent assemblages are suggested to be hematite associated alteration and magnetite-albite-calcsilicate alteration respectively (Skirrow et al. 2007, Conor et al. 2010). It is also important to note that biotite rich alteration aureoles that overprint scapolite spots occur adjacent to some of the sulphide veining. The relationship of this alteration phase to biotite-magnetite alteration is open to interpretation, however at the very least the ca. 1599 Ma age of the mineralised veins provides a minimum age for Na-Ca alteration (Skirrow et al. 2007). The two later ages reported by Skirrow et al. (2007) (an original and a repeat analysis) of a molybdenite grain are from a vein of quartz-chlorite-K feldspar ± hematite ± chalcopyrite ± pyrite ± tourmaline ± molybdenite. The vein cross cuts earlier magnetite-biotite alteration and yields Re-Os ages of 1574 ±6 Ma and 1577 ± 6 Ma (Skirrow et al. 2007) therefore representing the minimum age of biotite-magnetite alteration.

Uranium in Yorke Peninsula

Extensive uranium mineralisation occurred synchronously with biotite-magnetite alteration (Figure 8g, Figure 9), uraninite is visible by large radioactive decay haloes in

coarse-grained biotite and hornblende. Biotite-magnetite alteration appears to be directly associated with uraninite mineralisation in most samples, and is exhibited as coarse-grained biotite containing uraninite (e.g. Sample 2131463 U=167.8ppm; Figure 8g). However, other samples of biotite-magnetite alteration exhibited very little uraninite (e.g. Sample 2129388 U=8.7ppm; Figure 8p, s).

Maximum peaks of U did not coincide with maximum peaks for Cu-Au (Figure 10g-j) indicating that uraninite and Cu-Au mineralisation in the Doora Member are somewhat independent of one another. While it is suggested that U mineralisation is part of the regional mineralising event, drill hole assays by Adelaide Resources have shown a spatial removal between U enrichment and highly Cu-Au mineralised zones (pers. comm. Drown 2015). Uranium in the NYP is not well documented in published literature and is only mentioned briefly e.g. Keeling et al. (2003), Drexel et al. (1993) and Conor et al. (2010). However the relationship of U with at least one period of biotite-magnetite alteration at the Doora-Vulcan trend is consistent with the NYP being a part of the much larger Olympic IOCG(U) province.

Relationships with Eastern Proterozoic Australia

Alteration and mineralisation in the NYP is suggested to be broadly synchronous with emplacement of the Hiltaba Suite granites 1600-1580 Ma both in the NYP and elsewhere in the Olympic Domain (Conor 1995, Ferris et al. 2002, Hand et al. 2007, Conor et al. 2010, Groves et al. 2010). Although ages of volcanism and magmatism in the NYP have been successfully constrained by this and other studies (e.g. Fanning 1997, Fanning et al. 2007) only minimum ages constraining biotite-magnetite alteration and Cu-Au mineralisation have been suggested (Skirrow et al. 2007). Paragenetic

studies of the alteration phases both here, in Skirrow et al. (2007) and Conor et al. (2010) show that the minimum age of mineralisation of 1574 ±6 Ma suggested by Skirrow et al. (2007) can be fairly confidently defined. This minimum age of mineralisation is almost indistinguishable from the final stages of Hiltaba Suite magmatism in the NYP at ca. 1577 ±7 Ma (Skirrow et al. 2002). Alteration assemblages found in the Doora Member are similar to those in other regions of the Olympic Domain such as the magnetite rich alteration found at depth in the Olympic Dam Deposit (Hayward & Skirrow 2010) as well as that located laterally to the Prominent Hill Deposit (Belperio et al. 2007).

Styles of alteration and associated IOCG mineralisation throughout the Olympic Domain are suggested to vary due to the depth and temperature at which each deposit formed (e.g. Drexel et al. 1993, Bastrakov et al. 2007, Belperio et al. 2007, Skirrow 2010). In the NYP chalcopyrite is the dominant mineral responsible for Cu mineralisation, and pyrite dominated sulphide mineralisation shares a direct relation with magnetite-biotite alteration (Figure 8i, j) occurring at high temperatures. High temperatures also allowed boiling near surface and precipitation of Cu from mineralising fluids (Morales Ruano et al. 2002). Shallowly formed IOCG deposits such as Olympic Dam (Oreskes & Einaudi 1992, Johnson & McCulloch 1995, Reynolds 2001) and Prominent Hill (Belperio et al. 2007) and Moonta are associated with lower temperature fluids resulting in hematitic alteration dominating and in places chalcocite substituting for chalcopyrite as the main Cu bearing ore mineral (Skirrow 2010). A direct relationship between NYP style magnetite related Cu-Au mineralisation and OD/Prominent Hill style hematite-Cu-Au mineralisation is represented in the petrology

of the Doora Member, where hematitic alteration occurs as a temporally separated but genetically linked phase to biotite-magnetite alteration (Figure 8p, s-t). Belperio et al. (2007) and Williams *et al.* (2005) highlight the importance of this relationship between magnetite and hematite alteration when exploring for hematite dominated iron oxide systems by noting that mineralisation may occur in high density zones proximal to magnetic highs.

The occurrence of U in the NYP is contemporaneously associated with biotite-magnetite alteration (Figure 8g, Figure 9) adding to the model defining the formation of IOCG(U) mineralising systems in the Olympic Domain. Most IOCG(U) deposits show some degree of association with anomalous levels of U within and outside of mineralised zones e.g. Olympic Dam and Prominent Hill in the Olympic Domain (Hitzman & Valenta 2005). The NYP is similar to other mining regions outside of the Olympic Domain, in particular the Ernest Henry Cu-Au mine in the Cloncurry District. Similar to the drill hole assays done by Adelaide Resources in the NYP (pers. comm. Drown 2015), reconnaissance drilling in the region of the Ernest Henry mine has identified a several kilometre wide U enrichment zone surrounding the central zone of alteration (Hitzman & Valenta 2005). Based on the relationship between uraninite mineralisation and K-Fe alteration (Figure 8g, Figure 9) it is suggested that U enrichment in the NYP was associated with the biotite-magnetite mineralisation phase but was later remobilised by less pervasive oxidising hydrothermal fluids from the more highly sheared/fractured zones in which sulphide mineralisation tends to be enriched. This relationship is reflected by the sporadic relationship between Fe_2O_3, S and U in the whole rock geochemistry conducted on the Doora Member (Figure 10d, g) where what

are determined to be peaks in sulphide U mineralisation do not align. An increased geochemical sampling density is recommended for any investigations which follow this preliminary study to further verify this claim.

CONCLUSIONS

- A crystallisation age of the Moonta Porphyry in the vicinity of the Poona Mine was determined to be 1752 ±6 Ma which provided a corresponding minimum sedimentation age of the Doora Member of ca. 1752 Ma due to their interfingering relationship.
- The protolithic material which forms the Harlequin Stone was determined to be of detrital origin with the majority of zircon ages matching with the ca. 1850 Donington Suite Granitoids. A minimum sedimentation age of ca. 1708 Ma suggests a wider age of Wallaroo Group formation than previously reported in literature however additional geochronological work is needed to support this claim.
- The bulk of mineralisation within the Doora Member was determined to be genetically linked to biotite-magnetite alteration involving high temperature (>320°C) fluids. Zones of increased mineralisation were seen to correspond with coarsening grainsize of biotite. Later hematitic bearing alteration phases were responsible for Cu enrichment within carbonate rich zones. Uranium mineralisation was also associated with biotite-magnetite alteration but is suggested to have since been remobilised from the main mineralised zones by later less pervasive hydrothermal phases.
- Comparison of whole rock geochemistry from the Doora Member and the Oorlano Metasomatite showed deviation in alteration types and intensity from

similar protolithic sediments. It is suggested that this occurrence is due to the Oorlano Metasomatites proximity to the Arthurton and Tickera Granites.

- Alteration assemblages which resulted in economic mineralisation in the NYP are comparable to other areas in Eastern Proterozoic Australia. In particular, the Earnest Henry Cu-Au deposit in the Cloncurry District shares a similar progression of alteration assemblages with magnetite-biotite alteration associated with the main phase of mineralisation. Additionally, as in the NYP, uranium enrichment surrounds the central altered and mineralised zones.

ACKNOWLEDGMENTS

Firstly I would like to thank my primary supervisor Dr Caroline Forbes for her unwavering support and guidance throughout the duration of this study. Secondly I would like to thank my co-supervisors Colin Conor and Dr Anthon Reid for their valuable advice and wisdom regarding all things geology in the Northern Yorke Peninsula and beyond. The state drill core libraries at Glenside and Moonta are recognised for their assistance in lying out and sampling of drill core. Chris Drown from Adelaide Resources is acknowledged for providing extremely valuable information regarding uranium enrichment in the NYP without which many conclusions could not be made. Dr Benjamin Wade and the team at Adelaide Microscopy are thanked for their time patience in training and assistance with the SEM and LA-ICPMS. Lastly I would like to thank the honours coordinating staff for their help and advice regarding training and project issues throughout the year.

REFERENCES

BASTRAKOV E. N., SKIRROW R. G. & DAVIDSON G. J. 2007. Fluid evolution and origins of iron oxide Cu-Au prospects in the Olympic Dam district, Gawler Craton, South Australia. *Economic Geology* **102**, 1415-1440.

BELPERIO A., FLINT R. & FREEMAN H. 2007. Prominent Hill: a hematite-dominated, iron oxide copper-gold system. *Economic geology* **102**, 1499-1510.

BOTH R. A., HAFER M. R., MENDIS D. P. J. & KELTY B. T. 1993. The Moonta copper deposits, South Australia: Geology and ore genesis of the Poona and Wheal Hughes ore bodies. *Current Research in Geology Applied to Ore Deposits*, 49-52.

CLARK C., MUMM A. S. & FAURE K. 2005. Timing and nature of fluid flow and alteration during Mesoproterozoic shear zone formation, Olary Domain, South Australia. *Journal of Metamorphic Geology* **23**, 147-164.

CONOR C. 1995. Open File Envelope No. 8886. Mines and Energy South Australia.

CONOR C. 2002. The Palaeo-Mesoproterozoic geology of northern Yorke Peninsula, South Australia. Hiltaba Suite-related alteration and mineralisation of the Moonta-Wallaroo Cu-Au district. *Adelaide, South Australia, Australia*.

CONOR C. & FORBES C. J. 2012. IOCG-related metasomatism and metamorphism in the Yorke Peninsula South Australia - A field guidebook. In AUSTRALIA G. S. O.

CONOR C., RAYMOND O., BAKER T., TEALE G., SAY P. & LOWE G. 2010. Alteration and Mineralisation in the Moonta-Wallaroo Copper-Gold Mining Field Region, Olympic Domain, South Australia. *Hydrothermal Iron Oxide Copper-Gold & Related Deposits: A Global Perspective* **3**, 147-170.

COOPER B. 1999. Marketing Harlequin Stone. *MESA Journal* **14**, 18.

COWLEY W., CONOR C. & ZANG W. 2003. New and revised Proterozoic stratigraphic units on northern Yorke Peninsula. *MESA Journal* **29**, 46-58.

CREASER R. & FANNING C. 1993. AU-Pb zircon study of the Mesoproterozoic Charleston Granite, Gawler Craton, South Australia. *Australian Journal of Earth Sciences* **40**, 519-526.

DIREEN N. G. & LYONS P. 2007. Regional crustal setting of iron oxide Cu-Au mineral systems of the Olympic Dam region, South Australia: Insights from potential-field modeling. *Economic Geology*, **102**, 1397-1414.

DREXEL J. F., PREISS W. V. & PARKER A. 1993. The Geology of South Australia: The Precambrian. Mines and Energy, South Australia, Geological Survey of South Australia.

DUTCH R., HAND M. & KELSEY D. 2010. Unravelling the tectonothermal evolution of reworked Archean granulite facies metapelites using in situ geochronology: an example from the Gawler Craton, Australia. *Journal of Metamorphic Geology* **28**, 293-316.

FANNING C. 1997. Geochronological Synthesis of Southern Australia, Part II, The Gawler Craton. *South Australia Department of Mines and Energy, Open File Envelope* **8918**.

FANNING C., REID A. & TEALE G. 2007. A Geochrolological Framework for the Gawler Craton, South Australia. South Australia: Gological Survey.

FERRIS G. M., SCHWARZ M. P. & HEITHERSAY P. 2002. The geological framework, distribution, and controls of Fe-oxide Cu–Au mineralisation in the Gawler Craton, South Australia: Part 1—Geological and tectonic framework. *Hydrothermal iron oxide copper–gold and related deposits: a global perspective* **2**, 9-32.

FORBES C. 2012. Report on Sampling Strategy and Background Geochemistry. Interim Technical Report. School of Earth and Environmental Sciences, University of Adelaide: Deep Exploration Technologies Cooperative Research Centre.

FORBES C. J., BETTS P. G., GILES D. & WEINBERG R. 2008. Reinterpretation of the tectonic context of high-temperature metamorphism in the Broken Hill Block, NSW, and implications on the Palaeo- to Meso-Proterozoic evolution. *Precambrian Research* **166**, 338-349.

FORBES C. J., GILES D., HAND M., BETTS P. G., SUZUKI K., CHALMERS N. & DUTCH R. 2011. Using P–T paths to interpret the tectonothermal setting of prograde metamorphism: An example from the northeastern Gawler Craton, South Australia. *Precambrian Research* **185**, 65-85.

GAUTHIER L., HALL G., STEIN H. & SCHALTEGGER U. 2001. The Osborne deposit, Cloncurry district: a 1595 Ma Cu–Au skarn deposit. 58-59.

GILES D. & NUTMAN A. 2002. SHRIMP U–Pb monazite dating of 1600–1580 Ma amphibolite facies metamorphism in the southeastern Mt Isa Block, Australia. *Australian Journal of Earth Sciences* **49**, 455-465.

GRIFFIN W., POWELL W., PEARSON N. & O'REILLY S. 2008. Laser Ablation–ICP–MS in the Earth Sciences. Mineralogical Association of Canada Short Course Series.

GROVES D., BIERLEIN F., MEINERT L. & HITZMAN M. 2010. Iron Oxide Copper-Gold (IOCG) Deposits through Earth History: Implications for Origin, Lithospheric Setting, and Distinction from Other Epigenetic Iron Oxide Deposits. *Economic Geology* **105**, 641-654.

HAND M., REID A. & JAGODZINSKI L. 2007. Tectonic framework and evolution of the Gawler Craton, southern Australia. *Economic Geology* **102**, 1377-1395.

HAYNES D. W., CROSS K. C., BILLS R. T. & REED M. H. 1995. Olympic Dam ore genesis; a fluid-mixing model. *Economic Geology* **90**, 281-307.

HAYWARD N. & SKIRROW R. 2010. Geodynamic setting and controls on iron oxide Cu-Au (±U) ore in the Gawler Craton, South Australia. *Hydrothermal iron oxide copper-gold and related deposits: A global perspective* **3**, 105-131.

HESS F. L. 1924. Molybdenum Deposits: A Short Review. pp. 1-9. United States Geological Survey.

HITZMAN M. W. & VALENTA R. K. 2005. Uranium in iron oxide-copper-gold (IOCG) systems. *Economic Geology* **100**, 1657-1661.

JOHNSON J. P. & MCCULLOCH M. T. 1995. Sources of mineralising fluids for the Olympic Dam deposit (South Australia): Sm・Nd isotopic constraints. *Chemical Geology* **121**, 177-199.

KEELING J., MAUGER A. J., SCOTT K. M. & HARTLEY K. 2003. Alteration mineralogy and acid-sulphate weathering at Moonta copper mines, South Australia. *Advances in Regolith*, 230-233.

KONTONIKAS-CHAROS A., CIOBANU C. L. & COOK N. J. 2014. Albitization and redistribution of REE and Y in IOCG systems: Insights from Moonta-Wallaroo, Yorke Peninsula, South Australia. *Lithos* **208–209**, 178-201.

LUDWIG K. R. 2003. User's manual for Isoplot 3.00: a geochronological toolkit for Microsoft Excel. Kenneth R. Ludwig.

MARK G., OLIVER N. H. & WILLIAMS P. J. 2006. Mineralogical and chemical evolution of the Ernest Henry Fe oxide–Cu–Au ore system, Cloncurry district, northwest Queensland, Australia. *Mineralium Deposita* **40**, 769-801.

MORALES RUANO S., BOTH R. A. & GOLDING S. D. 2002. A fluid inclusion and stable isotope study of the Moonta copper–gold deposits, South Australia: evidence for fluid immiscibility in a magmatic hydrothermal system. *Chemical Geology* **192**, 211-226.

ORESKES N. & EINAUDI M. T. 1992. Origin of hydrothermal fluids at Olympic Dam; preliminary results from fluid inclusions and stable isotopes. Economic Geology, 87, 64-90.

RAYMOND O., FLETCHER I. & MCNAUGHTON N. 2002. Copper-gold mineral systems in the south-eastern Gawler Craton-Another Mt Isa Eastern succession. Geological Society of Australia Abstracts. pp. 69-69. Geological Society of Australia; 1999.

REID A., HAND M., JAGODZINSKI E., KELSEY D. & PEARSON N. 2008. Paleoproterozoic orogenesis in the southeastern Gawler Craton, South Australia∗. *Australian Journal of Earth Sciences* **55**, 449-471.

REID A. J. & HAND M. 2012. Mesoarchean to Mesoproterozoic evolution of the southern Gawler Craton, South Australia. *Episodes-Newsmagazine of the InternationalUnion of Geological Sciences* **35**, p.216.

REYNOLDS L. 2001. Geology of the Olympic Dam Cu-U-Au-Ag-REE deposit: MESA Journal

SKIRROW R. 2010. 'Hematite-Group' IOCG±U Ore Systems: Tectonic Settings, Hydrothermal Characteristics, and Cu-Au and U Mineralizing Processes. *Geological Association of Canada Shortcourse Notes* **20**, 39-58.

SKIRROW R., BASTRAKOV E., DAVIDSON G., RAYMOND O. & HEITHERSAY P. 2002. The geological framework, distribution and controls of Fe oxide Cu-Au mineralisation in the Gawler Craton, South Australia. Part II. Alteration and mineralisation. *Hydrothermal iron oxide copper-gold and related deposits: A global perspective.* Porter GeoConsultancy Publishing, Adelaide, 33-47.

SKIRROW R. G., BASTRAKOV E. N., BAROVICH K., FRASER G. L., CREASER R. A., FANNING C. M.,

RAYMOND O. L. & DAVIDSON G. J. 2007. Timing of iron oxide Cu-Au-(U) hydrothermal activity and Nd isotope constraints on metal sources in the Gawler Craton, South Australia. *Economic Geology* **102**, 1441-1470.

TAYLOR R. G. & POLLARD P. J. 2006. Ore Textures and Breccias. James Cook University.

Williams P. J., Barton M. D., Johnson D. A., Fontboté L., De Haller A., Mark G., Oliver N. H. & Marschik R. 2005. Iron oxide copper-gold deposits: Geology, space-time distribution, and possible modes of origin. *Economic Geology*, 371-405.

WILLIAMS P. J., DONG G., RYAN C. G., POLLARD P. J., ROTHERHAM J. F., MERNAGH T. P. & CHAPMAN L. H. 2001. Geochemistry of hypersaline fluid inclusions from the Starra (Fe oxide)-Au-Cu deposit, Cloncurry District, Queensland. *Economic Geology* **96**, 875-883.

WURST A. T. 1994. Analyses of late stage, Mesoproterozoic, syn and post tectonic, magmatic events in the Moonta Sub-domain: Implications for Cu-Au mineralisation in-the" Copper Triangle" of South Australia. University of Adelaide.

ZANG W. 2002. Late Palaeoproterozoic Wallaroo Group and Early Mesoproterozoic mineralisation in the Moonta Subdomain, eastern Gawler Craton, South Australia. *South Australia Department of Primary Industries and Resources, Report Book* **1**, 161.

APPENDIX A: WHOLE ROCK GEOCHEMICAL DATA

Appendix 1: Whole rock geochemical Data of the Doora Member samples selected from the Doora-Vulcan trend

				Sample Number								
ELEMENTS	UNITS	DETECTION	METHOD	2129382	2129383	2129384	2129385	2129386	2129387	2129388	2129389	2129382 (Check)
Au	ppb	1	FA25/MS	4	115	2	1	2	X	6	X	3
Ag	ppm	0.05	4AB/MS	X	0.15	X	X	X	X	0.07	X	X
Al2O3	%	0.01	FB6/OE	15.59	13.46	16.4	14.8	14.11	12.51	4.87	13.78	15.54
As	ppm	0.5	4AB/MS	2.6	4.7	3.9	3.6	5.4	26	21.2	6.6	3.5
Ba	ppm	0.5	FB6/MS	2034.6	2086.4	1675.8	1522.3	1179.4	764.8	410.7	552.4	2069.5
Be	ppm	0.5	FB6/MS	1	1.4	2.7	1.9	1.3	1.9	2.2	2	1.1
Bi	ppm	0.01	4AB/MS	0.01	0.74	0.01	X	X	0.31	1.87	0.18	0.02
CaO	%	0.01	FB6/OE	0.54	0.54	3	2.3	0.39	0.91	1.07	0.75	0.54
Cd	ppm	0.02	4AB/MS	X	0.05	0.05	X	X	0.05	X	X	X
Ce	ppm	0.5	FB6/MS	55.6	187.4	121.2	29.9	324.2	3436.2	646.3	212.6	57.8
Co	ppm	0.1	4AB/MS	34	14	17.5	25.4	34.7	45.8	540.9	47.6	34.6
Cr	ppm	20	FB6/OE	69	79	72	70	68	59	X	58	68
Cs	ppm	0.05	4AB/MS	7.12	9.66	9.79	8.53	14.42	24.48	7.97	14.26	7.12
Cu	ppm	1	4AB/OE	334	9983	52	205	238	127	2444	266	330
Dy	ppm	0.05	FB6/MS	3.47	8.34	5.7	3.78	3.67	23.62	12.8	3.9	3.54
Er	ppm	0.05	FB6/MS	2.17	6.64	3.2	2.47	2.24	11.53	8.49	2.3	2.23
Eu	ppm	0.05	FB6/MS	0.74	2.13	1.72	0.82	1.11	11.1	4.41	1.2	0.78
Fe2O3	%	0.01	FB6/OE	8.11	11.47	8.54	8.16	11.37	23.34	47.78	12.98	8.16
Ga	ppm	0.1	FB6/MS	20.1	20.8	21	20.9	19.4	23.7	19.1	21.4	20.5
Gd	ppm	0.05	FB6/MS	3.81	8.96	6.81	3.6	5.15	37.74	15.47	4.71	3.95
Ge	ppm	0.05	4AB/MS	0.44	0.28	0.22	0.19	0.21	X	0.43	0.18	0.4
Hf	ppm	0.1	FB6/MS	3.5	5	5.6	4	3.8	4.4	1.8	3.5	3.7
Ho	ppm	0.02	FB6/MS	0.75	2	1.14	0.78	0.75	4.48	2.75	0.8	0.76
In	ppm	0.005	4AB/MS	0.058	1.033	0.016	0.04	0.064	0.411	0.139	0.062	0.056
K2O	%	0.01	FB6/OE	8.2	7.71	6.41	6.91	8.31	7.63	3.13	5.06	8.22
La	ppm	0.2	FB6/MS	30.4	114.8	67.9	18.6	200.4	2199.7	382.1	132.5	30.7
Li	ppm	1	4AB/OE	40	52	56	61	49	118	14	42	38
Lu	ppm	0.02	FB6/MS	0.33	1.15	0.47	0.4	0.44	1.29	1.55	0.38	0.35
MgO	%	0.01	FB6/OE	3.11	4.12	3.56	3.44	4.22	7.56	2.87	4.36	3.15
MnO	%	0.01	FB6/OE	0.03	0.04	0.05	0.04	0.05	0.09	0.11	0.06	0.03
Mo	ppm	1	FB6/MS	X	X	X	X	X	X	X	X	X
Na2O	%	0.01	FB6/OE	2.17	0.69	2.32	1.9	1.95	0.32	0.15	3.2	2.2
Nb	ppm	0.1	FB6/MS	12.2	14.7	14.4	12.6	12.8	18.2	4.9	12.8	12
Nd	ppm	0.1	FB6/MS	23.9	62.7	42.9	13.7	77.2	751	172.5	55.6	25.2
Ni	ppm	1	4AB/OE	26	56	11	20	15	21	250	31	26
P2O5	%	0.01	FB6/OE	0.12	0.11	0.23	0.2	0.14	0.43	0.44	0.22	0.14
Pb	ppm	5	4AB/OE	6	6	6	7	X	14	X	X	5
Pr	ppm	0.05	FB6/MS	6.84	19.52	12.41	3.67	28.66	291.38	58.73	19.2	7.02
Rb	ppm	0.1	FB6/MS	267.9	324.9	312.6	310.6	428.2	595.4	203.1	328.4	270.5
Re	ppm	0.002	4AB/MS	0.008	0.006	X	X	X	X	0.018	X	0.009
S	ppm	50	4AB/OE	5650	15155	X	2386	3919	2630	77532	8620	5557
Sb	ppm	1	FB6/MS	X	X	X	X	X	X	X	X	X
Sc	ppm	10	FB6/OE	14	17	14	15	11	20	X	12	14
Se	ppm	0.5	4AB/MS	X	X	X	X	X	1.7	9.3	0.6	X
SiO2	%	0.01	FB6/OE	59.88	58.15	56.11	59.43	58.21	43.51	28.05	56.44	59.61
Sm	ppm	0.05	FB6/MS	4.54	11.12	8.23	3.52	8.46	70.12	22.31	6.88	4.69
Sn	ppm	1	FB6/MS	7	21	14	10	4	9	4	7	7
Sr	ppm	0.2	FB6/MS	65.6	43.6	52.3	54.8	35.8	34.1	17	28.4	66.2
Ta	ppm	0.1	FB6/MS	1.2	1.5	1.5	1.3	1.1	1.4	0.4	1.2	1.2
Tb	ppm	0.02	FB6/MS	0.55	1.3	0.96	0.58	0.67	4.43	2.17	0.64	0.56
Te	ppm	0.1	4AB/MS	0.1	0.8	X	X	X	X	0.7	X	0.1
Th	ppm	0.05	FB6/MS	16.28	22.62	22.51	18.77	16.89	20.3	17.57	13.92	16.05
TiO2	%	0.01	FB6/OE	0.56	0.67	0.67	0.57	0.54	0.6	0.23	0.52	0.56
Tl	ppm	0.02	4AB/MS	0.77	0.94	0.84	0.81	1.15	1.7	0.71	1.06	0.79
Tm	ppm	0.05	FB6/MS	0.35	1.09	0.51	0.37	0.36	1.52	1.39	0.37	0.36
U	ppm	0.05	FB6/MS	36.88	21.62	25.1	16.35	8.5	21.78	8.7	5.49	37.93
V	ppm	10	FB6/OE	118	140	122	101	69	206	104	71	118
W	ppm	1	FB6/MS	X	X	2	X	X	X	X	X	X
Y	ppm	0.5	FB6/MS	22.6	62.7	30.6	22.3	21.7	118.4	83.8	22.8	22.5
Yb	ppm	0.05	FB6/MS	2.27	7.67	3.16	2.53	2.63	8.88	9.63	2.38	2.21
Zn	ppm	1	4AB/OE	32	44	15	21	43	76	79	26	30
Zr	ppm	1	FB6/MS	112	161	186	128	128	148	59	115	113

Appendix 2: Standard values acquired during whole rock geochemistry data collection of the Doora Member samples from the Doora-Vulcan trend.

Standards									
GSP-2	OREAS 45d	OREAS 45d	OREAS 901	OxC109	SY-4	MPL-5	OREAS 45e	OREAS 624	Control Blank
		25		196			51		X
	0.18		0.31			27.3			X
14.81					20.72			7.95	X
	13		72			992			X
1339.3					349.6			1017.2	X
1.3					2.9			0.8	X
	0.29		4.56			39.18			X
2.07					8.16			2.1	X
	0.04		0.08			2.81			X
427.2					119.5			28.6	X
	29.5		74.7			129.1			X
20					X			37	X
	3.9		5.21			24.02			X
	389		1355			1841			X
5.48					18.66			2.65	X
2.22					14.49			1.75	X
2.2					2.05			1.42	X
4.96					6.25			22.82	X
21					36.3			21.4	X
11.84					14.32			3.25	X
	1.12		0.28			6.92			X
14.1					10.5			2.9	X
0.95					4.49			0.59	X
	0.102		0.222			19.849			X
5.39					1.68			1.09	X
180.1					56.2			16.9	X
	28		17			42			X
0.22					2.11			0.28	X
1.01					0.54			2.19	X
0.04					0.11			0.09	X
X					X			X	X
2.74					7.17			0.64	X
25.9					13.5			4.4	X
201.4					56.6			14.3	X
	241		39			2266			X
0.28					0.14			0.07	X
	25		18			2020			X
53.89					14.59			3.59	X
244.7					54.7			31.6	X
	0.005		X			1.585			X
	477		345			11576			X
X					X			71	X
X					X			X	X
	2.5		2.8			126			X
67.01					50.33			42.96	X
25.84					13.08			3.42	X
8					7			13	X
233.9					1222.1			37.4	X
0.9					0.9			0.4	X
1.22					2.56			0.44	X
	0.2		X			29.2			X
108.73					1.42			3.67	X
0.67					0.29			0.25	X
	0.27		0.79			6.72			0.02
0.29					2.32			0.27	X
2.41					0.81			1.23	X
56					X			32	X
3					X			X	X
26.3					124.7			16.4	X
1.64					14.68			1.79	X
	47		23			1272			X
533					530			100	X

Appendix 3: Whole Rock Geochemical data collected by Dr Caroline Forbes from samples of the Oorlano Metasomatite at various locations across the Northern Yorke Peninsula.

Samp_R#	1960849	1933075	1933076	1949812	1949813	1949050	1949051	1949008	1949009	1946895	1946896	1949055	1949780	1933085	1933086
DH_No	22962	23265	23265	23669	23669	23674	23674	30060	30060	139474	139474	139488	139488	143968	143968
DH_Name	SYP 602	Nth Kadina 1	Nth Kadina 1	DDH 153	DDH 153	DDH 158	DDH 158	Bute B31	Bute B31	PB 24	PB 24	PBD 38	PBD 38	PJ 1A	PJ 1A
East	767704	747787	747787	751171	751171	759856	759856	777888	777888	771179	771179	759504	759504	761879	761879
North	6214605	6247265	6247265	6243568	6243568	6246503	6246503	6243276	6243276	6264821	6264821	6267846	6267846	6160620	6160620
Zone	53	53	53	53	53	53	53	54	54	53	53	53	53	53	53
East - original	767704	747787	747787	751171	751171	759856	759856	223555	223555	771179	771179	759504	759504	761879	761879
Depth from	134	3.05	12.72	116.74	126.8	116.48	126.5	137.3	147.3	54.6	64.6	157.3	167.3	209.3	219.3
Depth to	136	4.26	13.71	117.8	127.8	117.5	127.5	138.3	148.3	55.6	65.6	158.3	168.3	210.3	220.3
Base_Cover	Basement	Basement	Basement	Basement	Basement	Basement	Basement	Basement	Basement	Basement	Basement	Basement	Basement	Basement	Basement
Date_req	27-Aug	16-Apr	16-Apr	15-Aug	15-Aug	18-Jul	18-Jul	4-Jul	4-Jul	14-May	14-May	18-Jul	18-Jul	16-Apr	16-Apr
Samp_type	Cuttings	Drill core	Drill core	Drill core	Drill core	Drill core	Drill core	Drill core	Drill core	Drill core	Drill core	Drill core	Drill core	Drill core	Drill core
Samp_from	B1	B1	B2	B1	B2	B1	B2	B1	B2	B1	B2	B1	B2	B1	B2
Au_ppb	0.5	0.5	0.5	0.5	2	0.5	0.5	1	1	0.5	0.5	8	0.5	0.5	0.5
Ag_ppm	0.025	0.025	0.025	0.025	0.025	0.025	0.025	0.21	0.07	0.025	0.025	0.09	0.06	0.31	0.025
Al2O3_pct	15.31	7.73	20.85	16.95	9.08	9.43	11.38	2.26	12.84	15.8	14.2	10.43	11.43	10.63	9.8
As_ppm	9	4.3	0.5	8	8	17.9	16.4	31.3	9.2	13.4	4.7	20.7	16.7	9.4	4
Ba_ppm	657.8	455.2	593.3	555.1	233.1	293.9	84.4	331.3	549.1	414.5	242.4	301.1	14.6	225	183.9
Be_ppm	5.7	1.8	3.8	1.2	1.4	0.6	1	0.5	2.2	3.1	1.5	11.1	3	3.1	4.1
Bi_ppm	0.03	0.05	0.05	0.13	0.005	0.15	1.37	0.15	0.09	0.13	0.06	1.3	0.05	0.04	0.09
CaO_pct	1.39	0.86	6.11	0.58	13.35	0.28	0.35	18.38	3.57	0.93	9.54	6.94	4.54	8.18	0.55
Cd_ppm	0.01	0.15	0.46	0.1	0.01	0.01	0.01	0.01	0.01	0.01	0.01	0.09	0.04	0.01	0.01
Ce_ppm	103	25.3	97.2	121.3	112.6	38.9	67.1	14.8	144	53	58.8	632.6	37.8	11.6	13.6
Co_ppm	7.4	3.5	13.6	19.1	35.5	5.8	20.9	8.8	14.8	43.6	28.4	34	10.9	23.8	102.9
Cr_ppm	71	23	96	71	54	22	44	32	71	393	309	66	58	39	36
Cs_ppm	15.46	0.88	6.1	3.2	1.88	0.31	1.28	0.58	7.58	4.54	4.09	0.93	0.44	2.63	1.84
Cu_ppm	33	26	51	25	33	96	426	35	14	55	29	135	34	92	42
Dy_ppm	6.93	2.36	6.51	3.03	2.66	1.8	4.1	2.36	3.02	2.97	2.78	8.41	8.87	2.42	1.84
Er_ppm	4.31	1.58	3.71	2.09	1.86	1.2	2.37	1.19	1.64	1.68	1.64	4.21	5.64	1.59	1.38
Eu_ppm	1.54	0.55	1.76	1.36	0.89	0.43	0.93	0.78	1.95	1.05	0.76	2.21	1.28	0.26	0.22
F_ppm	2306	410	2070	1536	782	369	626	356	2057	2652	1937	539	859	411	687
Fe2O3_pct	9.49	3.65	6.37	6.84	3.53	2.32	4.14	3.61	11.32	11.73	8.38	21.54	12.59	13.16	29.78
Ga_ppm	21	9.4	32.6	22.2	10.4	9.2	13.7	5.2	22.7	19.3	14.8	12.9	18.9	21.4	19.7
Gd_ppm	6.89	2.13	6.51	4.63	3.51	2.09	4.7	2.55	4.61	3.54	2.7	12.27	8.12	1.65	1.23
Ge_ppm	1.1	0.11	0.7	0.8	0.7	0.12	0.025	0.19	0.55	0.71	1.56	0.91	0.79	2.3	1.7
Hf_ppm	3.5	15.5	5.4	10.4	6.6	5.4	5.9	0.3	2.9	1.8	1.1	3.9	5.8	5.4	3.5
Ho_ppm	1.45	0.5	1.33	0.67	0.6	0.41	0.85	0.45	0.58	0.61	0.6	1.63	1.92	0.52	0.43
In_ppm	0.03	0.027	0.06	0.01	0.02	0.011	0.041	0.031	0.043	0.051	0.065	0.475	0.202	0.036	0.05
K2O_pct	8.08	2.96	3.13	10.56	2.27	2.1	1.8	0.71	3.79	3.3	2.4	3.1	0.1	2.96	1.81

La_ppm	54.8	12.2	49.6	88.3	60.9	19.6	35.3	6.3	72.9	28.9	36.9	356.4	12.3	5.9	6.8
Li_ppm	22.4	0.7	45.7	41	26.1	15.4	36.6	9.3	44.3	121.8	37.9	11.5	3.4	21.6	57.6
Lu_ppm	0.62	0.36	0.56	0.55	0.42	0.19	0.35	0.14	0.3	0.26	0.28	0.7	0.9	0.33	0.32
MgO_pct	1.94	0.74	2.13	5.06	3.7	1.82	2.62	12.31	6.65	10.1	8.87	4.56	3.2	2.05	6.12
MnO_pct	0.04	0.01	0.04	0.01	0.17	0.04	0.1	0.58	0.15	0.3	0.18	0.42	0.15	0.06	0.06
Mo_ppm	0.9	2.4	2	0.05	0.8	0.5	0.8	0.5	0.05	2.3	8	0.05	0.2	0.7	0.5
Na2O_pct	0.23	2.27	6.01	0.15	3.21	2.9	2.7	0.02	0.09	1.56	2.91	2.83	6.75	2.9	2.21
Nb_ppm	13.05	9.5	19.3	16.24	8.09	4.77	10.57	0.72	4.26	7.7	7.5	18.07	18.19	24.6	12.3
Nd_ppm	39.5	10.8	42.8	63.8	37	16.6	29.1	8.1	52.8	23.3	17.8	178.6	28.7	5.3	5.6
Ni_ppm	53	3	28	39	10	7	15	4	37	145	94	133	24	12	20
P2O5_pct	0.19	0.14	0.35	0.41	0.19	0.18	0.28	0.08	0.21	0.1	0.09	0.23	0.31	0.16	0.21
Pb_ppm	10	16	2.5	9	10	6	2.5	2.5	2.5	2.5	2.5	7	17	2.5	2.5
Pd_ppb	0.05	0.05	0.05	0.05	0.05	0.05	0.05	0.05	1	10	8	3	0.05	0.05	3
Pr_ppm	11.03	2.76	11.17	18.46	11.24	4.45	7.64	1.9	15.36	6.08	5.52	59.69	6.17	1.37	1.6
Pt_ppb	3	0.05	1	2	0.05	0.05	0.05	0.05	0.05	7	6	0.05	0.05	0.05	0.05
Rb_ppm	290.5	162.3	239.5	473	103.2	77.8	79.2	37	217.7	305.4	180.5	197.2	11.5	211.2	105
Re_ppm	0.002	0.002	0.002	0.002	0.002	0.002	0.002	0.002	0.002	0.007	0.004	0.002	0.002	0.002	0.002
S_ppm	218	148	703	176	954	25	108	6075	796	1215	167	25	25	1789	25
Sb_ppm	0.41	0.21	0.32	0.23	0.34	0.025	0.13	0.39	0.87	3.25	0.9	0.63	0.18	0.26	0.14
Sc_ppm	13	10	16	11	1	10	10	10	14	49	42	10	10	10	10
Se_ppm	0.025	4.4	3	0.025	0.025	0.025	1.4	1.8	0.7	2	4.8	2.4	1.6	2.7	4
SiO2_pct	59.37	80.03	51.22	56.3	53.45	78.55	70.98	32.09	50.83	47.57	48.72	46.77	58.88	52.32	45.93
Sm_ppm	7.58	2.39	7.83	9.12	5.49	2.83	5.51	2.25	8.05	4.4	3.16	20.26	7.67	1.32	1.12
Sn_ppm	6	19	15	5	3	2	2	2	31	3	2	11	12	9	20
Sr_ppm	30.3	87.3	184	23.6	66.4	18.2	20.2	33.7	20.7	46.9	143.6	88.5	15.6	40.3	14.7
Ta_ppm	1.4	1.2	2	1.7	1.2	0.7	1	0.2	1.1	0.5	0.4	1.2	1.3	22.1	2.8
Tb_ppm	1.01	0.35	0.96	0.53	0.45	0.28	0.64	0.4	0.54	0.49	0.42	1.46	1.29	0.31	0.23
Te_ppm	0.05	0.05	0.05	0.1	0.05	0.07	0.06	0.05	0.18	0.05	0.05	0.64	0.08	0.05	0.05
Th_ppm	16.93	18.11	24.22	26.06	16.06	9.52	17.76	1.71	19.19	2.39	2.79	19.4	35.83	14.03	12.37
TiO2_pct	0.56	0.39	0.8	0.69	0.39	0.23	0.41	0.08	0.52	0.71	0.65	0.48	0.51	0.37	0.5
Tl_ppm	0.8	0.27	0.4	0.92	0.25	0.36	0.6	0.28	0.73	0.92	0.4	0.36	0.01	0.45	0.27
Tm_ppm	0.63	0.31	0.59	0.4	0.31	0.2	0.35	0.17	0.27	0.26	0.27	0.62	0.85	0.34	0.27
U_ppm	3.11	7.09	8.9	6.7	5.1	2.18	4.47	1.67	4.11	3.12	1.12	2.96	7.94	6.39	4.63
V_ppm	95	40	103	84	40	21	53	18	79	253	197	197	123	74	112
W_ppm	4	3	2	2	0.05	2	5	2	12	28	1	0.05	1	0.05	2
Y_ppm	44.6	14.7	38.1	18.8	17.8	11.5	23.9	14	17.6	16.2	16.6	58.6	55.3	16.5	12.3
Yb_ppm	3.97	1.92	3.52	2.89	2.3	1.3	2.27	0.96	1.72	1.69	1.68	4.09	5.28	1.73	1.72
Zn_ppm	15	11	30	156	37	18	212	9	17	89	31	29	17	30	69
Zr_ppm	120	620	193	368	245	208	225	13	95	63	40	138	212	115	118

APPENDIX B: GEOCHRONOLOGICAL DATA

Appendix 4: Radiogenic isotope ratios of LA-ICPMS data of the Moonta Porphyry sample selected from the Poona Mine.

Analysis_#	Pb207/Pb206		Pb206/U238		Pb207/U235		Pb208/Th232	
STDGJ-01	0.06047	0.00087	0.10047	0.00134	0.83762	0.0138	0.03111	0.00084
STDGJ-02	0.06097	0.00088	0.09871	0.00132	0.82988	0.01362	0.0305	0.00082
STDGJ-03	0.05976	0.00086	0.09717	0.0013	0.80058	0.01317	0.02925	0.00079
STDGJ-04	0.06013	0.00087	0.09698	0.00129	0.80391	0.01319	0.0306	0.00082
PLES-01	0.06012	0.00078	0.05294	0.0007	0.43883	0.00669	0.02429	0.0004
PLES-02	0.05303	0.0007	0.05286	0.0007	0.38649	0.00598	0.01549	0.00027
STDGJ-05	0.0587	0.00085	0.09761	0.0013	0.79001	0.01301	0.03312	0.00087
MOONT-01	0.10764	0.00148	0.31203	0.00421	4.63056	0.07352	0.0861	0.00138
MOONT-02	0.01461	0.00215	0.38268	0.03203	0.66815	0.08772	0.00167	0.00035
MOONT-03	0.10542	0.00129	0.1967	0.00262	2.85895	0.04185	0.03292	0.00047
MOONT-04	0.10817	0.00122	0.26546	0.00351	3.95901	0.05528	0.06136	0.00085
MOONT-05	0.11367	0.00142	0.29765	0.00398	4.66443	0.06945	0.07595	0.00115
MOONT-06	0.10867	0.00149	0.30087	0.00407	4.50793	0.07121	0.07943	0.00117
MOONT-07	0.1064	0.00126	0.30414	0.00403	4.46161	0.06413	0.08165	0.00118
MOONT-08	0.11079	0.00123	0.17886	0.00235	2.73219	0.0376	0.04243	0.0006
MOONT-09	0.10602	0.00114	0.26846	0.00353	3.92424	0.05321	0.06468	0.0009
MOONT-10	0.1067	0.00143	0.30974	0.00413	4.55655	0.0707	0.0883	0.00138
MOONT-11	0.10725	0.0013	0.30948	0.00412	4.57628	0.06672	0.08421	0.00122
MOONT-12	0.10343	0.0019	0.20594	0.00287	2.93684	0.05766	0.03069	0.00061
MOONT-13	0.10622	0.00121	0.30894	0.00409	4.52454	0.06347	0.08359	0.0012
MOONT-14	0.10553	0.00138	0.2991	0.00397	4.35209	0.0661	0.08028	0.00125
MOONT-15	0.10739	0.00123	0.25007	0.00331	3.70264	0.0521	0.05193	0.00074
STDGJ-06	0.06088	0.00087	0.09761	0.0013	0.81923	0.01344	0.03121	0.00085
STDGJ-07	0.06051	0.00087	0.09776	0.00131	0.81554	0.01343	0.0304	0.00086
STDGJ-08	0.05985	0.00087	0.09699	0.0013	0.80039	0.01323	0.02929	0.00083
STDGJ-09	0.06007	0.00086	0.09824	0.00131	0.81354	0.01337	0.03043	0.00084
PLES-03	0.05672	0.00075	0.05327	0.00071	0.4166	0.00644	0.02014	0.00034
PLES-04	0.0536	0.00071	0.05284	0.0007	0.39047	0.00606	0.01547	0.00028
STDGJ-10	0.06139	0.00088	0.09728	0.0013	0.82331	0.0135	0.03343	0.0009
MOONT-16	0.1089	0.0014	0.30733	0.00412	4.61431	0.06998	0.08508	0.00128
MOONT-17	0.10772	0.00134	0.29861	0.00399	4.43469	0.06596	0.07938	0.00118
MOONT-18	0.10426	0.00115	0.1922	0.00254	2.76281	0.03798	0.0384	0.00053
MOONT-19	0.10635	0.00131	0.28433	0.00378	4.16901	0.0613	0.04143	0.00063
MOONT-20	0.10749	0.00129	0.29979	0.00399	4.44264	0.06436	0.08022	0.00119
MOONT-21	0.10537	0.00123	0.29177	0.00386	4.23867	0.06031	0.07152	0.00106
MOONT-22	0.10776	0.0014	0.31544	0.00423	4.68639	0.07145	0.08827	0.00132
MOONT-23	0.10733	0.00145	0.28129	0.00379	4.16248	0.06515	0.07332	0.00113
MOONT-24	0.10719	0.00147	0.3018	0.00407	4.46028	0.07063	0.08393	0.00131
MOONT-25	0.10789	0.00129	0.29653	0.00395	4.41062	0.06386	0.05115	0.00074
MOONT-26	0.10567	0.00132	0.30654	0.00409	4.46599	0.0663	0.07905	0.00119
MOONT-27	0.10753	0.00136	0.30422	0.00407	4.51027	0.0677	0.08306	0.00127
MOONT-28	0.10589	0.00137	0.30711	0.00413	4.48338	0.06849	0.08258	0.00123
MOONT-29	0.10733	0.00135	0.26465	0.00354	3.91617	0.05842	0.05951	0.00091
MOONT-30	0.10538	0.00123	0.28162	0.00374	4.09176	0.05844	0.0486	0.00072
STDGJ-11	0.05919	0.00087	0.09762	0.00131	0.79662	0.01332	0.02832	0.00085
STDGJ-12	0.06043	0.00088	0.09803	0.00131	0.81675	0.01359	0.03065	0.00088
STDGJ-13	0.06021	0.00089	0.09684	0.0013	0.80385	0.01348	0.0309	0.00088
STDGJ-14	0.06015	0.00089	0.09737	0.00131	0.80739	0.01355	0.03309	0.00092
PLES-05	0.05445	0.00073	0.05362	0.00071	0.40252	0.00631	0.01756	0.00032
PLES-06	0.05336	0.00072	0.05307	0.00071	0.39044	0.00617	0.01603	0.0003
STDGJ-15	0.06035	0.00089	0.09698	0.0013	0.80694	0.01347	0.03134	0.0009
MOONT-31	0.10756	0.0013	0.27248	0.00363	4.04075	0.05906	0.02988	0.00045
MOONT-32	0.1075	0.00128	0.2253	0.003	3.3393	0.04826	0.05013	0.00076
MOONT-33	0.10658	0.00142	0.30736	0.00414	4.51637	0.07016	0.0837	0.00132
MOONT-34	0.10669	0.00143	0.26029	0.00351	3.82884	0.05976	0.03078	0.00048
MOONT-35	0.10458	0.00126	0.21296	0.00284	3.07056	0.04479	0.03425	0.00052
MOONT-36	0.10587	0.00129	0.21475	0.00287	3.13465	0.04587	0.02321	0.00035
MOONT-37	0.10732	0.00148	0.28456	0.00386	4.2103	0.06709	0.07437	0.00118
MOONT-38	0.10565	0.00139	0.30026	0.00404	4.37352	0.06759	0.07422	0.0012
MOONT-39	0.10141	0.00149	0.22518	0.00305	3.14837	0.05239	0.01769	0.00029
MOONT-40	0.1068	0.00129	0.28759	0.00384	4.23465	0.06192	0.06718	0.00103
MOONT-41	0.10611	0.00121	0.2858	0.0038	4.18126	0.05875	0.04884	0.00067
MOONT-42	0.10766	0.00143	0.30275	0.00409	4.49376	0.06969	0.07914	0.00122
MOONT-43	0.10914	0.00151	0.15149	0.00205	2.2795	0.03634	0.01451	0.00023
MOONT-44	0.10553	0.00132	0.23252	0.00313	3.38311	0.05063	0.02216	0.00036
MOONT-45	0.10677	0.0013	0.30278	0.00404	4.45724	0.06536	0.08124	0.00128
STDGJ-16	0.06028	0.00089	0.09695	0.0013	0.80571	0.01358	0.03142	0.0009
STDGJ-17	0.05981	0.0009	0.09645	0.0013	0.79534	0.01349	0.02971	0.00087

STDGJ-18	0.06076	0.00091	0.09651	0.0013	0.80838	0.01375	0.02938	0.00088
STDGJ-19	0.05932	0.00089	0.09701	0.0013	0.79332	0.01354	0.03085	0.00091
PLES-07	0.05378	0.00072	0.05306	0.00071	0.39342	0.00617	0.01729	0.00032
PLES-08	0.05568	0.00074	0.05335	0.00071	0.40958	0.0064	0.01848	0.00033
STDGJ-20	0.05893	0.00088	0.09798	0.00132	0.796	0.0135	0.03194	0.00092
MOONT-46	0.10642	0.00141	0.30946	0.00416	4.5405	0.07041	0.08453	0.00142
MOONT-47	0.10537	0.00146	0.29705	0.00401	4.31521	0.06893	0.05451	0.00094
MOONT-48	0.1066	0.00173	0.30212	0.00421	4.44017	0.08028	0.05219	0.00113
MOONT-49	0.10712	0.00125	0.19927	0.00265	2.94302	0.04217	0.05648	0.00092
MOONT-50	0.10596	0.00144	0.30217	0.00409	4.41424	0.06988	0.08077	0.00134
MOONT-51	0.11013	0.00152	0.29777	0.00403	4.52131	0.0722	0.07893	0.00134
MOONT-52	0.10807	0.00147	0.29424	0.00397	4.3837	0.0692	0.07855	0.00135
MOONT-53	0.10636	0.00134	0.29193	0.00391	4.28064	0.06431	0.04239	0.00071
MOONT-54	0.10572	0.00129	0.27973	0.00374	4.07718	0.06013	0.05466	0.0009
MOONT-55	0.10752	0.00148	0.30729	0.00415	4.55531	0.07247	0.08547	0.00146
MOONT-56	0.10627	0.00131	0.31227	0.00417	4.57522	0.06778	0.0833	0.0014
MOONT-57	0.10688	0.00149	0.29636	0.00401	4.36702	0.07025	0.07677	0.00137
MOONT-58	0.10735	0.00134	0.29901	0.004	4.42535	0.06601	0.06941	0.00117
MOONT-59	0.0997	0.00123	0.20066	0.00268	2.75815	0.04079	0.02473	0.0004
MOONT-60	0.10861	0.00148	0.2867	0.00388	4.29319	0.06787	0.07194	0.0012
STDGJ-21	0.06016	0.00091	0.0974	0.00131	0.8078	0.01384	0.03102	0.00092
STDGJ-22	0.06049	0.00091	0.09704	0.00131	0.80923	0.01384	0.03097	0.00091
STDGJ-23	0.06035	0.00091	0.09674	0.0013	0.80484	0.01381	0.02853	0.00088
STDGJ-24	0.06026	0.00092	0.09707	0.00131	0.80643	0.01386	0.03054	0.00092
PLES-09	0.05418	0.00075	0.05421	0.00072	0.40491	0.0065	0.01746	0.00035
PLES-10	0.05482	0.00076	0.05366	0.00072	0.40557	0.00653	0.01857	0.00037
STDGJ-25	0.05926	0.0009	0.09781	0.00132	0.79911	0.01371	0.02842	0.00088
MOONT-61	0.10782	0.00141	0.30556	0.00412	4.54225	0.07019	0.07987	0.00139
MOONT-62	0.10762	0.00146	0.10916	0.00148	1.61954	0.02567	0.03541	0.00069
MOONT-63	0.10467	0.00148	0.26479	0.00358	3.82093	0.06197	0.02453	0.00045
MOONT-64	0.10938	0.00143	0.31746	0.00426	4.78705	0.0736	0.09972	0.00186
MOONT-65	0.10846	0.00141	0.30669	0.00413	4.58589	0.07027	0.0743	0.00126
MOONT-66	0.10637	0.00129	0.31111	0.00416	4.56262	0.06687	0.08078	0.00136
MOONT-67	0.10798	0.00142	0.29999	0.00405	4.46578	0.0693	0.07502	0.00132
MOONT-68	0.1066	0.00155	0.30822	0.00419	4.52989	0.07497	0.08656	0.00166
MOONT-69	0.10708	0.00141	0.30907	0.00416	4.56253	0.07061	0.08421	0.00152
MOONT-70	0.10648	0.00152	0.30845	0.0042	4.52823	0.07439	0.08283	0.00153
MOONT-71	0.10569	0.00146	0.21368	0.00289	3.11348	0.04987	0.05376	0.00099
MOONT-72	0.10534	0.0014	0.13346	0.0018	1.93825	0.02979	0.06683	0.00091
MOONT-73	0.10762	0.00145	0.31117	0.00421	4.61691	0.0727	0.08464	0.00157
MOONT-74	0.11119	0.00197	0.30393	0.00432	4.65864	0.08997	0.07349	0.00167
MOONT-75	0.10985	0.00157	0.31171	0.00424	4.72051	0.07739	0.08724	0.00165
STDGJ-26	0.06005	0.00092	0.0989	0.00134	0.8188	0.01415	0.02852	0.00089
STDGJ-27	0.05983	0.00093	0.09826	0.00133	0.81059	0.01417	0.02747	0.00088
STDGJ-28	0.05854	0.00091	0.09792	0.00133	0.79029	0.01382	0.02896	0.00091
STDGJ-29	0.06207	0.00095	0.09846	0.00133	0.84263	0.01459	0.04148	0.00115
PLES-11	0.0521	0.00074	0.05418	0.00073	0.38912	0.00638	0.0162	0.00034
PLES-12	0.05713	0.0008	0.05374	0.00072	0.42328	0.00686	0.02162	0.00044
STDGJ-30	0.0606	0.00093	0.09784	0.00132	0.81745	0.01419	0.02932	0.00092
MOONT-76	0.11054	0.00156	0.29433	0.00399	4.48524	0.07303	0.08318	0.00165
MOONT-77	0.10824	0.00153	0.30972	0.00421	4.62169	0.07525	0.08453	0.00163
MOONT-78	0.10721	0.00163	0.2954	0.00403	4.36642	0.07478	0.05468	0.00117
MOONT-79	0.1066	0.00141	0.29548	0.00398	4.3425	0.06761	0.04701	0.00091
MOONT-80	0.10659	0.00147	0.19532	0.00264	2.87002	0.04603	0.02055	0.00041
MOONT-81	0.10779	0.00145	0.2895	0.00392	4.3024	0.06761	0.06825	0.00123
MOONT-82	0.10826	0.00144	0.30016	0.00405	4.47986	0.06992	0.07031	0.00137
MOONT-83	0.10639	0.00142	0.1977	0.00268	2.89977	0.04576	0.01481	0.0003
MOONT-84	0.10428	0.00147	0.22115	0.003	3.17942	0.05184	0.02238	0.00044
MOONT-85	0.10727	0.0018	0.30659	0.00411	4.53337	0.08352	0.09451	0.00326
MOONT-86	0.10357	0.00145	0.17306	0.00234	2.47104	0.04005	0.01945	0.00039
MOONT-87	0.10685	0.00147	0.23489	0.00318	3.46033	0.05531	0.03559	0.00071
MOONT-88	0.10042	0.00123	0.14067	0.00188	1.94758	0.02888	0.01929	0.00036
STDGJ-31	0.05976	0.00094	0.09801	0.00133	0.80749	0.0143	0.03043	0.00093
STDGJ-32	0.06108	0.00096	0.09794	0.00133	0.82478	0.01458	0.03551	0.00107

Appendix 5: Ages of zircon spots from LA-ICPMS of the Moonta Porphyry sample selected from the Poona Mine.

Analysis_#	Pb207/Pb206		Pb206/U238		Pb207/U235		Pb208/Th232	
STDGJ-01	620.4	30.89	617.2	7.85	617.8	7.62	619.2	16.45
STDGJ-02	638.3	30.65	606.9	7.72	613.5	7.56	607.3	16.17
STDGJ-03	594.5	31.19	597.8	7.62	597.2	7.42	582.8	15.57

STDGJ-04	608.1	30.81	596.7	7.6	599	7.43	609.2	16.14
PLES-01	607.8	27.84	332.6	4.29	369.4	4.72	485.1	7.82
PLES-02	329.9	29.66	332.1	4.29	331.8	4.38	310.7	5.36
STDGJ-05	556.1	31.19	600.4	7.64	591.2	7.38	658.7	16.97
MOONT-01	1759.9	24.96	1750.7	20.68	1754.8	13.26	1669.3	25.62
MOONT-02	0.1	0	2088.8	149.33	519.6	53.39	33.7	7.07
MOONT-03	1721.7	22.26	1157.6	14.11	1371.2	11.01	654.6	9.13
MOONT-04	1768.8	20.56	1517.7	17.9	1625.8	11.32	1203.7	16.15
MOONT-05	1858.8	22.48	1679.6	19.76	1760.9	12.45	1479.5	21.67
MOONT-06	1777.3	24.79	1695.6	20.15	1732.4	13.13	1544.8	21.87
MOONT-07	1738.6	21.64	1711.8	19.93	1723.9	11.92	1586.5	22.02
MOONT-08	1812.4	20.03	1060.8	12.87	1337.3	10.23	840	11.69
MOONT-09	1732.1	19.67	1533	17.96	1618.7	10.97	1266.9	17.16
MOONT-10	1743.7	24.33	1739.4	20.33	1741.4	12.92	1710.2	25.6
MOONT-11	1753.3	21.98	1738.1	20.27	1745	12.15	1634.2	22.82
MOONT-12	1686.5	33.51	1207.2	15.34	1391.5	14.87	611	11.93
MOONT-13	1735.6	20.77	1735.5	20.13	1735.5	11.67	1622.5	22.31
MOONT-14	1723.6	23.76	1686.8	19.68	1703.3	12.54	1560.9	23.45
MOONT-15	1755.7	20.74	1438.8	17.08	1571.9	11.25	1023.4	14.14
STDGJ-06	634.9	30.61	600.4	7.66	607.6	7.5	621.1	16.64
STDGJ-07	621.7	30.81	601.3	7.67	605.6	7.51	605.3	16.84
STDGJ-08	598.3	31.08	596.8	7.62	597	7.46	583.6	16.37
STDGJ-09	605.9	30.79	604.1	7.7	604.4	7.48	605.8	16.47
PLES-03	480	29.17	334.6	4.33	353.6	4.61	403	6.8
PLES-04	354.2	29.63	331.9	4.29	334.7	4.42	310.2	5.48
STDGJ-10	652.8	30.45	598.4	7.64	609.9	7.52	664.6	17.51
MOONT-16	1781.1	23.3	1727.6	20.33	1751.9	12.66	1650.4	23.9
MOONT-17	1761.2	22.59	1684.4	19.82	1718.8	12.32	1544	22.19
MOONT-18	1701.4	20.13	1133.3	13.74	1345.6	10.25	761.6	10.36
MOONT-19	1737.8	22.37	1613.1	18.99	1668	12.04	820.6	12.18
MOONT-20	1757.2	21.7	1690.3	19.78	1720.3	12.01	1559.6	22.24
MOONT-21	1720.8	21.29	1650.3	19.28	1681.5	11.69	1396.1	19.96
MOONT-22	1761.9	23.46	1767.4	20.74	1764.8	12.76	1709.6	24.6
MOONT-23	1754.6	24.39	1597.8	19.08	1666.7	12.81	1430.1	21.36
MOONT-24	1752.2	24.82	1700.2	20.16	1723.6	13.13	1629	24.49
MOONT-25	1764	21.65	1674.1	19.65	1714.3	11.98	1008.3	14.23
MOONT-26	1726	22.7	1723.7	20.17	1724.7	12.32	1537.8	22.27
MOONT-27	1758	22.93	1712.2	20.11	1732.9	12.47	1612.7	23.66
MOONT-28	1729.7	23.62	1726.5	20.36	1727.9	12.68	1603.8	22.9
MOONT-29	1754.6	22.7	1513.6	18.03	1617	12.07	1168.5	17.37
MOONT-30	1721	21.35	1599.5	18.81	1652.7	11.65	959.2	13.87
STDGJ-11	574.1	31.65	600.4	7.68	594.9	7.53	564.5	16.62
STDGJ-12	619.1	31.18	602.8	7.71	606.2	7.59	610.3	17.17
STDGJ-13	611	31.56	595.9	7.63	599	7.59	615.1	17.24
STDGJ-14	608.8	31.62	599	7.67	601	7.61	658	17.91
PLES-05	389.5	29.75	336.7	4.37	343.5	4.57	351.9	6.28
PLES-06	344.2	30.3	333.3	4.32	334.7	4.5	321.4	5.89
STDGJ-15	616.3	31.37	596.7	7.64	600.7	7.57	623.8	17.57
MOONT-31	1758.5	21.96	1553.4	18.4	1642.4	11.9	595.1	8.86
MOONT-32	1757.5	21.58	1309.8	15.77	1490.3	11.29	988.7	14.61
MOONT-33	1741.7	24.08	1727.7	20.42	1734	12.91	1624.6	24.56
MOONT-34	1743.7	24.25	1491.3	17.95	1598.8	12.57	612.8	9.36
MOONT-35	1707	22.06	1244.6	15.1	1425.4	11.17	680.7	10.17
MOONT-36	1729.5	22.13	1254.1	15.22	1441.2	11.27	463.7	6.82
MOONT-37	1754.4	24.98	1614.3	19.37	1676	13.07	1449.9	22.12
MOONT-38	1725.6	24.03	1692.6	20.01	1707.3	12.77	1447.1	22.57
MOONT-39	1650.1	27	1309.2	16.06	1444.6	12.82	354.5	5.78
MOONT-40	1745.5	21.94	1629.5	19.23	1680.8	12.01	1314.2	19.5
MOONT-41	1733.7	20.78	1620.5	19.06	1670.4	11.51	963.8	12.96
MOONT-42	1760.2	23.99	1704.9	20.22	1729.8	12.88	1539.5	22.93
MOONT-43	1785	25.02	909.3	11.47	1206	11.25	291.2	4.63
MOONT-44	1723.7	22.74	1347.7	16.35	1500.5	11.73	442.9	7.19
MOONT-45	1745.1	22.02	1705.1	20	1723	12.16	1578.8	23.85
STDGJ-16	613.6	31.72	596.5	7.65	600	7.63	625.4	17.64
STDGJ-17	596.7	32.09	593.6	7.62	594.2	7.63	591.7	17.15
STDGJ-18	630.6	32.03	593.9	7.63	601.5	7.72	585.3	17.21
STDGJ-19	578.8	32.43	596.8	7.66	593.1	7.66	614.2	17.93
PLES-07	361.9	30.02	333.3	4.33	336.9	4.49	346.4	6.29
PLES-08	439.3	28.95	335.1	4.35	348.6	4.61	370.2	6.58
STDGJ-20	564.5	32.23	602.5	7.73	594.6	7.63	635.5	18.02
MOONT-46	1739	24.06	1738	20.5	1738.4	12.9	1640.2	26.39
MOONT-47	1720.7	25.21	1676.7	19.94	1696.3	13.17	1072.8	18.09
MOONT-48	1742.1	29.45	1701.8	20.84	1719.9	14.98	1028.3	21.8
MOONT-49	1751	21.22	1171.4	14.24	1393.1	10.86	1110.5	17.51
MOONT-50	1731	24.79	1702	20.24	1715	13.1	1569.9	25.12
MOONT-51	1801.6	24.91	1680.2	20.04	1734.9	13.28	1535.5	25.18

MOONT-52	1767	24.65	1662.7	19.79	1709.3	13.05	1528.5	25.25
MOONT-53	1737.9	22.94	1651.2	19.5	1689.6	12.37	839.2	13.76
MOONT-54	1726.9	22.31	1590	18.82	1649.8	12.03	1075.7	17.34
MOONT-55	1757.9	24.85	1727.4	20.48	1741.1	13.25	1657.7	27.25
MOONT-56	1736.4	22.43	1751.9	20.5	1744.8	12.34	1617.2	26.14
MOONT-57	1747	25.27	1673.2	19.94	1706.1	13.29	1495	25.71
MOONT-58	1754.9	22.53	1686.4	19.87	1717.1	12.35	1356.3	22.1
MOONT-59	1618.5	22.7	1178.8	14.41	1344.3	11.02	493.8	7.93
MOONT-60	1776.2	24.65	1625	19.46	1692.1	13.02	1404.1	22.68
STDGJ-21	609.3	32.39	599.1	7.71	601.2	7.77	617.5	18.03
STDGJ-22	621	32.25	597	7.68	602	7.77	616.5	17.84
STDGJ-23	616	32.39	595.3	7.67	599.6	7.77	568.5	17.38
STDGJ-24	612.9	32.5	597.2	7.69	600.5	7.79	608	18
PLES-09	378.4	30.92	340.3	4.43	345.2	4.7	349.8	6.87
PLES-10	404.9	30.49	337	4.39	345.7	4.72	371.9	7.27
STDGJ-25	576.7	32.61	601.6	7.74	596.3	7.74	566.5	17.21
MOONT-61	1763	23.74	1718.8	20.32	1738.7	12.86	1553.1	26.06
MOONT-62	1759.5	24.51	667.8	8.61	977.8	9.95	703.4	13.46
MOONT-63	1708.5	25.72	1514.3	18.26	1597.2	13.05	489.8	8.84
MOONT-64	1789	23.58	1777.3	20.83	1782.6	12.91	1921.3	34.18
MOONT-65	1773.6	23.5	1724.4	20.4	1746.7	12.77	1448.6	23.68
MOONT-66	1738.2	21.99	1746.2	20.46	1742.5	12.21	1570.2	25.44
MOONT-67	1765.5	23.95	1691.2	20.07	1724.6	12.87	1462.1	24.85
MOONT-68	1742.2	26.25	1731.9	20.65	1736.5	13.77	1678	30.82
MOONT-69	1750.2	23.79	1736.1	20.49	1742.5	12.89	1634.2	28.33
MOONT-70	1740	26	1733.1	20.7	1736.2	13.66	1608.5	28.55
MOONT-71	1726.3	25.18	1248.4	15.35	1436	12.31	1058.3	19.08
MOONT-72	1720.3	24.27	807.6	10.25	1094.4	10.3	1307.6	17.23
MOONT-73	1759.5	24.35	1746.4	20.68	1752.3	13.14	1642.2	29.27
MOONT-74	1818.9	31.75	1710.8	21.36	1759.8	16.14	1433.4	31.52
MOONT-75	1796.8	25.77	1749.1	20.85	1770.9	13.74	1690.6	30.74
STDGJ-26	605.4	32.7	608	7.84	607.4	7.9	568.3	17.55
STDGJ-27	597.6	33.26	604.2	7.8	602.8	7.95	547.8	17.3
STDGJ-28	550.1	33.51	602.2	7.78	591.3	7.84	577	17.83
STDGJ-29	676.7	32.43	605.4	7.81	620.6	8.04	821.4	22.26
PLES-11	289.7	32.09	340.1	4.45	333.7	4.66	324.8	6.81
PLES-12	496	30.72	337.4	4.41	358.4	4.89	432.4	8.69
STDGJ-30	625.1	32.8	601.8	7.77	606.6	7.93	584.1	18
MOONT-76	1808.2	25.48	1663.1	19.88	1728.2	13.52	1615	30.79
MOONT-77	1769.9	25.6	1739.3	20.71	1753.2	13.59	1640.1	30.39
MOONT-78	1752.6	27.45	1668.5	20.05	1706	14.15	1076.1	22.46
MOONT-79	1742.1	23.94	1668.9	19.81	1701.5	12.85	928.6	17.49
MOONT-80	1741.8	25.06	1150.1	14.22	1374.1	12.08	411.2	8.13
MOONT-81	1762.5	24.3	1639	19.59	1693.8	12.95	1334.4	23.32
MOONT-82	1770.2	24.06	1692.1	20.06	1727.2	12.96	1373.4	25.8
MOONT-83	1738.5	24.34	1163	14.41	1381.9	11.91	297.2	6.02
MOONT-84	1701.7	25.82	1287.9	15.84	1452.2	12.59	447.4	8.6
MOONT-85	1753.6	30.34	1723.9	20.26	1737.1	15.33	1825.3	60.28
MOONT-86	1689.1	25.64	1029	12.85	1263.6	11.72	389.4	7.81
MOONT-87	1746.4	24.84	1360.1	16.58	1518.2	12.59	706.8	13.92
MOONT-88	1631.9	22.6	848.5	10.64	1097.6	9.95	386.2	7.09
STDGJ-31	594.7	34.12	602.7	7.81	601	8.04	606	18.22
STDGJ-32	642.2	33.44	602.3	7.8	610.7	8.11	705.2	20.93

Appendix 6: Radiogenic isotope ratios of LA-ICPMS data of the Oorlano Metasomatite (Harlequin Stone) sample selected from the Orallaw Quarry.

Grain Spot	Pb206/U238	±	Pb207/U235	±	Pb207/Pb206	±
1.1	0.31901	0.00479	4.79505	0.07409	0.10903	0.00121
2.1	0.24037	0.0036	3.833	0.05864	0.11567	0.00126
3.1	0.25395	0.0038	3.78127	0.05735	0.108	0.00115
4.1	0.25615	0.00384	5.97067	0.09057	0.16907	0.00181
5.1	0.24267	0.00364	3.81731	0.05839	0.1141	0.00124
6.1	0.283	0.00423	5.70667	0.08604	0.14626	0.00154
7.1	0.29344	0.00439	6.24458	0.094	0.15436	0.00162
8.1	0.22996	0.00344	4.09935	0.0618	0.1293	0.00136
9.1	0.23462	0.00351	3.83481	0.05846	0.11855	0.00128
10.1	0.37427	0.00559	11.72111	0.17469	0.22716	0.00233
11.1	0.35065	0.00525	6.15541	0.09299	0.12733	0.00135
12.1	0.26133	0.00392	4.48707	0.06869	0.12454	0.00136
13.1	0.2844	0.00426	4.51704	0.0692	0.1152	0.00126
14.1	0.31928	0.00478	6.23344	0.09464	0.14161	0.00151
15.1	0.32116	0.00481	7.43716	0.11181	0.16797	0.00176

16.1	0.25619	0.00385	4.24765	0.06617	0.12026	0.00136
17.1	0.31587	0.00473	6.02034	0.09128	0.13825	0.00147
18.1	0.16601	0.00248	3.91411	0.05874	0.17102	0.00178
19.1	0.30479	0.00468	4.39777	0.07957	0.10466	0.00155
20.1	0.27184	0.0041	4.68313	0.07407	0.12496	0.00145
21.1	0.25129	0.00376	4.91846	0.07384	0.14198	0.00148
22.1	0.33799	0.00506	7.58675	0.11454	0.16282	0.00171
23.1	0.30903	0.00463	5.51642	0.08417	0.12948	0.0014
24.1	0.40643	0.00609	10.12375	0.1531	0.18068	0.00191
25.1	0.31493	0.00473	5.077	0.07885	0.11693	0.00131
26.1	0.26687	0.004	4.92599	0.07447	0.13389	0.00141
27.1	0.3121	0.00467	5.65195	0.08536	0.13136	0.00138
28.1	0.17281	0.00259	3.16943	0.04864	0.13304	0.00145
29.1	0.17688	0.00265	3.2464	0.049	0.13313	0.0014
30.1	0.18392	0.00276	4.82271	0.07333	0.1902	0.00204
31.1	0.3109	0.00467	4.73787	0.07317	0.11054	0.00122
32.1	0.22786	0.00341	4.23496	0.06418	0.13482	0.00143
33.1	0.27629	0.00416	4.2344	0.06658	0.11117	0.00127
34.1	0.327	0.00491	5.15036	0.07905	0.11425	0.00124
35.1	0.33182	0.00497	5.19436	0.07912	0.11355	0.00121
36.1	0.31705	0.00477	5.13757	0.08007	0.11754	0.00132
37.1	0.28764	0.00433	5.03891	0.07839	0.12707	0.00142
38.1	0.30127	0.00453	4.57956	0.07094	0.11026	0.00122
39.1	0.2339	0.00356	5.79511	0.09435	0.17971	0.00222
40.1	0.31956	0.00485	5.00336	0.08231	0.11357	0.00142
41.1	0.31497	0.00474	5.04022	0.07888	0.11608	0.00131
41.2	0.21116	0.00317	3.87834	0.05936	0.13323	0.00144
42.1	0.32319	0.00484	5.04017	0.07677	0.11312	0.00121
43.1	0.367	0.00551	7.79029	0.11936	0.15397	0.00167
44.1	0.22441	0.00336	3.78348	0.05743	0.12229	0.0013
45.1	0.29291	0.0044	5.03084	0.07764	0.12459	0.00137
46.1	0.36098	0.00541	12.20724	0.18432	0.2453	0.00256
47.1	0.26494	0.00399	4.5128	0.07075	0.12356	0.0014
48.1	0.3121	0.00472	4.92568	0.07916	0.11448	0.00136
48.2	0.32348	0.00489	5.12061	0.08255	0.11482	0.00138
49.1	0.29636	0.00445	4.61303	0.07153	0.11291	0.00125
50.1	0.2896	0.00435	4.65221	0.07206	0.11653	0.00129
51.1	0.25664	0.00385	3.59763	0.05537	0.10168	0.00111
52.1	0.27733	0.00416	5.96689	0.09114	0.15607	0.00167
53.1	0.25367	0.00381	5.52244	0.08515	0.15791	0.00173
54.1	0.18646	0.0028	2.99397	0.04643	0.11647	0.00129
55.1	0.32293	0.00485	5.06929	0.07868	0.11387	0.00126
55.2	0.33031	0.00497	5.18303	0.0811	0.11382	0.00128
56.1	0.37028	0.00556	8.84898	0.13471	0.17335	0.00184
57.1	0.18013	0.00271	3.5471	0.05479	0.14284	0.00157
58.1	0.30178	0.00454	4.56498	0.0715	0.10973	0.00124
59.1	1.15501	0.01732	52.14968	0.79089	0.32752	0.00344
60.1	0.31245	0.00471	5.69132	0.08924	0.13213	0.00149
61.1	0.14211	0.00215	2.4001	0.0384	0.12251	0.00144
62.1	0.30121	0.00455	5.0243	0.08062	0.121	0.00143
63.1	0.31522	0.00475	5.02951	0.07884	0.11574	0.0013
64.1	0.28775	0.00433	4.52404	0.07089	0.11405	0.00128
65.1	0.30111	0.00453	5.53576	0.08584	0.13336	0.00147
66.1	0.1165	0.00176	2.20107	0.03463	0.13705	0.00156
67.1	0.24528	0.00371	3.90196	0.06331	0.1154	0.00139
68.1	0.19224	0.0029	2.94318	0.04678	0.11105	0.00129
69.1	0.29824	0.00448	4.58562	0.07074	0.11153	0.00121
70.1	0.26533	0.00399	4.70481	0.07262	0.12863	0.0014
71.1	0.2857	0.0043	4.71549	0.07412	0.11972	0.00136
72.1	0.29041	0.00437	4.57754	0.07139	0.11434	0.00127
73.1	0.46104	0.00694	16.72282	0.25786	0.26311	0.00286
74.1	0.29634	0.00448	7.15609	0.11364	0.17517	0.00203
74.2	0.28549	0.00434	7.30586	0.11742	0.18563	0.00221
75.1	0.24539	0.0037	4.35832	0.06824	0.12884	0.00144
76.1	0.25685	0.00388	4.07616	0.0648	0.11512	0.00133
77.1	0.17502	0.00263	3.07191	0.0476	0.12732	0.00139
78.1	0.30608	0.00461	4.6838	0.07323	0.111	0.00124
79.1	0.28159	0.00425	4.50766	0.0712	0.11612	0.00132
80.1	0.12275	0.00185	2.42008	0.03767	0.14301	0.00158
81.1	0.31753	0.00479	5.13146	0.08149	0.11723	0.00135
82.1	0.17027	0.00257	3.00801	0.04796	0.12815	0.00149
83.1	0.2252	0.00339	3.56017	0.05603	0.11468	0.0013
84.1	0.34782	0.00523	8.0774	0.12499	0.16846	0.00184
85.1	0.18233	0.00274	3.24548	0.05024	0.12912	0.00141
85.2	0.20906	0.00314	3.06404	0.04751	0.10631	0.00116
86.1	0.25492	0.00385	3.86346	0.06137	0.10994	0.00126

86.2	0.19899	0.003	3.33169	0.05289	0.12145	0.0014
87.1	0.27078	0.00408	4.11028	0.06514	0.11011	0.00126
88.1	0.30863	0.00465	4.7973	0.07487	0.11275	0.00125
89.1	0.06268	0.00095	1.04964	0.0166	0.12147	0.00138
90.1	0.29476	0.00448	4.46805	0.07419	0.10996	0.00138
91.1	0.2989	0.00453	4.48083	0.07342	0.10874	0.00133
92.1	0.23659	0.00357	3.57042	0.05685	0.10947	0.00126
93.1	0.18771	0.00283	3.50116	0.05485	0.1353	0.00151
94.1	0.26396	0.00398	4.18018	0.06645	0.11488	0.00132
95.1	0.25298	0.00381	4.3693	0.06849	0.12528	0.0014
96.1	0.32988	0.00497	6.07425	0.09571	0.13357	0.00151
97.1	0.24075	0.00363	6.02671	0.094	0.18159	0.00201
98.1	0.33325	0.00503	5.65873	0.08927	0.12317	0.00139
99.1	0.31057	0.00468	4.87484	0.07723	0.11386	0.0013
100.1	0.22773	0.00343	4.36375	0.06844	0.139	0.00155
101.1	0.20849	0.00315	4.14543	0.06563	0.14423	0.00164
102.1	0.24914	0.00376	4.0971	0.06537	0.11929	0.00138
103.1	0.25895	0.00391	4.39307	0.06977	0.12306	0.00141
104.1	0.18957	0.00286	3.20993	0.05144	0.12283	0.00143
105.1	0.12164	0.00183	3.40637	0.0534	0.20314	0.00226
106.1	0.24894	0.00376	4.52179	0.07173	0.13176	0.0015
107.1	0.26255	0.00396	4.62198	0.07326	0.1277	0.00145
107.2	0.39005	0.00589	9.24982	0.14664	0.17202	0.00196
108.1	0.30397	0.00459	4.82302	0.0774	0.1151	0.00134
109.1	0.25066	0.00378	3.99707	0.06304	0.11567	0.0013
110.1	0.26063	0.00394	4.56261	0.07347	0.12699	0.00149
111.1	0.29289	0.00443	4.61441	0.07414	0.11428	0.00134
112.1	0.45248	0.00686	12.47098	0.20012	0.19993	0.00234
113.1	0.21187	0.0032	3.43283	0.05542	0.11753	0.00139
114.1	0.33406	0.00504	8.74801	0.13824	0.18996	0.00214
115.1	0.24891	0.00376	4.44978	0.07104	0.12968	0.00149
116.1	0.31126	0.00472	6.25829	0.10218	0.14585	0.00176
116.2	0.30433	0.00462	7.12747	0.11559	0.16989	0.00202
117.1	0.33311	0.00507	5.40737	0.09035	0.11775	0.00148
118.1	0.21753	0.00328	5.45182	0.08626	0.1818	0.00205
119.1	0.26719	0.00405	4.64469	0.07563	0.1261	0.00151
120.1	0.20155	0.00305	3.76855	0.06063	0.13563	0.00159
121.1	0.31298	0.00476	4.86947	0.08127	0.11286	0.00142
121.2	0.31536	0.0048	4.8866	0.0819	0.1124	0.00142
122.1	0.22802	0.00345	3.55886	0.05787	0.11321	0.00135
123.1	0.35231	0.00533	7.31128	0.11688	0.15053	0.00174
124.1	0.24073	0.00364	3.98612	0.0642	0.12011	0.00141
125.1	0.4286	0.00647	9.38684	0.14931	0.15887	0.00181
126.1	0.30843	0.00471	4.72105	0.08119	0.11103	0.00147
127.1	0.39337	0.00595	9.63144	0.15483	0.17761	0.00207
128.1	0.28381	0.00431	5.8411	0.09588	0.14929	0.00181
129.1	0.12131	0.00183	1.94021	0.03126	0.11602	0.00136
130.1	0.31698	0.00479	5.03822	0.08122	0.1153	0.00135
131.1	0.27317	0.00416	4.12948	0.06966	0.10965	0.0014
131.2	0.27707	0.00421	4.1637	0.06978	0.10901	0.00138
133.1	0.30758	0.00469	4.71282	0.07998	0.11114	0.00144
134.1	0.37767	0.00571	10.90423	0.17449	0.20943	0.00241
135.1	0.35227	0.00532	10.95552	0.1748	0.22559	0.00258
135.2	0.13521	0.00205	2.59694	0.04194	0.13932	0.00163
136.1	0.22979	0.00347	3.57523	0.05748	0.11286	0.00131
137.1	0.26494	0.00401	4.64358	0.07535	0.12714	0.0015
137.2	0.30972	0.00469	5.48577	0.0891	0.12848	0.00152
138.1	0.21056	0.0032	3.28076	0.05481	0.11302	0.00142
139.1	0.31147	0.00472	4.78125	0.07876	0.11135	0.00136

Appendix 7: Ages of zircon spots from LA-ICPMS of the Oorlano Metasomatite (Harlequin Stone) sample selected from the Orallaw Quarry.

Grain Spot	Pb206/U238	±	Pb207/U235	±	Pb207/Pb206	±
1.1	1784.9	23.39	1784	12.98	1783.2	20.18
2.1	1388.6	18.72	1599.7	12.32	1890.3	19.48
3.1	1458.8	19.53	1588.8	12.18	1765.9	19.43
4.1	1470.1	19.7	1971.6	13.19	2548.5	17.83
5.1	1400.5	18.86	1596.4	12.31	1865.7	19.52
6.1	1606.5	21.28	1932.4	13.03	2302.7	18.01
7.1	1658.7	21.88	2010.7	13.18	2394.8	17.77
8.1	1334.3	18.03	1654.2	12.3	2088.5	18.42
9.1	1358.7	18.35	1600.1	12.28	1934.5	19.21

10.1	2049.4	26.23	2582.4	13.94	3032.1	16.36
11.1	1937.7	25.04	1998.1	13.2	2061.5	18.54
12.1	1496.6	20.02	1728.6	12.71	2022.3	19.17
13.1	1613.5	21.4	1734.1	12.74	1883.1	19.51
14.1	1786.2	23.37	2009.2	13.28	2247	18.36
15.1	1795.4	23.45	2165.5	13.46	2537.5	17.44
16.1	1470.3	19.76	1683.3	12.8	1960.1	19.95
17.1	1769.5	23.18	1978.8	13.2	2205.4	18.35
18.1	990.1	13.73	1616.6	12.14	2567.6	17.29
19.1	1715	23.13	1711.9	14.97	1708.4	26.93
20.1	1550.1	20.77	1764.2	13.23	2028.3	20.46
21.1	1445.1	19.36	1805.4	12.67	2251.4	17.85
22.1	1877	24.39	2183.3	13.54	2485.1	17.65
23.1	1735.9	22.82	1903.2	13.11	2091	18.82
24.1	2198.6	27.92	2446.1	13.98	2659.1	17.41
25.1	1764.9	23.2	1832.3	13.18	1909.9	19.95
26.1	1524.9	20.33	1806.7	12.76	2149.6	18.31
27.1	1751	22.95	1924.1	13.03	2116.2	18.33
28.1	1027.6	14.25	1449.7	11.84	2138.5	18.95
29.1	1049.9	14.5	1468.3	11.72	2139.7	18.26
30.1	1088.4	15.02	1788.9	12.79	2743.9	17.49
31.1	1745.1	22.95	1774	12.95	1808.3	19.9
32.1	1323.3	17.92	1680.8	12.45	2161.6	18.34
33.1	1572.6	21	1680.7	12.91	1818.6	20.62
34.1	1823.8	23.83	1844.5	13.05	1868.1	19.49
35.1	1847.2	24.07	1851.7	12.97	1857	19.19
36.1	1775.3	23.34	1842.3	13.25	1919.2	20
37.1	1629.7	21.66	1825.9	13.18	2057.8	19.62
38.1	1697.6	22.42	1745.6	12.91	1803.7	20.02
39.1	1354.9	18.61	1945.7	14.1	2650.2	20.34
40.1	1787.6	23.67	1819.9	13.92	1857.3	22.4
41.1	1765.1	23.24	1826.1	13.26	1896.6	20.21
41.2	1235	16.86	1609.2	12.36	2140.9	18.76
42.1	1805.3	23.6	1826.1	12.91	1850.2	19.17
43.1	2015.3	25.99	2207.1	13.79	2390.5	18.3
44.1	1305.2	17.7	1589.2	12.19	1989.9	18.72
45.1	1656	21.94	1824.5	13.07	2023	19.3
46.1	1986.8	25.62	2620.5	14.17	3154.7	16.48
47.1	1515	20.33	1733.3	13.03	2008.2	19.99
48.1	1751	23.17	1806.7	13.57	1871.7	21.33
48.2	1806.7	23.82	1839.5	13.69	1877.1	21.44
49.1	1673.2	22.15	1751.6	12.94	1846.8	19.87
50.1	1639.6	21.76	1758.7	12.94	1903.6	19.7
51.1	1472.6	19.76	1549	12.23	1655.1	20.02
52.1	1577.9	21.01	1971	13.28	2413.5	18.07
53.1	1457.4	19.61	1904.1	13.26	2433.5	18.42
54.1	1102.2	15.23	1406.1	11.8	1902.8	19.74
55.1	1804	23.66	1831	13.16	1862.1	19.85
55.2	1839.9	24.09	1849.8	13.32	1861.3	20.2
56.1	2030.7	26.13	2322.6	13.89	2590.3	17.6
57.1	1067.7	14.79	1537.8	12.23	2261.9	18.79
58.1	1700.1	22.49	1742.9	13.04	1794.9	20.37
59.1	4949.5	51.82	4034.2	15.11	3605.5	16
60.1	1752.7	23.13	1930.1	13.54	2126.5	19.64
61.1	856.6	12.11	1242.6	11.47	1993.1	20.79
62.1	1697.3	22.56	1823.4	13.59	1971	20.93
63.1	1766.4	23.27	1824.3	13.28	1891.4	20.14
64.1	1630.3	21.69	1735.4	13.03	1864.9	20.19
65.1	1696.8	22.44	1906.2	13.34	2142.6	19.13
66.1	710.4	10.14	1181.4	10.98	2190.2	19.64
67.1	1414.1	19.22	1614.1	13.11	1886.1	21.61
68.1	1133.5	15.68	1393.1	12.05	1816.7	20.91
69.1	1682.6	22.25	1746.7	12.86	1824.5	19.6
70.1	1517	20.31	1768.1	12.92	2079.3	19.05
71.1	1620	21.58	1770	13.17	1952.1	20.08
72.1	1643.6	21.83	1745.2	13	1869.5	19.95
73.1	2444.2	30.63	2919.1	14.77	3265.4	16.98
74.1	1673.1	22.3	2131.1	14.15	2607.7	19.16
74.2	1619	21.74	2149.5	14.35	2703.8	19.48
75.1	1414.7	19.13	1704.5	12.93	2082.1	19.59
76.1	1473.7	19.88	1649.5	12.96	1881.7	20.68
77.1	1039.7	14.44	1425.7	11.87	2061.3	19.19
78.1	1721.4	22.74	1764.3	13.08	1815.9	20.12
79.1	1599.4	21.36	1732.4	13.13	1897.3	20.36
80.1	746.4	10.61	1248.6	11.18	2264	18.95
81.1	1777.6	23.45	1841.3	13.49	1914.4	20.53

82.1	1013.6	14.17	1409.7	12.15	2072.8	20.36
83.1	1309.3	17.85	1540.7	12.48	1874.8	20.26
84.1	1924.2	25.03	2239.7	13.98	2542.4	18.16
85.1	1079.7	14.95	1468.1	12.02	2086	19.06
85.2	1223.8	16.76	1423.7	11.87	1737.1	19.93
86.1	1463.8	19.76	1606.1	12.81	1798.3	20.79
86.2	1169.9	16.14	1488.5	12.4	1977.7	20.33
87.1	1544.8	20.72	1656.3	12.94	1801.2	20.67
88.1	1734	22.88	1784.4	13.11	1844.2	19.9
89.1	391.9	5.73	728.7	8.22	1977.9	20.15
90.1	1665.3	22.29	1725.1	13.78	1798.6	22.66
91.1	1685.8	22.48	1727.4	13.6	1778.4	22.17
92.1	1368.9	18.61	1543	12.63	1790.6	20.9
93.1	1109	15.35	1527.5	12.37	2167.9	19.31
94.1	1510.1	20.32	1670.1	13.03	1877.9	20.58
95.1	1453.8	19.61	1706.6	12.95	2032.8	19.62
96.1	1837.8	24.12	1986.6	13.74	2145.4	19.58
97.1	1390.6	18.84	1979.7	13.58	2667.4	18.18
98.1	1854.1	24.3	1925.1	13.61	2002.7	19.94
99.1	1743.5	23.04	1797.9	13.35	1861.9	20.45
100.1	1322.6	18.02	1705.5	12.96	2214.8	19.2
101.1	1220.8	16.78	1663.3	12.95	2278.6	19.46
102.1	1434	19.42	1653.7	13.02	1945.6	20.51
103.1	1484.5	20.01	1711	13.14	2001.1	20.14
104.1	1119	15.52	1459.6	12.41	1997.7	20.54
105.1	740	10.54	1505.9	12.3	2851.6	18.02
106.1	1433	19.39	1735	13.19	2121.5	19.85
107.1	1502.9	20.23	1753.2	13.23	2066.5	19.93
107.2	2123.1	27.33	2363.1	14.53	2577.4	18.91
108.1	1711	22.71	1788.9	13.5	1881.4	20.88
109.1	1441.9	19.48	1633.6	12.81	1890.3	20.11
110.1	1493.1	20.16	1742.5	13.41	2056.7	20.6
111.1	1655.9	22.07	1751.9	13.41	1868.6	20.95
112.1	2406.3	30.46	2640.5	15.08	2825.6	18.95
113.1	1238.8	17.05	1511.9	12.69	1919	21.03
114.1	1858	24.36	2312.1	14.4	2741.8	18.43
115.1	1432.9	19.41	1721.7	13.24	2093.6	20.1
116.1	1746.9	23.23	2012.6	14.29	2297.8	20.6
116.2	1712.7	22.82	2127.5	14.44	2556.5	19.81
117.1	1853.5	24.51	1886	14.32	1922.4	22.42
118.1	1268.8	17.38	1893	13.58	2669.3	18.59
119.1	1526.5	20.6	1757.3	13.61	2044.2	21.03
120.1	1183.6	16.36	1586.1	12.91	2172.2	20.23
121.1	1755.3	23.36	1797	14.06	1845.9	22.56
121.2	1767	23.51	1799.9	14.13	1838.6	22.76
122.1	1324.1	18.12	1540.4	12.89	1851.6	21.43
123.1	1945.6	25.39	2150.2	14.28	2352	19.57
124.1	1390.5	18.91	1631.4	13.07	1957.9	20.69
125.1	2299.4	29.21	2376.5	14.6	2443.6	19.16
126.1	1733	23.21	1771	14.41	1816.4	23.9
127.1	2138.4	27.55	2400.2	14.79	2630.6	19.21
128.1	1610.5	21.64	1952.5	14.23	2337.8	20.67
129.1	738.1	10.54	1095.1	10.8	1895.8	20.87
130.1	1774.9	23.46	1825.8	13.66	1884.5	20.9
131.1	1556.9	21.06	1660.2	13.79	1793.6	23.11
131.2	1576.6	21.27	1666.9	13.72	1782.8	22.87
133.1	1728.8	23.11	1769.5	14.21	1818.2	23.27
134.1	2065.4	26.72	2515	14.88	2901.2	18.53
135.1	1945.4	25.37	2519.4	14.85	3021	18.22
135.2	817.5	11.62	1299.8	11.84	2218.8	20.19
136.1	1333.4	18.2	1544.1	12.76	1845.9	20.85
137.1	1515	20.44	1757.1	13.56	2058.8	20.72
137.2	1739.3	23.09	1898.4	13.95	2077.2	20.72
138.1	1231.8	17.04	1476.5	13	1848.5	22.5
139.1	1747.9	23.22	1781.6	13.83	1821.5	21.94